CryoVex 2004 and 2005 (BoB) data acquisition and final report

ESA Contract C18677/04/NL/GS

by

V. Helm[1], S.Hendricks[1], S. Goebell[1], W. Rack[1], C. Haas[1], U. Nixdorf[1], T. Boebel[2]

1) Alfred Wegener Institute – Bremerhaven, Germany
2) Optimare Sensor Systems AG – Bremerhaven, Germany

February 22nd 2006

Table of content

List of figures

List of tables

1 Introduction

CryoVex 2004 and 2005 (CryoSat Validation EXperiment) were the second and third combined airborne and surface campaigns for the preparation of the CryoSat mission, after successful completion of CryoVex 2003 by Danish colleagues. The new key element was the implementation and operation of ESA's Airborne SAR Interferometric Radar Altimeter System (ASIRAS) on a German Do-228 aircraft. ASIRAS was designed to simulate the SIRAL radar altimeter onboard CryoSat, to investigate the nature of CryoSat waveforms and their dependence on different surface properties. Data were gathered together with airborne nadir looking and laser and laser scanner measurements as well as video recordings.

The primary goal of CryoVex 2004 was to conduct measurements over the glacial ice caps of Svalbard, Greenland, and Devon Island. CryoVex 2005 was performed over the sea ice of the Bay of Bothnia (BoB). In addition, in March 2005 ASIRAS was operated in the Low Altitude Mode (LAM), now allowing measurements at flying altitudes below 1100 m to obtain simultaneous observations with range-limited laser scanners. Airborne measurements during CryoVex 2004 and 2005 were carried out by AWI, DLR, Optimare and RST. Simultaneous ground observations were performed by the international ESA CVRT groups.

This reports is split into two parts: Part A describes the data acquisition activity of AWI carried out in two separate campaigns in 2004 (CryoVex2004A, CryoVex2004B) and 2005 (CryoVex 2005 BoB). Part B gives an overview on data processing, aircraft operations and selected results.

1.1 Definitions, Acronyms and Abbreviations

AAR	Actual Aircraft Reference Frame
ALS	Airborne Laser Scanner
AMR	Aircraft Mechanical Reference Frame
ASIRAS	Airborne SAR Interferometric Radar Altimeter System
AWI	Alfred Wegener Institute
BoB	Bay of Bothnia
CALVAL	CALibration VALidation
CRYOVEX	CRYOSAT Validation Experiment
DEM	Digital Elevation Model
DGPS	Differential Global Positioning System
DLR	Deutsche Luft und Raumfahrt
EM	Electro Magnetic induction
ESA	European Space Agency
GEF	Global Earth Fixed Frame
HAM	High Altitude Mode
ITRF	International Terrestrial Reference Frame
LAM	Low Altitude Mode
LD90	single beam laser altimeter
NAR	Nominal Aircraft Reference Frame
SAR	Synthetic Aperture Radar
SIRAL	SAR Interferometric Radar Altimeter System
WB	weak backscatter

1.2 References

R1. ASIRAS Product Description,CS-LI-ESA-GS-0371, version 1.6, 13/1/2006

R2. LMS-Q280 Airborne Laser Scanner, Technical Documentation and User's Instruction, version 5.2, 22/01/03

R3. Hawley,R.L., et al. (2006), ASIRAS airborne radar resolves internal annual layers in the dry-snow zone of Greenland, Geophys. Res. Letters, Vol. 33

R.4 Mavrocordatos, C. et al. (), Development of ASIRAS (Airborne SAR/Interferometric Altimeter System)

R.5 _Ferraro, E., et al. (1995), Comparison of Retracking Algorithms Using Airborne Radar and Laser Altimeter Measurements of the Greenland Ice Sheet, IEEE Trans. on Geoscience and Remote Sens., vol. 33, no. 3

R.6 ASIRAS Design Description. ASIRAS-RST-ADD-0001.

2 Hardware installation, configuration and system overview

Installation of the complex radar and laser equipment in the Polar 4 aircraft AWI was accomplished by Optimare before campaign start in Bremerhaven.

Main components of the equipment are (see Figure 2.1-1):
RST – Radar Altimeter System (ASIRAS – Airborne Synthetic Interferometric Radar Altimeter System)

Riegl – Laser Scanner LMSQ280 (ALS)

Riegl – Laser Altimeter LD90

Sony – Nadir Video Camera

Trimble – two DGPS antenna and one automatically recording basis station

Basic data acquisition system

Honeywell INS
GNS-X
Basic meteorological sensor (BMET/NAVP)

2.1 Instrument information and reference frame of aircrafts

Table 2.1-1 Local reference frame of the aircraft (Polar 4) and installation positions of the devices

Reference frame of the aircraft (Polar 4):				
positive x – direction	Through nose of aircraft			
positive y – direction	to right wing side			
positive z – direction	Downwards ($x \times y$)			
zero datum	Front left edge of ASIRAS antenna			
Components	X[mm]	Y[mm]	Z[mm]	
GPS-REAR (Pos. 2)	-211	320	-1843	GPS antenna ground
GPS-FRONT (Pos. 1)	4649	540	-1923	GPS antenna ground
RIEGL-LD90 (Pos. 19)	1442	770	+90	Midpoint of transmit-receive optic
RIEGL-LMSQ280 (Pos. 18)	1109	770	-458	Origin of measurement
RST-RADAR1 (Pos. 21)	-197	390	+20	Midpoint of patch antenna
RST-RADAR2 (Pos. 21)	-197	1150	+20	Midpoint of patch antenna
SONY – Video Camera (Pos. 20)	4624	1205	-294	Midpoint of camera lens

Units are [mm]. Measurements were carried out with a measuring stick and a balance.

The AWI-Polar4 aircraft was used during the CryoVex2004A and CryoVex2004B campaigns.

Table 2.1-2 Local reference frame of the aircraft (D-CODE) and installation positions of the devices

Reference frame of the aircraft (D-CODE):				
positive x – direction	Through nose of aircraft			
positive y – direction	to right wing side			
positive z – direction	Downwards ($x \times y$)			
zero datum	Front left edge of ASIRAS antenna			
Components	X[mm]	Y[mm]	Z[mm]	
GPS-REAR (Pos. 2)	18	1398	-1819	GPS antenna ground
GPS-FRONT (Pos. 1)	4836	561	-1996	GPS antenna ground
RIEGL-LD90 (Pos. 19)	1180	770	+115	Midpoint of transmit-receive optic
RIEGL-LMSQ280 (Pos. 18)	1080	763	-441	Origin of measurement
RST-RADAR1 (Pos. 21)	-216	390	+15	Midpoint of patch antenna
RST-RADAR2 (Pos. 21)	-216	1150	+15	Midpoint of patch antenna
SONY – Video Camera (Pos. 20)	4446	1417	-100	Midpoint of camera lens

The D-CODE aircraft was used during the CryoVex2004A Bay of Bothnia campaign.
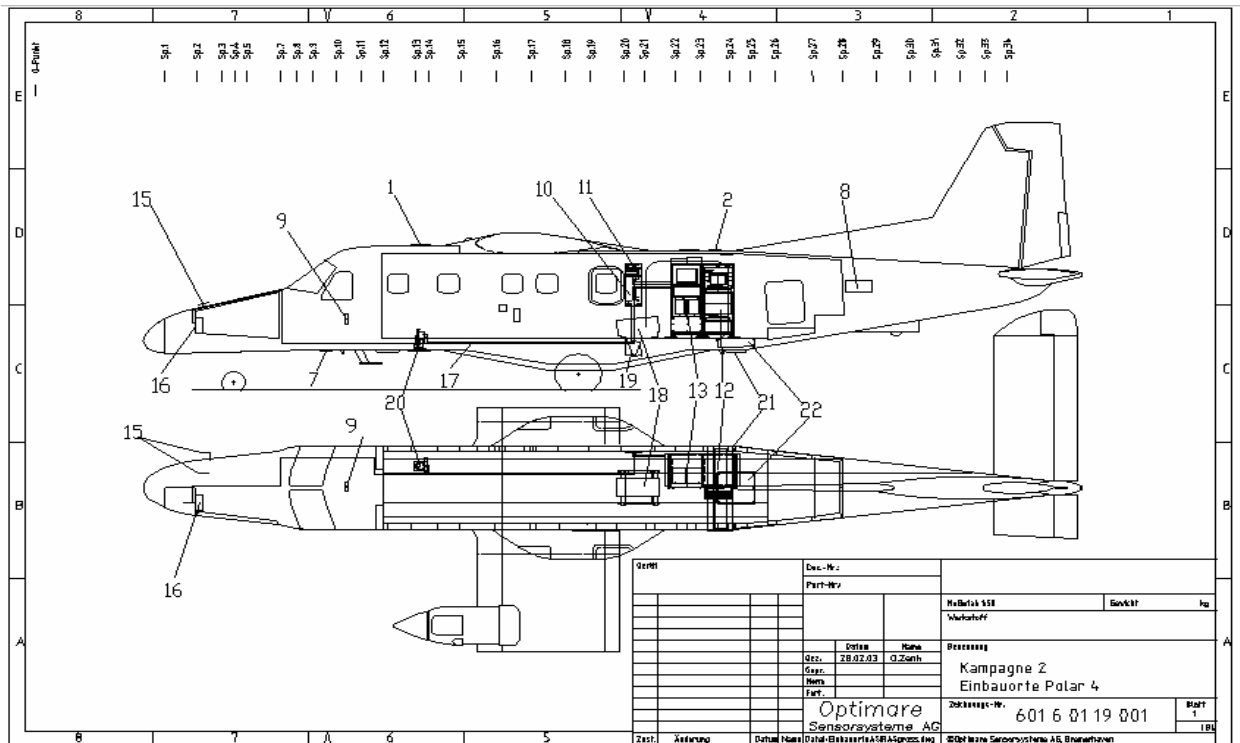
Figure 2.1-1 Sketch of aircraft showing positions of measuring devices

1+2 GPS antenna (Trimble receiver)

7 Radar altimeter

8 INS

9 GNS-X

10 Power distribution module

11 Data distribution module

12 Rack I

13 Rack II

15 Basis meteorology sensors

16 BMET I/O module

17 Fiber optic

18 Riegl laser scanner LMSQ-280

19 Riegl LD90 laser altimeter

20 Sony video camera

21 RST ASIRAS antenna

22 Antenna cable slot

Detailed information to the devices:

ASIRAS
        Laptop for measurement control
        PC1 and PC2 for data acquisition (two channels)
        ASIRAS transceiver
        ASIRAS antenna
        Chirp Bandwidth: 1GHz
        Pulse Length: 4.0E-06 s
        PRF: 4000 Hz
        Altitude Window: 1100 – 7000m
        Range Window: 18 m
        (design description see [R.4, R.6])

Laser Scanner LMSQ280
        Laser scanner
        Laser scanner sensor processor for data acquisition
        Laser scanner key switch to switch a time impulse
        measurement range: 30 m – 1200 m
        measurement resolution: 20 mm with typ. ± 25 mm accuracy
        data channels: range, amplitude, quality, true color
        measurement rate: PRR: 18.5 kHz, data: 9250 Hz
        beam divergence: 0.5 mrad
        scanning range: nominal 45° - 60°
        scanning rate 4 Hz to 80 Hz

The scanner provides cross-track scans at a user selectable frequency. Per scan 113 single points were measured. The width of the swath is dependent on flight elevation (1100 m flight elevation ---> swath width ca. 800m). During CryoVex2004 ALS was running with a scan angle of 45° by appr. 80 scans/second. Start and stop time of ALS recording is listed in table 4 (see [R.2]).

Laser Altimeter LD90
        Laser Altimeter (Single Beam)
        data recording at NAVP sensor processor
        measurement rate: PRR: 2000 Hz, data: 4 Hz
        measurement range: up to 2500 m
        minimum distance: 1.5 m
        measurement resolution: 2 mm with typ. ± 25 mm accuracy
        beam divergence: 0.5 mrad

INS – Inertial Navigation System

Honeywell Laser NAVP2 platform is equipped with accelerometer and ring laser gyros. The data is recorded at NAVP sensor. Processor Data output to ARINC 429. Primary data are acceleration and angle rates with highest data rate of 50 Hz. Several other secondary labels with reduced data output rate available, e.g. drift angle, true heading, pitch angle, roll angle, wind speed, wind direction.

2.2 Concept of data flow
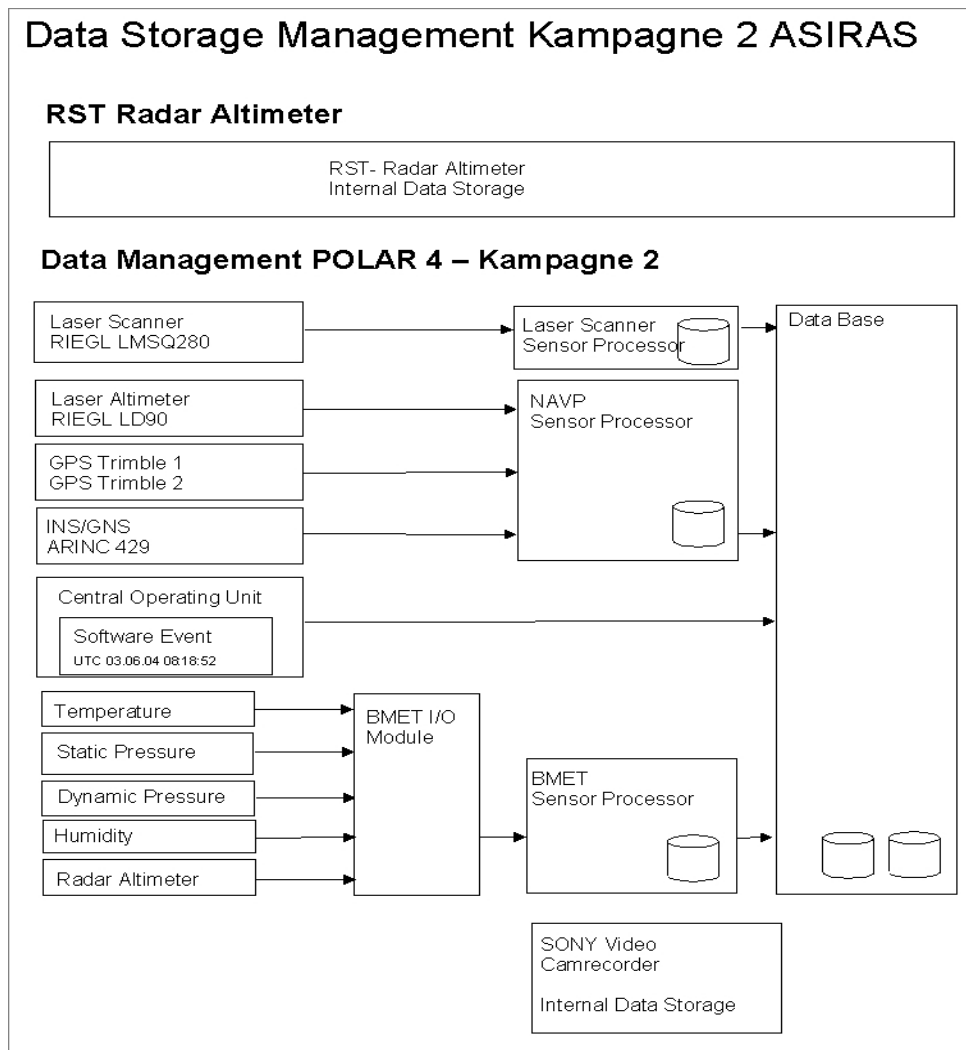
Figure 2.2-1 Concept of data flow

During flight data recorded by the sensor processors is stored in ring buffers (20 min). The whole bunch of data recorded on a flight is stored on hard disk (data storage system) and backed up at LTO-tapes for the campaigns.

2.3 Time concept

A UTC time tag and 1 PPS pulse from one of the GPS receivers is the primary time information for the complete system. The system tact is derived from a GPS receiver and coupled via the time-server with all devices. The time stamp of the data is added as soon as the data is acquired by the Medusa-P system. In general the sensor processor or the I/O Module does this job to merge either the analog signals or digital system together with the time information immediately when the data shows up in the system. These time stamped data packages are forwarded via Ethernet link to the database and the online visualization. Every measurement gets its specific data at occurrence in the system.

In the normal time server / time client application the time accuracy should about $+\text{-}1^{-6}$ s and the resolution is about 1^{-3} s.

Exception:
The ALS has as additional opportunity to reset an internal time counter with a PPS impulse. But no direct link to UTC time stamps.
Therefore the ALS and its Sensor Processor gets the same PPS signal. When the signal reaches the ALS the internal time counter is reset and stored in the data stream. At the same time the ALS writes the UTC time, which is derived from the GPS and PPS time settings of the sensor Processor, at occurrence of this pulse to a data file called "trigdata".

The normal ALS data stream is logged in the rawdata file.
Both instruments the ALS and the Sensor Processor has different start up times. So, in order to prevent that one of these systems archives the PPS earlier, the PPS can be switched on by hand, specially for the Laser scanner by hand at a definitive time during system start up. To this On/OFF switch the PPS signal is switched on at a time when both systems are operable and the ALS time reset counter is checked, whether it is increasing (OK) or not (FALSE).

VIDEO:
The absolute camera time is set to UTC at the beginning of a flight. The camera records the set time at the tape. Additional a PPS pulse is recorded on the audio trace as transformed audio signal. This is only possible in the installation at the POLAR 4. The CODE has a different design, where the audio input of the camera is not function able.

ASIRAS:
ASIRAS has his own time concept and is described by RST documentation [R.6]. In operation GPS-synchronization is applied. The accurate GPS time datation provides the synchronization to the ancillary aircraft equipment. Once the GPS-time of the first radar pulse is known, echoes at any given time can be computed by simply adding to the start time the pulse number multiplied by the PRF.

Synchronisation Data Acquisition System

Primary Time Information

TRIMBLE GPS Receiver

UTC 03.06.04 08:18:52

Sync Puls

Time Server

08:18:52

UTC 03.06.04 08:18:52 → RST- Radar Altimeter Transceiver

Sync Puls +/- 1 μs

UTC 03.06.04 08:18:52 → Laser Scanner Sensor Processor

Sync Puls +/- 1 μs

Sync Counter

Time Counter

Sync Puls +/- 1 μs → Laser Scanner RIEGL LMSQ280

Sync Puls +/- 1 μs → Laser Altimeter RIEGL LD90

Time Counter

LWL Time Signal
Sync Puls +/- 1 μs
Resolution 1/1000 s → NAVP Sensor Processor

INS/GNS ARINC 429

GPS Time Stamp
UTC 03.06.04 08:18:52 → Central Operating Unit

Software Event
UTC 03.06.04 08:18:52

LWL Time Signal
Sync Puls +/- 1 μs
Resolution 1/1000 s → BMET Sensor Processor

LWL Time Signal
Sync Puls +/- 1 μs
Resolution 1/1000 s → BMET I/O Module

AD-Converter add absolute time stamp to single datum
Sync: 1/100000 s
Resolution: 1/1000 s

Temperature

Static Pressure

Dynamic Pressure

Humidity

Radar Altimeter

Software Event
UTC 03.06.04 08:18:52

User interactive visuale synchronisation to Tape Frame Counter and UTC-Time

SONY Video Camrecorder

Framerate 1/25 s

Sync Puls +/- 1 μs → Puls/Audio Coupler

Audio Signal →

Audio Track

Figure 2.3-2 Time concept

3 Part A.1: CryoVex 2004 data acquisition report

In general, the two campaigns (CryoVex2004a April 19th – May 9th 2004, CryoVex 2004b August 30th – September 17th 2004) measured continental ice cap profiles. Flights were performed in Svalbard across Austfonna (CyroVex2004a) at the Greenlandic Ice sheet along the EGIG line (CyroVex2004 a/b) and at Devon ice cap (CryoVex 2004 a/b). In general each profile was measured twice in high and low altitude, respectively. This was necessary because of the very small overlap of measurement ranges between the ASIRAS instrument and the laser scanner system. ASIRAS SARIn Mode is operable in altitudes from 1096 m above ground upwards and the laser scanner system is limited to 1280 m for targets with 100 % reflectivity. This range is degraded if the reflectivity is less. The nominal flight elevation during low altitude flights was around 300 m and during high altitude flights around 1150 m above ground. For each flight a GPS base station was operated on ground. Some minor data leaks exist, which are caused by a none operating ground station at Sep 16th and GPS receiver problems at one of the two on board receivers at May 6th. In general for each flight, all data is collected, backed up and stored at the AWI.

Partners in the contract are AWI, DLR, Optimare Sensor Systems AG, and RST. AWI's responsibilities were project planning, coordination and data analysis of the campaigns. DLR maintained and operated the aircraft, Optimare integrated the system, operated the data acquisition and ancillary equipment, and RST was designer and operator of ASIRAS.

The field operations of the airborne survey proceeded as follows:
In general each measurement flight was tried to accompany by at least one runway-over flight. The runway-overpasses, if possible, were done twice, to have first an overlap between ASIRAS and Laser Scanner System at an altitude of 1150 m and second to get a high topographic resolution information of the runway from the laser scanner system at altitudes of 300 m. All runway overpasses are listed in Table 3.1-2 and Table 3.1-7. The comment column includes a short description of the data quality of both ASIRAS and scanner. In coordination with the ground teams corner reflectors were built up at selected profiles. In some cases the corner reflector was missed during the overpass. A closer look into successful runway and corner overflights will follow in section 5.
Section 3.1 summarizes the measurement activity for both campaigns and lists all runway over passes.

3.1 CryoVex2004A & Cryovex2004B measurement activity

Table 3.1-1 CryoVex2004A measurement activity: April 19th – May 9th 2004

April 19	Scientific equipment unpacked, checked and installed in the aircraft Polar 4 in hangar in Svalbard. Setup automatically PC-logging reference GPS receiver. First test flight.
April 20	Checking data of test flight
April 21 – 24	bad weather
April 25	Austfonna flight (Problems with data acquisition ancillary system only GPS Receiver data and ASIRAS RST System available, problems with aircraft power system)
April 26 – 28	fixing aircraft inverter problem and data acquisition system problems
May 01	transfer flight to Resolute Bay
May 02	flight activity at Devon ice cap, operation over profile normal
May 03	bad weather
May 04	transfer flight to Ilulissat

May 05	flight activity at EGIG line first part
May 06	flight activity at EGIG line, ASIRAS PC crashed at high altitude do to pressure problems and non pressurize hard disc.
May 07	transfer to Longyearbyen
May 08	Disintegration of system in Longyearbyen
May 09	transfer to Bremerhaven

In total 27 airborne hours were flown during CryoVex2004A. An overview of flight activity is given in Table 3.1-4. The flown tracks are shown in Figure 3.1-1, Figure 3.1-2, Figure 3.1-3, Figure 3.1-4, Figure 3.1-5 and Figure 3.1-6.

Table 3.1-2 CryoVex2004A runway over passes.

RUNWAY	DAY	Start time	Stop time	ASIRAS	ALS High	ALS Low	Comment ASIRAS	Comment ALS
Longyearbyen	404190101	55942	55974	A040419_01	•			weak backscatter
		56438	56472	A040419_02	•			weak backscatter
		61768	61800		•			weak backscatter
		62054	62086		•			weak backscatter
		62362	62394		•			weak backscatter
Longyearbyen	404200201	57824	57858	A040420_00	•			weak backscatter
		72134	72165	A040420_06	•		no data	no data
		72781	72809	A040420_07	•		no data	no data
Resolute	405020401	78119	78162	A040502_05	•		hit, retracking ok	ok
		788546	78586			•		ok
Ilulissat	405050501	72557	72587	A040505_03	•		no hit, retracking ok, roll > 1°	weak backscatter
		72898	72916			•		ok
Ilulissat	405060601	61536	61566			•		ok

Table 3.1-3 CryoVex2004A, ALS measurement activity

Day	UTC time	Comment in user_event
April19	15:14:00	Laser sync on
April19	15:14:30	Laser sync on real
April20	15:41:45	Start sync pulses
April20	19:33:11	als restart
April20	20:18:29	Stop sync als

April25	-	-
May 02	17:57:45	Sync on
May 02	18:51:03	Laser scanner off
May 02	19:03:38	Laser scanner sync on
May 02	19:48:12	Sync pulse on
May 06	12:45:00	Sync on
May 06	13:12:31	Sync on
May 06	15:49:15	Sync on

Table 3.1-4 Flight activity of CryoVex2004A by Julian day and UTC time

Date/JD	Location	ASIRAS tracks	Take off (UTC)	Landing (UTC)	Airborne
April 19	Austfonna	A040419_00 - A040419_08	14:38	17:42	3 h 04 min
April 20	Austfonna	A040420_00 - A040420_07	15:23	20:22	4 h 59 min
April 25	Austfonna	A040425_00 - A040425_04	06:30	09:21	2 h 51 min
May 01	transfer	-	-	-	-
May 02	Resolute	A040502_00 - A040502_05	17:29	21:58	4 h 29 min
May 04	transfer	-	-	-	-
May 05	Ilulissat	A040505_00 - A040505_03	17:44	20:24	2 h 40 min
May 06	Ilulissat	A040506_00 - A040506_02	12:34	17:17	4 h 43 min
May 07	transfer	-	-	-	-

Table 3.1-5 CryoVex2004B measurement activity: August 30th – September 17th 2004

Aug 30	Scientific equipment unpacked, checked and installed in the aircraft Polar 4 in hangar in Luneort (Bremerhaven). Setup automatically PC-logging reference GPS receiver. Test flights over North Sea and river Weser. Operation normal.
Sep 01 – 02	Transfer aircraft and scientific equipment to Kangerlussuaq.
Sep 03	Arrival of scientific crew from AWI, RST and OPTIMARE in Kangerlussuaq.

Sep 04	Setup automatically PC-logging reference GPS receiver. Test flight across glacier, runway overpasses at Kangerlussuaq airport
Sep 05 – 08	Problems with IGI are solved. Planning of transfer to Resolute Bay.
Sep 09	Alternative flight activity (EGIG line), because of bad a weather period in Canada.
Sep 10	Transfer to Resolute Bay.
Sep 11	One flight over Devon ice cap (high altitude mode) with immediately returning to Ilulissat. The transfer flight had to be used as measurement flight , no further landing and refueling was possible at Resolute Bay due to bad weather and fuel problems at the Canadian station. Therefore, no reference GPS receiver could be built up at Resolute Bay!
Sep 12 –13	Data backup. Briefing and short analysis of data with Malcolm Davidson (ESA).
Sep 14	Setup automatically PC-logging reference GPS receiver in Ilulissat. flight activity (EGIG line).
Sep 15	Data backup, ESA Film team operation during CryoVex 2004 B in Ilulissat
Sep 16	Setup automatically PC-logging reference GPS receiver in Ilulissat. Flight activity (EGIG line). Installing pressurized hard disc in ASIRAS System by OPTIMARE in Kangerlussuaq. GPS ground station did not operate. Laser calibration flights.
Sep 17	Setup automatically PC-logging reference GPS receiver in Ilulissat. Flight activity (EGIG line). Laser calibration flights.

In total 18 airborne hours were flown during CryoVex2004B. An overview of flight activity is given in Table 3.1-6. The flown tracks are shown in Figure 3.1-7, Figure 3.1-8, Figure 3.1-9, Figure 3.1-10 and Figure 3.1-11

Table 3.1-6 Flights of CryoVex2004B by Julian day and UTC time

Date/JD	Location	ASIRAS tracks	Take off (UTC)	Landing (UTC)	Airborne
Aug 30	Bremerhaven	A040830_00 - A040830_08	-	-	-
Sep 04	Kangerlussuaq	A040904_00 - A040904_08	11:38	13:44	2 h 06 min
Sep 09	Kangerlussuaq	A040909_00 - A040909_05	14:45	18:53	4 h 08 min
Sep 11	Resolute	A040911_00 - A040911_01	16:27	18:15	1 h 48 min
Sep 14	Ilulissat	A040914_00 - A040914_07	14:42	18:37	3 h 55 min

Date/JD	Location	ASIRAS tracks	Take off (UTC)	Landing (UTC)	Airborne
Sep 16	Ilulissat	A040916_00 - A040916_02	-	-	-

Table 3.1-7 CryoVex2004B runway over passes.

RUNWAY	DAY	Start time	Stop time	ASIRAS	ALS High	ALS Low	Comment ASIRAS	Comment ALS
Kangerlussuaq	409040201	48400	48500	A040904_08	•		partly hit, retrack bad, roll >1°	weak backscatter
		48800	48840			•		ok
Kangerlussuaq	409090301	66625	66652	A040909_04	•		no hit, retrack, roll >1	weak backscatter
		67010	67055	A040909_05	•		partly hit, retrack bad, roll >1°	weak backscatter
		67340	67380			•		ok
Ilulissat	409140501	54144	54159			•		no INS
		54539	54555	A040914_00	•		hit, retrack bad	weak backscatter
		54906	54916	A040914_01	•		perfect hit, retrack gaps	weak backscatter
		64846	64858	A040914_04	•		hit, retrack very bad	weak backscatter
		65224	65241	A040914_06	•		hit, no retracking	weak backscatter
		65682	65694	A040914_07	•		hit, no retracking	weak backscatter

Table 3.1-8 CryoVex2004B, ALS measurement activity

Day	UTC time	Comment in user_event
Aug 30	-	-
Sep 04	12:19:46	Switch on lmsq280 sync pulse
Sep 09	14:50:45	Switch on lmsq280 sync pulse
Sep 09	15:52:29	Laser on
Sep 09	17:25:45	Laser off
Sep 09	18:08:38	Laser on
Sep 09	18:45:42	Ld90 als laser off
Sep 11	17:13:31	Switch on lmsq280 sync pulse
Sep 14	14:48:00	Switch on lmsq280 sync pulse

Sep 14	15:00:28	Switch on laser lmsq280
Sep 14	15:16:55	Laser off lmsq280
Sep 14	15:52:37	Switch on laser lmsq280
Sep 14	16:52:08	Laser signal
Sep 14	17:10:30	Switch off laser
Sep 14	17:41:43	Switch on laser lmsq280
Sep 16	18:34:32	Switch on sync jump from 4 to 8
Sep 17	13:09:46	Switch sync pulse on lmsq280
Sep 17	13:14:59	Switch laser source off
Sep 17	14:13:09	Switch on lmsq280 laser
Sep 17	16:56:45	Laser 12.5 Ausfälle
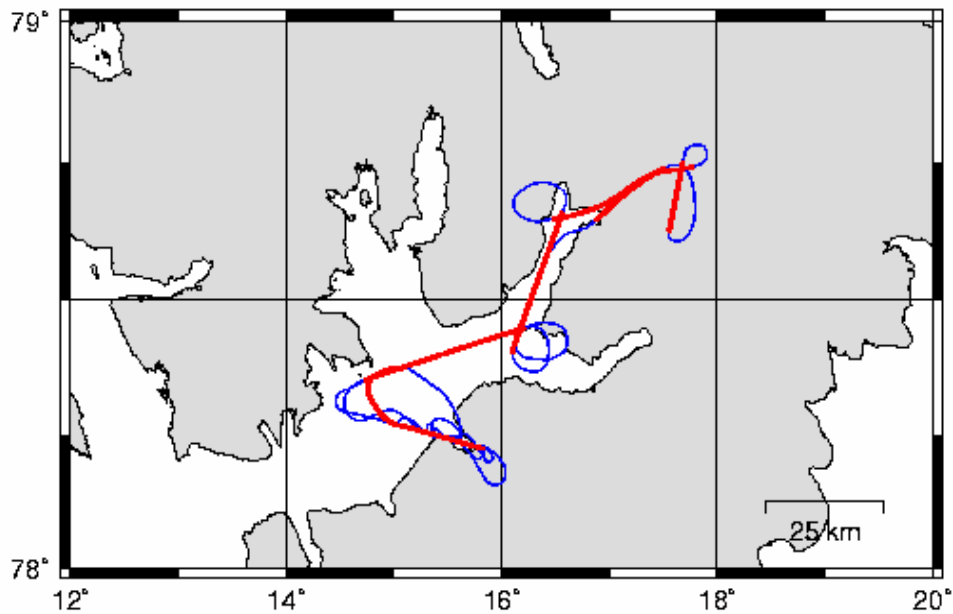
Figure 3.1-1CryoVex 2004A, 19th of April - Map of DGPS (blue) and ASIRAS (red) profiles.

Austfonna Ice Cap CryoVex 2004A – 040420
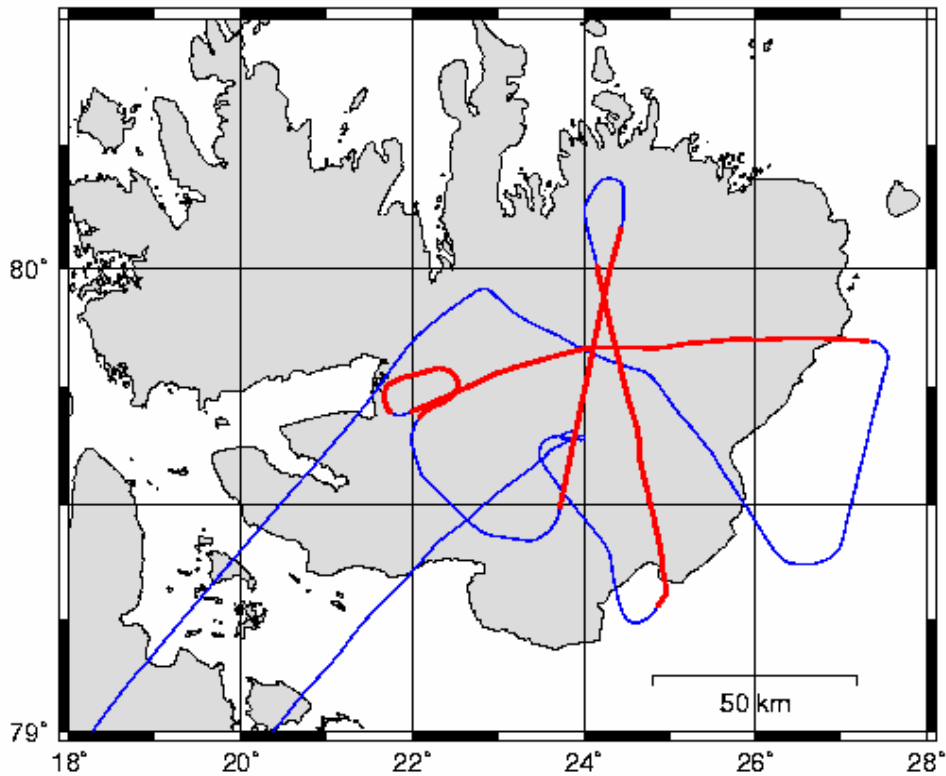
Figure 3.1-2CryoVex 2004A, 20th of April - Map of DGPS (blue) and ASIRAS (red) profiles.

Devon Ice Cap CryoVex 2004A – 040502
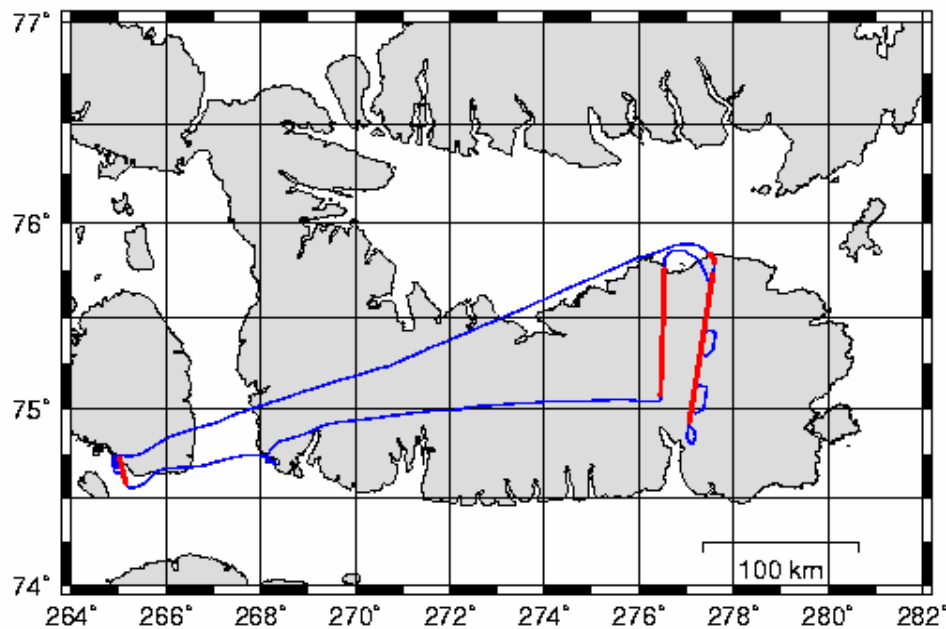
Figure 3.1-3 CryoVex 2004A, 2nd of May - Map of DGPS (blue) and ASIRAS (red) profiles.

Austfonna Ice Cap CryoVex 2004A – 040425
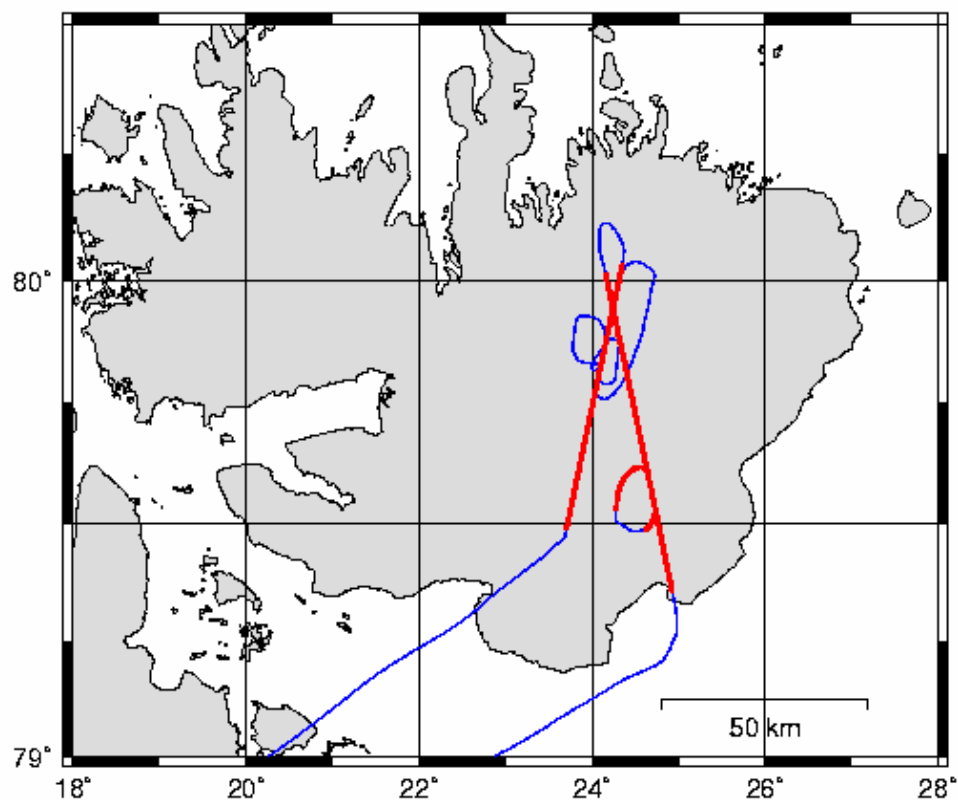
Figure 3.1-4CryoVex 2004A, 25th of April - Map of DGPS (blue) and ASIRAS (red) profiles.

EGIG–line CryoVex 2004A – 040505
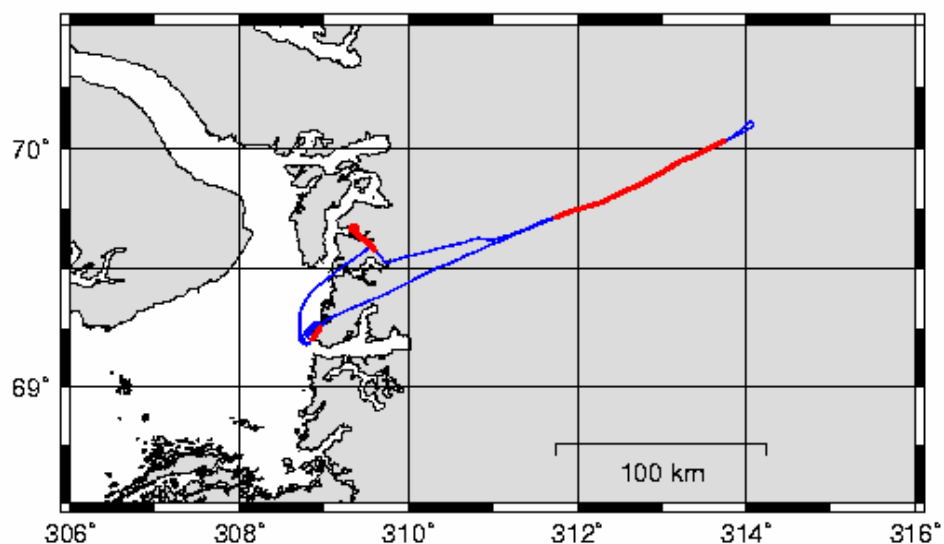
Figure 3.1-5 CryoVex 2004A, 5th of May - Map of DGPS (blue) and ASIRAS (red) profiles.

EGIG–line CryoVex 2004A – 040506
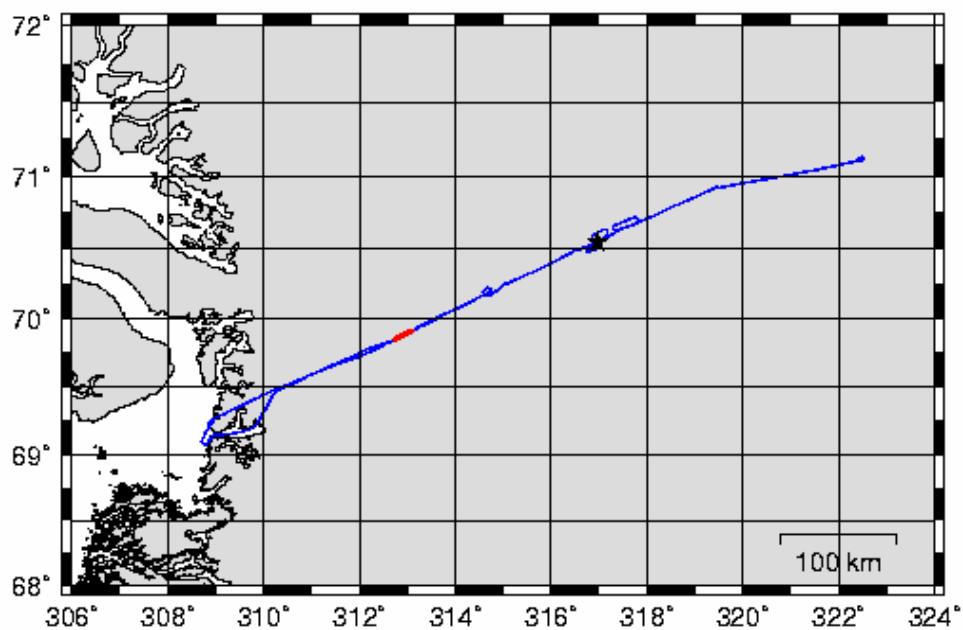
Figure 3.1-6 CryoVex 2004A, 6th of May - Map of DGPS (blue) and ASIRAS (red) profiles.

EGIG–line CryoVex 2004B – 040904
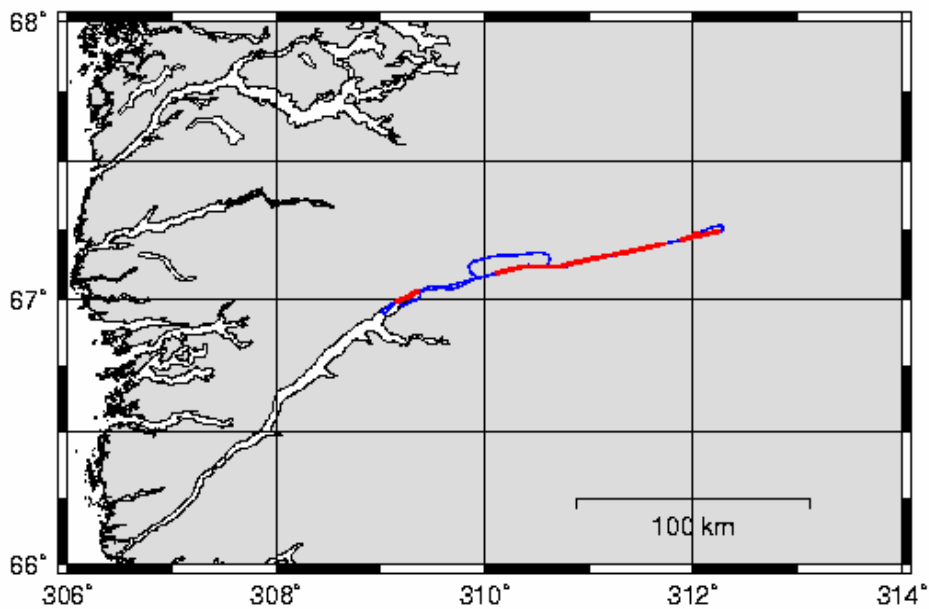
Figure 3.1-7CryoVex 2004B, 4th of Sep. - Map of DGPS (blue) and ASIRAS (red) profiles.

EGIG-line CryoVex 2004B – 040909
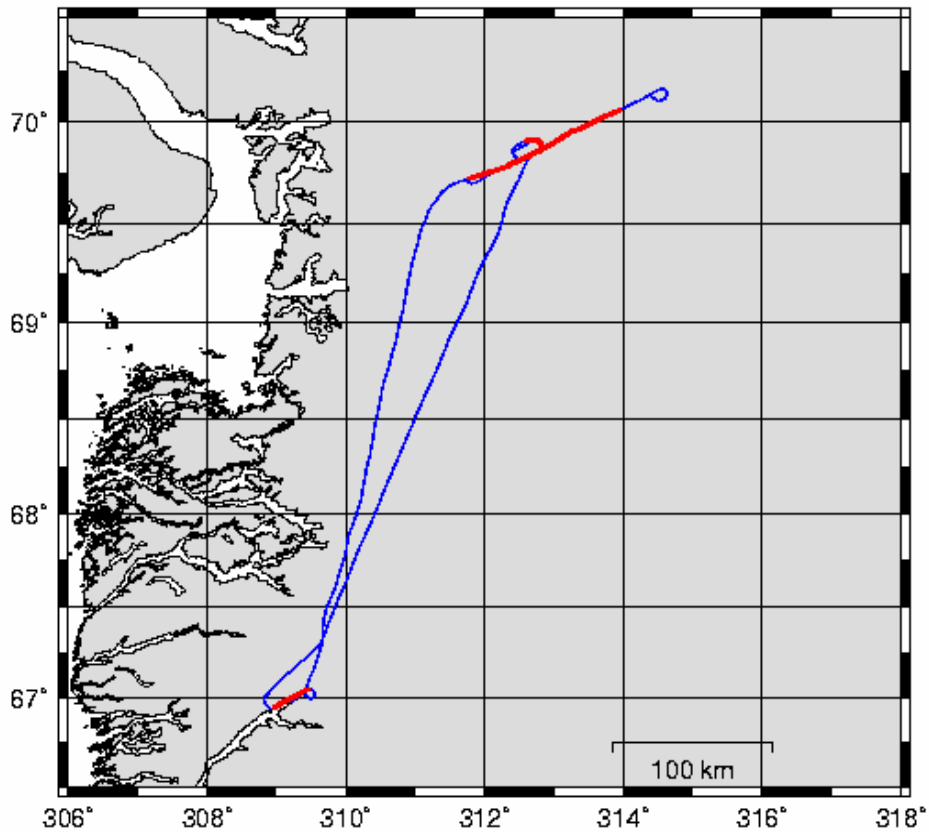
Figure 3.1-8 CryoVex 2004B, 9th of Sep. - Map of DGPS (blue) and ASIRAS (red) profiles.

Devon Ice Cap CryoVex 2004B – 040911
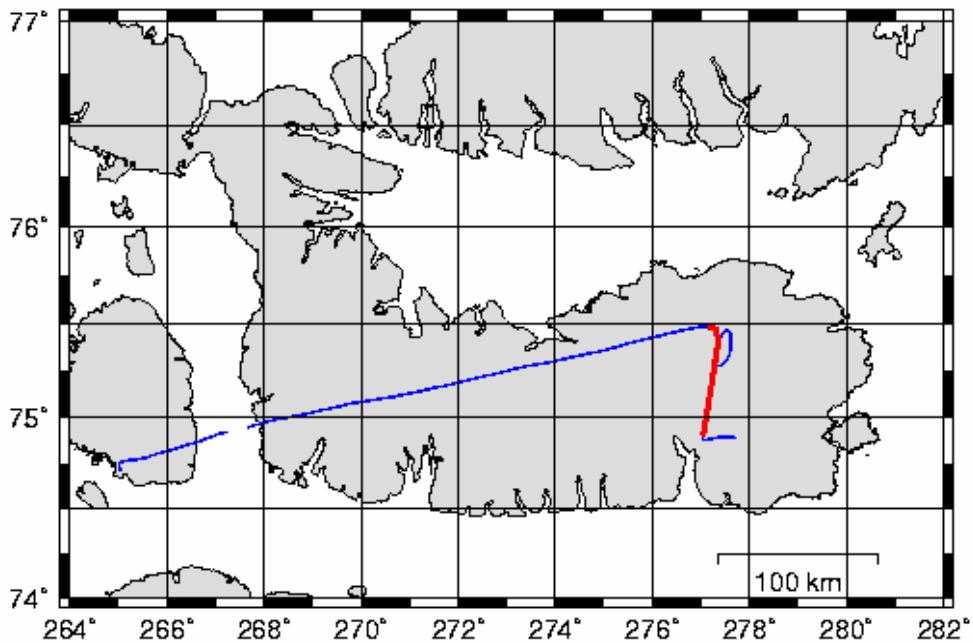
Figure 3.1-9CryoVex 2004B, 11th of Sep. - Map of DGPS (blue) and ASIRAS (red) profiles.

EGIG-line CryoVex 2004B – 040914
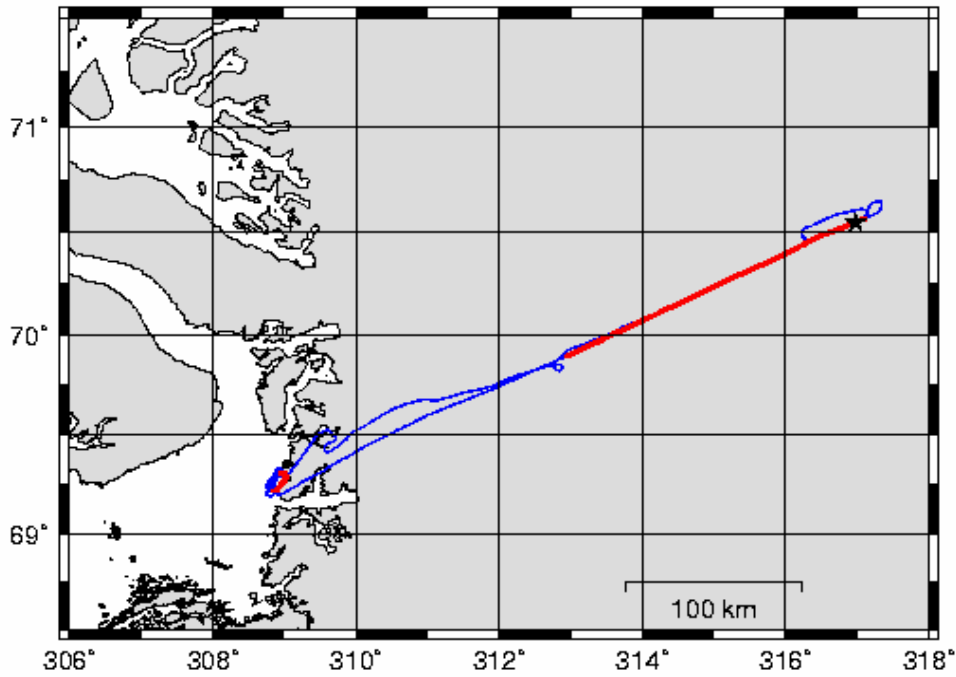
Figure 3.1-10CryoVex2004B, 14th of Sep. - Map of DGPS (blue) and ASIRAS (red) profiles.

EGIG-line CryoVex 2004B – 040917
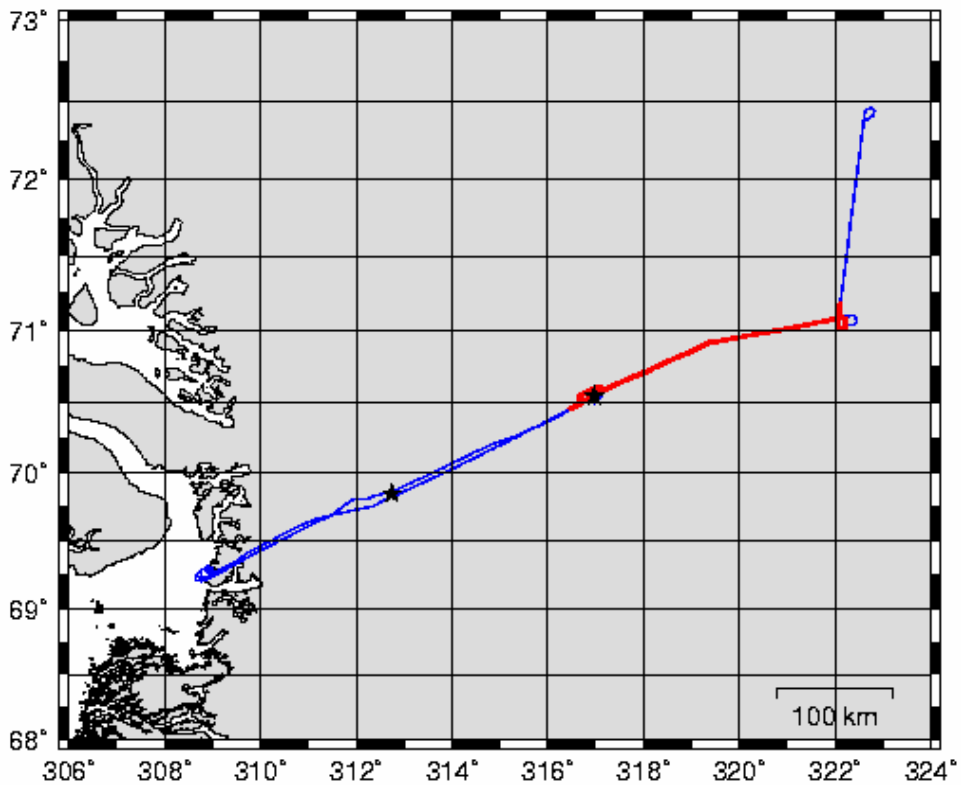
Figure 3.1-11CryoVex2004B, 17th of Sep. - Map of DGPS (blue) and ASIRAS (red) profiles.

4 PART A.2: Bay of Bothnia 2005 Data Aquistion Report

4.1 Measurement Activity

Prior to the measurement campaign in the Bay of Bothnia, an installation and test period of two weeks took place (see Campaign Report ASIRAS 01/05 including Test Report of LAMode by T. Boebel, S. Göbell, Ch. Haas, 2005).

On March 13, 2005 the campaign began with the transfer flight of the equipped D-CODE aircraft from Braunschweig to Stockholm. During the flight from Stockholm to Oulu ASIRAS was switched on for the first time as soon as sea ice was present (Figure 4.1-1). Due to clouds the laser scanning system could only record data at a later stage. The beginning darkness prevented the video camera from further recording. All other systems were operating successfully.

On March 14, 2005 two measurement flights were planned. During the first flight several corner reflectors had been over flown which marked the beginning and end of the validation lines (Figure 4.1-2 and Figure 4.1-3). The validation line between WP1 and WP2 was the same used for ground measurements. The flights were performed in four different altitudes (300 m, 500 m, 700 m, 1130 m). Both validation lines had been over flown twice at the same altitude. Due to a long warm-up of the laser scanning system no laser data could be recorded during the first two turns. Only after the third over flight the system was fully operational. Therefore, the lowest flight altitude was flown a third time at the end to assure a simultaneous recording of laser and ASIRAS radar data. In the following, a runway over flight at the Oulu airport was performed at 500 m. The second flight was the return flight to Stockholm along the same line from the outward flight. At the end roll (up to +- 10°) and pitch experiments (up to +- 5°) were performed. The measurement flight ended one flight hour before Stockholm when open water was reached.

On March 15, 2005 the campaign ended with the transfer flight from Stockholm to Bremerhaven. The very last action included the cross-over flight over the hangar at the airport Luneort in Bremerhaven. This enables a verification of the mounting of the laser scanning system relative to ASIRAS, INS and GPS.

March 13   Location:
Transfer flight to Stockholm
                            Start of recording at ice edge
                            Flying along pre-defined waypoints to Oulu

                            Flight Status:
Scattered clouds at flight altitude
Ice edge reached after 1.5 h flight
Flying into evening and night
Operation of System:
ASIRAS Operation with small hard disc
Video camera switched off because of darkness

Result:
Flight of LAMode successful
Only short recording times due to large data volumes
Harddiscs had to be changed every 60 min

March 14   Location:
                            Measurement flight Oulu near RV ARANDA (finish ice breaker)

                            Flight Status:
System has a long warm up time
Flight over 2 pre-defined validation lines at 4 different altitudes
(3 x 300m, 2 x 500m, 2 x 700m, 2x 1130m, 1x 300m)
Calibration flight over Oulu runway limited to one overpass because of air traffic
Good weather conditions

Operation of System:

No problems with ASIRAS after warm-up
Laser Scanner warm-up ends after the first 3 turns at 300 m, then ok

Result:
Successful recording of data
Successful hitting of corner reflectors

March 14   Location:
                  Measurement flight Oulu to Stockholm

                  Flight Status:
Good weather conditions, some scattered clouds near leads and open sea

Operation of System:
Normal

Result:
Successful flight

March 15   Location:
                  Transfer flight to Bremerhaven
                  Cross-over flights over hangar building at airport Luneort in Bremerhaven

Flight Status:
Moderate weather conditions, some scattered clouds

Operation of System:
Laser Scanner normal
ASIRAS switched off

Result:
Successful calibration flight

Table 4.1-1 ASIRAS, LD90 and ALS Processing on March 13.

Profile	Length (min)	Alt (m)	Comment	Profile	Length (min)	Alt (m)	Comment
8 val2	2.5	320	L1B ok, no LD90 / ALS	18 val2	2.5	691	L1B ok
9 val1	2.5	320	L1B ok, no ALS	19 val1	2.5	690	L1B ok
10 val2	2.5	321	L1B ok, no ALS	20 val2	2.5	689	L1B ok
11 val1	2.5	320	L1B ok, no ALS	21 val1	2.5	1062	L1B ok, no LD90
12 val2	2.5	294	L1B ok, no ALS	22 val2	2.5	1061	L1B ok, no LD90
13 val1	2.5	511	L1B ok, no ALS	23 val1	2.5	1061	L1B ok, no LD90
14 val2	2.5	506	L1B ok, no ALS	24 val2	2.5	1062	L1B ok, no LD90
15 val1	2.5	506	L1B ok	25 val1	2.5	311	L1B failed
16 val2	2.5	507	L1B ok	26 val2	2.5	325	L1B failed
17 val1	2.5	690	L1B ok	27 val1	2.5	326	L1B ok

Table 4.1-2 ASIRAS, LD90 and ALS Processing on March 14

Profile	Length (min)	Alt (m)	Comment	Profile	Length (min)	Alt (m)	Comment
7 val2	18	498	L1B ok, no ALS	30 val2	2	538	L1B ok
8 val1	35	508	L1B ok	31 val1	8	540	L1B ok
9 val2	25	514	L1B ok	32 val2	2	544	L1B ok
10 val1	9	513	L1B ok	33 val1	8	546	L1B ok
				34 val2	42	550	L1B ok
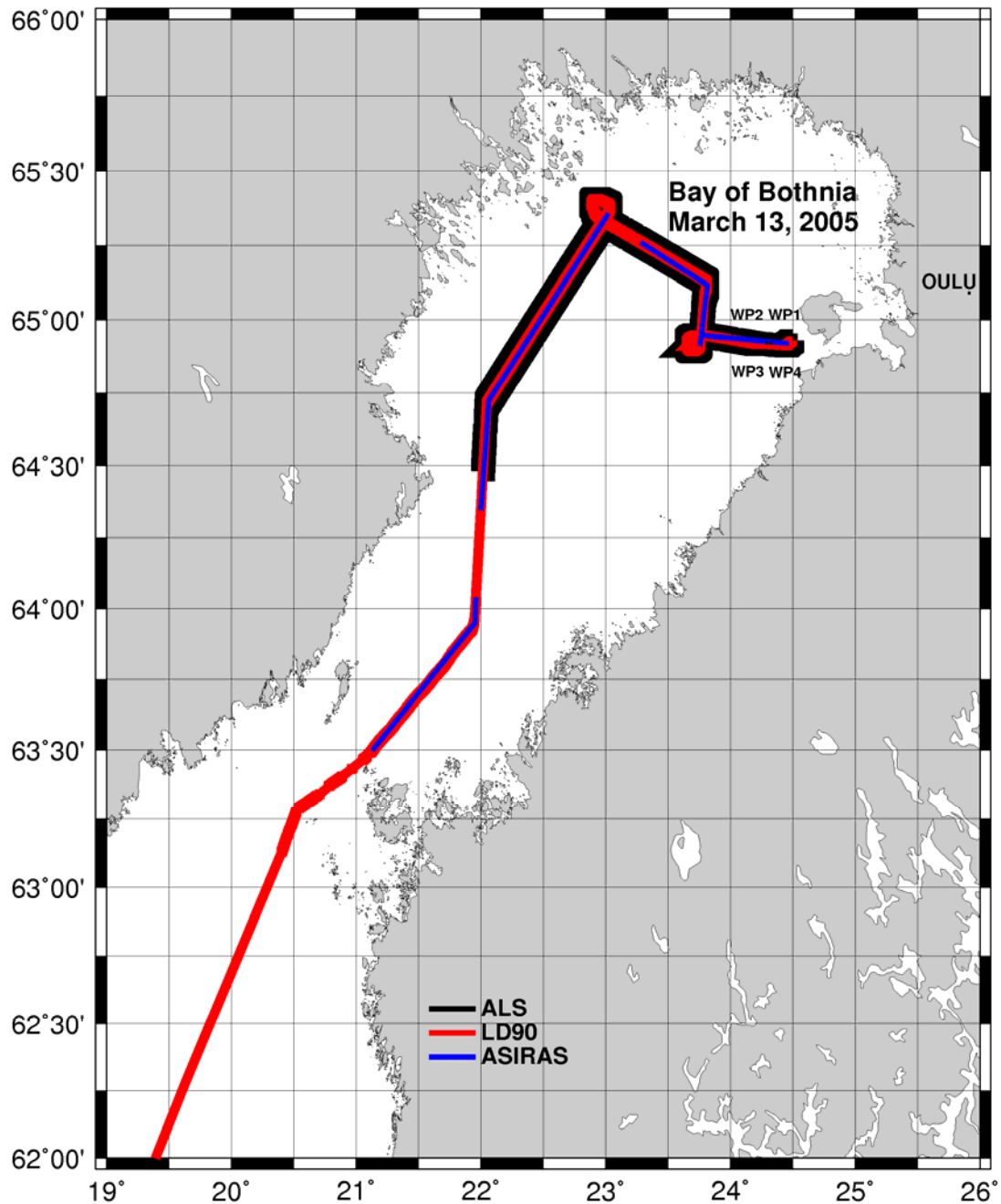
Figure 4.1-1 Measurement flight with operation periods of LD90 and ASIRAS on March 13
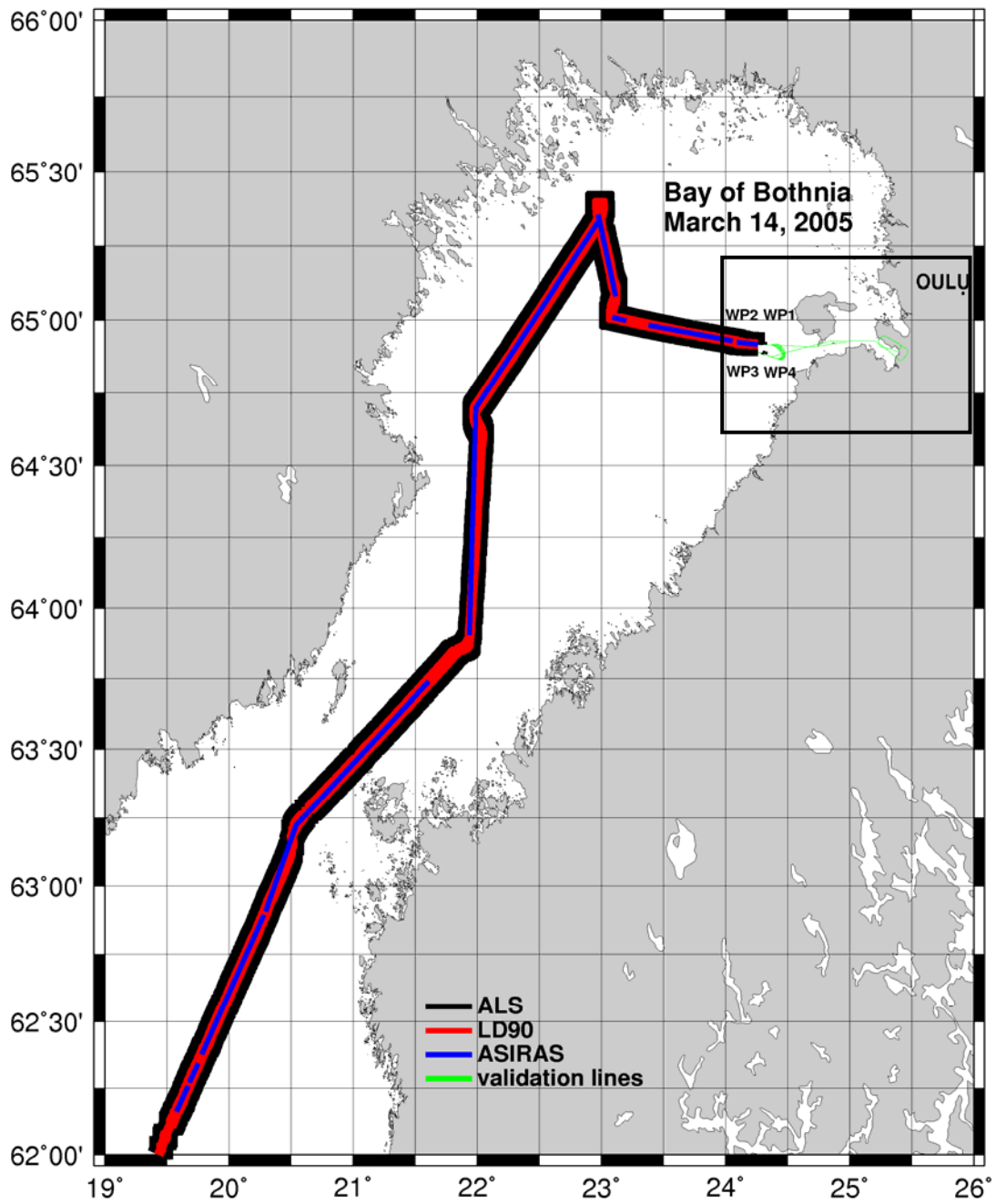
Figure 4.1-2Measurement flight with operation periods of LD90 and ASIRAS on March 14 .
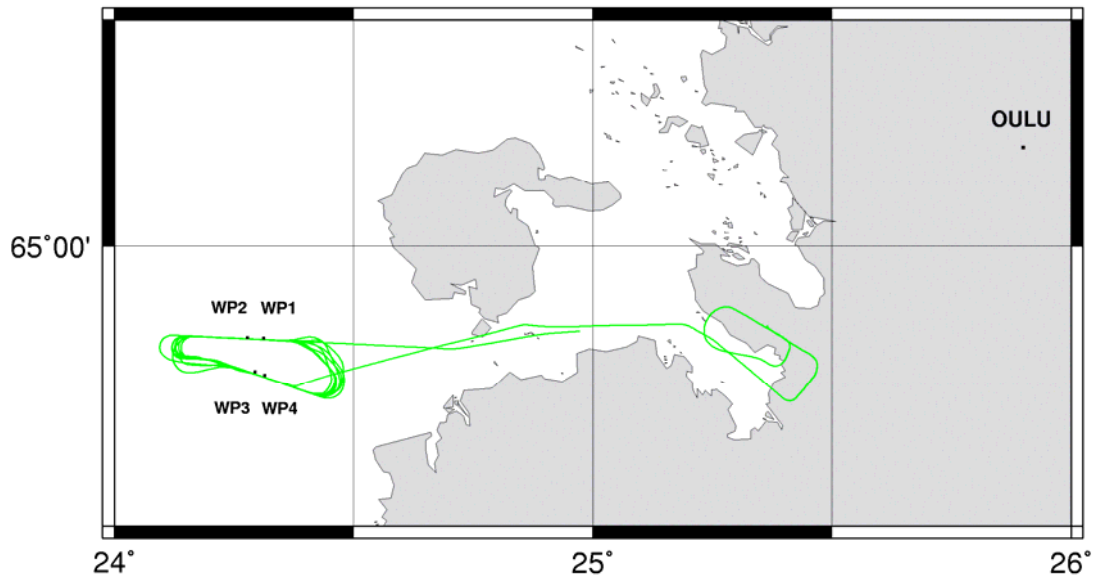
Figure 4.1-3 : Measurement flight over the validation lines from WP1 to WP2 and WP3 to WP4 and runway over flight on March 14.

Table 4.1-3 Flight activity of Bay of Bothnia 2005 by day and UTC time

Date	Location	ASIRAS tracks	Start (UTC)	Stop (UTC)	Airborne
March 13	transfer	-	-	-	2 h 40 min
March 13	Stockholm-Oulu	A050313_07 – A050313_10	16:27:59	18:07:56	3 h 30 min
March 14	Oulu	A050314_09 – A050314_27	12:06:58	13:47:06	1 h 57 min
March 14	Oulu – Stockholm	A050314_30 – A050314_38	15:29:05	17:32:28	3 h 11 min
March 15	transfer	-	-	-	2 h 40 min
March 15	Bremerhaven	laser scanner	11:56:23	12:16:40	30 min

5 Part B.1: Final CryoVex 2004 processing report

5.1 Overview and Introduction

For calibration and validation of ASIRAS a precise digital elevation model (DEM) of the measured profiles is required. This DEM is calculated from the Airborne Laser Scanner (ALS) data, which is measured with the Riegl – LMSQ80 instrument. The reference DEM (ALS-DEM) is calculated on a 1x1 m grid using a trigrid delauny triangulation.

After DGPS and ALS standard processing, it is necessary to calibrate the ALS system. This includes corrections for possible time shifts and inevitable installation inaccuracies (squint angles) in the aircraft. This procedure is required for every device.

After applying these corrections to the ALS and the Single Beam Laser (LD90) the calibration of the ASIRAS with the ALS-DEM is possible. For calibrating the ASIRAS and LD90 a couple of runway over flights were flown. Detailed ASIRAS processing and product information see in [R.1].
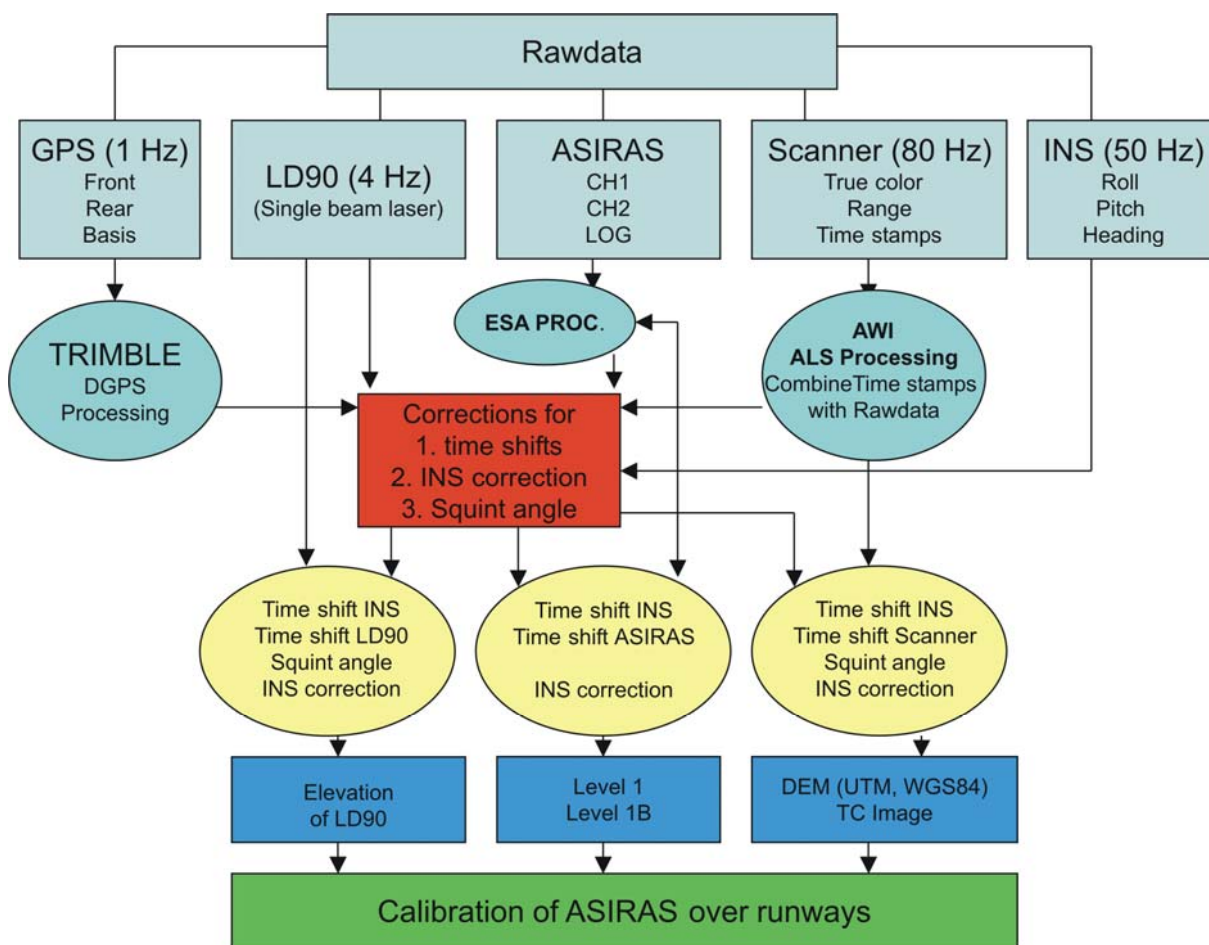
Figure 5.1-1 Processing flow of the calibration and validation of ASIRAS

The flow chart in Figure 5.1-1 shows the content of the whole processing scheme. In the following sections two main tasks are of special importance:

Determination of device dependent timeshifts
Determination of squint angles of ALS (airborne laser scanner) and LD90 (single beam laser)

Both depend on each other and are used in the determination of the correction values using a Newton approximation. The obtained values are used as correction constants in the processing flow. In Table 5.8-1 and Table 5.8-2 the results for both campaigns are listed. The campaign solutions are variable which has to be considered when comparing results.

5.2 DGPS data processing

Kinematic GPS is the key positioning method for the aircraft. GPS data were logged at 1 Hz using a reference ground receiver and 2 aircraft receivers (see PartA). The aircraft GPS receivers are named *airf* (front antenna) and *airr* (rear antenna). All GPS data were processed at AWI using Trimble Geomatic Office Software and precise ephemeredes.

First step of GPS processing was computing the reference positions of the GPS reference ground stations relative to IGS international network. This ensures that GPS coordinates are consistent with the global IGS coordinate system at an accuracy level of a few cm. The used ITRF basis stations and claculated GPS ground station reference coordinates are listed in Table 5.2-1 and Table 5.2-2.

Table 5.2-1 CryoVex2004A, GPS reference stations

Day	ITRF reference station	Ground station	Latitude	Longitude	Height (WGS84) in [m]	RMS in [m]
April 19	NYAL	Longyearbyen	78,246941078 N	15,490947926 E	64,53131	0,022
April 20	NYAL	Longyearbyen	78,246941054 N	15,490948263 E	64,50853	0,010
April 25	NYAL	Longyearbyen	78,246943200 N	15,490950170 E	64,65481	0,043
May 02	RESO	Resolute	74,718792996 N	94,986931302 W	62,30963	0,018
May 05	THU3	Ilulissat	69,240379632 N	51,065740216 W	59,03862	0,015
May 06	THU3	Ilulissat	69,240379710 N	51,065740548 W	58,97577	0,010

Table 5.2-2 CryoVex2004B, GPS reference stations

Day	ITRF reference station	Ground station	Latitude	Longitude	Height (WGS84) in [m]	RMS in [m]
Aug 30		Bremerhaven				
Sep 04	THU2	Kangerlussuaq	67,00924758 N	50,688730744 W	78,19316	0,008
Sep 09	KELY	Kangerlussuaq	67,00924832 N	50,688731743 W	78,20513	0,010
Sep 11	EURK	Eureka	79,988538479°N	85,939888870°W	29,71959	
Sep 14	THU2	Ilulissat	69,240379024 N	51,065740541 W	59,22907	0,018
Sep 16		Ilulissat				
Sep 17	THU3	Ilulissat	69,240379105 N	51,065740639 W	59,25281	0,020

The second step is computing DGPS solutions for the aircraft antennas. This was done on a single baseline basis to available reference stations using the Trimble software. These solutions are generally estimated to be accurate to the 10-40 cm rms level. The accuracy is dependent on the distance from the reference station to the aircraft (baseline) and on the number of satellites and their geometry. The number of satellites was usually quite high, often around 8-10, with some limited periods with fewer satellites.

5.2.1 DGPS – ground stations CryoVex 2004A

GPS ground stations:

Parallel to all measuring flights a Trimble 4000SSI ground station was installed. Data were recorded with the GPS receiver and downloaded with the program GPLOAD 2.75 after landing.

Figure 5.2-1 Longyearbyen: DGPS ground station, antenna on the roof of the hangar building. Receiver was installed in a separate room of the hangar. Data was named with LYR.

Figure 5.2-2 Resolute: DGPS ground station, antenna on top of the construction building (ca. 3 m above the runway) Receiver was powered by 110 V and was installed in the construction building. Data was named with RESU

Figure 5.2-3 Ilulissat: DGPS ground station, antenna was installed on top of the fire ladder at the tower. Data was named ILLU.

5.2.2 GPS – ground stations CryoVex2004B

GPS ground stations:

Parallel to all measuring flights a Trimble 4000SSI ground station was installed. Data were recorded with the GPS receiver and downloaded with the program GPLOAD 2.75 after landing.

Kangerlussuaq: Antenna was installed on top of the KISS building.
The antenna was established twice. Therefore the reference coordinates of the first test flights and the first profile are different. Data was named with KANG.

Figure 5.2-4 Kangerlussuaq: DGPS ground station.

Resolute:
Station could not be established. Ground reference data has to be bought by a special provider.

Ilulissat:
Antenna was situated on top of the fire ladder at the tower. Data were named with ILLU.
Same Picture as in CryoVex 2004A.

5.3 ALS standard data processing

Laser scanner (RIEGL – LMSQ80) data were recorded in both campaigns, in most cases in low and a high altitude, respectively.
The ALS laser scanner data were logged in binary files during flights. Pairs of size limited files were created (trigdata and rawdata). The rawdata includes range, beam angle, quality, true color and internal time stamp information whereas the trigdata file includes the PPS trigger pulses of the Trimble GPS receiver and therefore the time information.
During ALS standard processing the rawdata line timestamps are combined with the trigdata UTC time information see section 5.3 for more precise description of the ALS time concept).
While checking the data quality, which in overall is very good, AWI discovered several bugs in the rawdata file of the scanner. Table 5.3-1 addresses the errors and their correction.

> Note:
> Every scan line includes next to the timestamp of every single shot a syncounter. This counter counts the PPS trigger pulses. Every time a synccounter is set, the timestamp will be reset to zero. In normal case the line timestamp which is additional information should be the same as the first shot time in the scan.

Table 5.3-1 ALS raw data bugs and their solution

Problem	Solution
Time within a single beam is sometimes not steadily increasing. Jumps of single shots are possible. The amplitude of the jumps is not constant and is varying between microsec and deca seconds.	Creating steadily increasing shot times within a beam with a constant time difference of 55 micsec (median value). First shot is the original line timestamp.
Time of the first shot in a scan is sometimes unequal to the line time stamp.	Needs no correction because the line time stamp is used.
Time of line timestamp is sometimes not correct.	Line timestamp is reset by the mean of the value before and the value after the occurring error, or is reset by the 1st laser shot time in the corresponding scan line.
The number of synccounters is sometimes not equal to the number of trigger pulses	File is cutted after reaching the minimum of both values.
Reset of time is sometimes not corresponding with the synccounter information – this leads to a wrong sorting of the trigger pulse time.	A procedure will detect those errors and then sort the reset to the corresponding line where the syncounter took place.
The trigger pulse which should be close to 1 sec is varying within millisec – this can also lead to a decreasing time after combining trigger pulse and laser shot time.	Trigger time is set to 1 sec as long as true trigger time is not matching the 1 sec trigger time.
Beam angle is not always within the range of –22.5° to +22.5°. Jumps are up to 20°.	Jumps are detected and reset by the median value of the corresponding beam angle.

Table 5.3-2 Processed ALS data (CryoVex2004A) including start – stop time.

Day	File number	Number of Scans with trigdata info	Number of trigger pulse corrections	Bad trigger data quality in [%]	Start time In seconds of the day	Stop time In seconds of the day
040419	1	729340	544	6,22	54870	63609
040420	1	1092337	697	5,33	56505	69576
040425	1	75109	49	5,31	30892	31790
040502	1	203076	163	6,65	68619	71066
040502	2	638834	519	6,71	71292	79023
040505	1	668779	698	8,68	65320	73365
040506	1	71540	58	6,73	45900	46764
040506	2	757918	9106	99,76	47551	56685
040506	3	431932	378	7,22	56955	62184

Table 5.3-3 Processed ALS data (CryoVex2004B) including start – stop time.

Day	File number	Number of Scans with trigdata info	Number of trigger pulse corrections	Bad trigger data quality in [%]	Start time In seconds of the day	Stop time In seconds of the day
040904	1	409109	435	8,67	44387	49400
040909	1	966956	1097	9,21	53445	65353
040909	2	208840	154	6,00	65358	67922
040911	1	301852	304	8,32	62011	65661
040914	1	968819	832	7,00	53280	65160
040914	2	152914	202	10,77	65165	67037
040917	1	974457	823	6,95	47386	59233
040917	2	604969	547	7,39	59237	66639

5.4 Concept for the correction of time shifts

In section 2.3 the time concept of the measuring system was introduced. Here we have to consider the possibility of time biases between the individual instruments. This is because of an undependent developement of each instrument and their common usage within the CryoVex campaigns. The time stamp for every single data packet is first given when registered at the Medusa_P server (valid for LD90 and INS).

ASIRAS and ALS following own time concepts. Therefore comparisons between all devices need a common basis which is the DGPS UTC time stamp. If all time biases are known and corrected the system is consistent and therefore a comparison between the instruments within the system can be carried out. In the following sub sections we explain in short words how the time bias with respect to the DGPS UTC time of every single instrument was determined.

Timeshifts between DGPS and INS
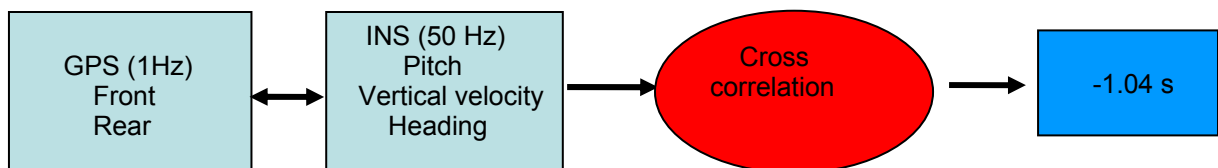
The time delay between DGPS (1 Hz) and INS (50 Hz) is calculated by a cross correlation. Three measured INS parameters (pitch, vertical velocity and heading) are correlated with the equivalent value calculated out of the resampled DGPS data. We split the whole profile within parts, determined the rate of change of the parameters and calculated the cross correlation. Median of the time biases determined from the maximum CC value of each part yields to the final solution for the whole profile. Table 5.8-1 and Table 5.8-2 presenting the results for both campaigns. We decided to take -1,04 s as the overall timeshift for the whole campaign because the altimeter data is most sensitive to the pitch.
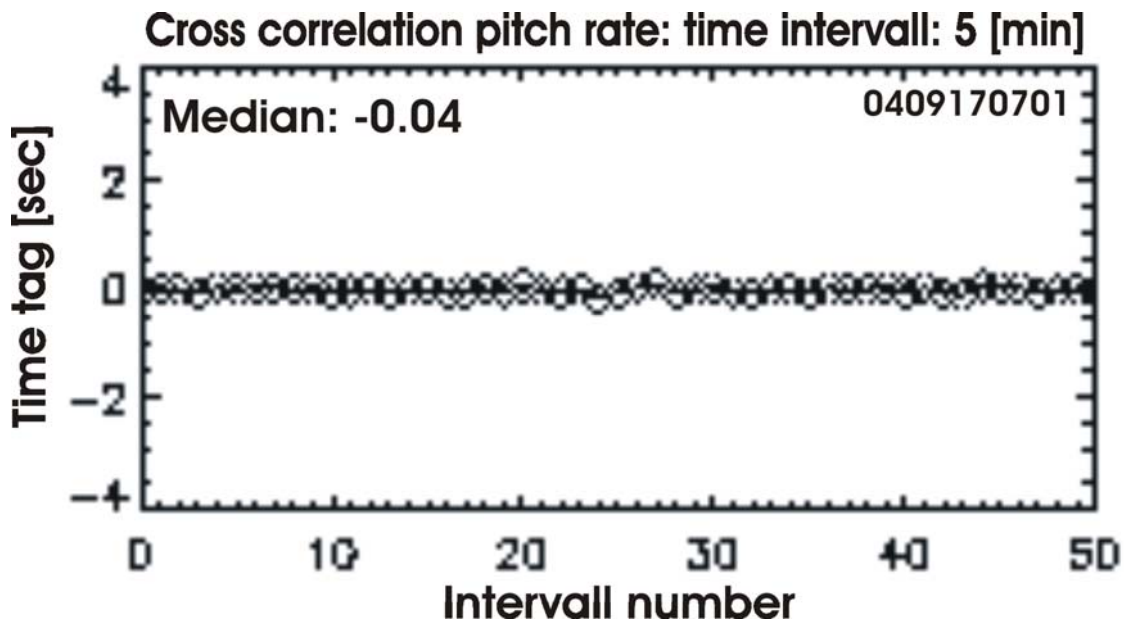
Figure 5.4-1 Results of cross correlation of the pitch rate at 17th of September 2004. INS was formerly shifted by -1.0 s to get better correlation results. Overall time shift is therefore -1.04 s.

Timeshift between DGPS and ALS
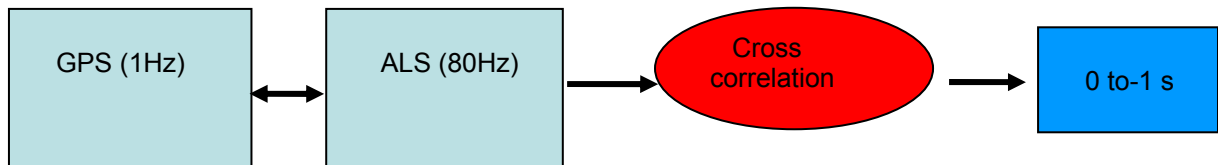
The timeshift between DGPS (1 Hz) and ALS (80 Hz) is calculated similar to the INS time shift. The rate of change of the measured ALS – center beam range is cross correlated with the rate of change of the DGPS altiude after resampling the GPS data to 80 Hz and split the profile into parts. Results are not consistent for the whole camapign and has to be applied for every single ALS profile.

Timeshift between DGPS and LD90 and DGPS and ASIRAS
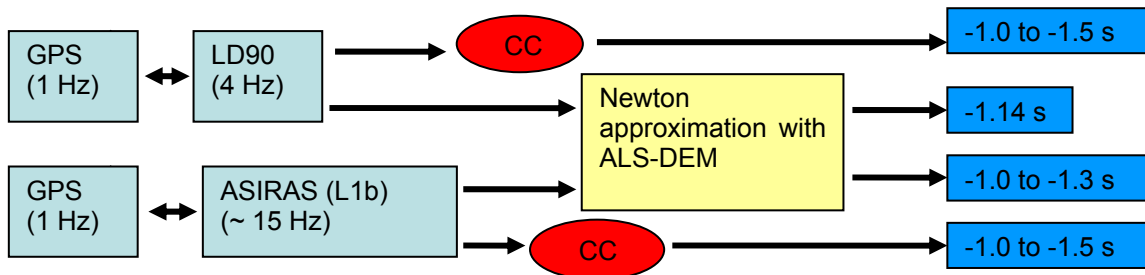
Two methods are used for the determination of the timeshifts between DGPS and ASIRAS and DGPS and LD90. First we are using the same technique by calculating the cross correlation which is described in the last sub section. Both the timeshift for LD90 and ASIRAS are not consistent within a measuring day and showing high uncertainties. Therefore a second method was developed, which is much more time consuming than the cross correlation method. The idea behind is to compare time segments of high quality range measurements for every single profile with the ALS-DEM. The ALS-DEM needs to be corrected for the ALS time shift and the ALS squint angle (see section 1.1) before using in the comparison. A newton approximation computes the closest approach of the ALS-DEM and the LD90/ASIRAS profile segment by changing the timeshift. Results are presented in Table 5.8-11 and Table 5.8-12. The LD90 timeshift is constant over a whole campaign, whereas a different ASIRAS timeshift has to be applied for every single profile. In some cases the data quality of ASIRAS was very weak and no timeshift could be determined. These profiles are corrected with -1.0 s.
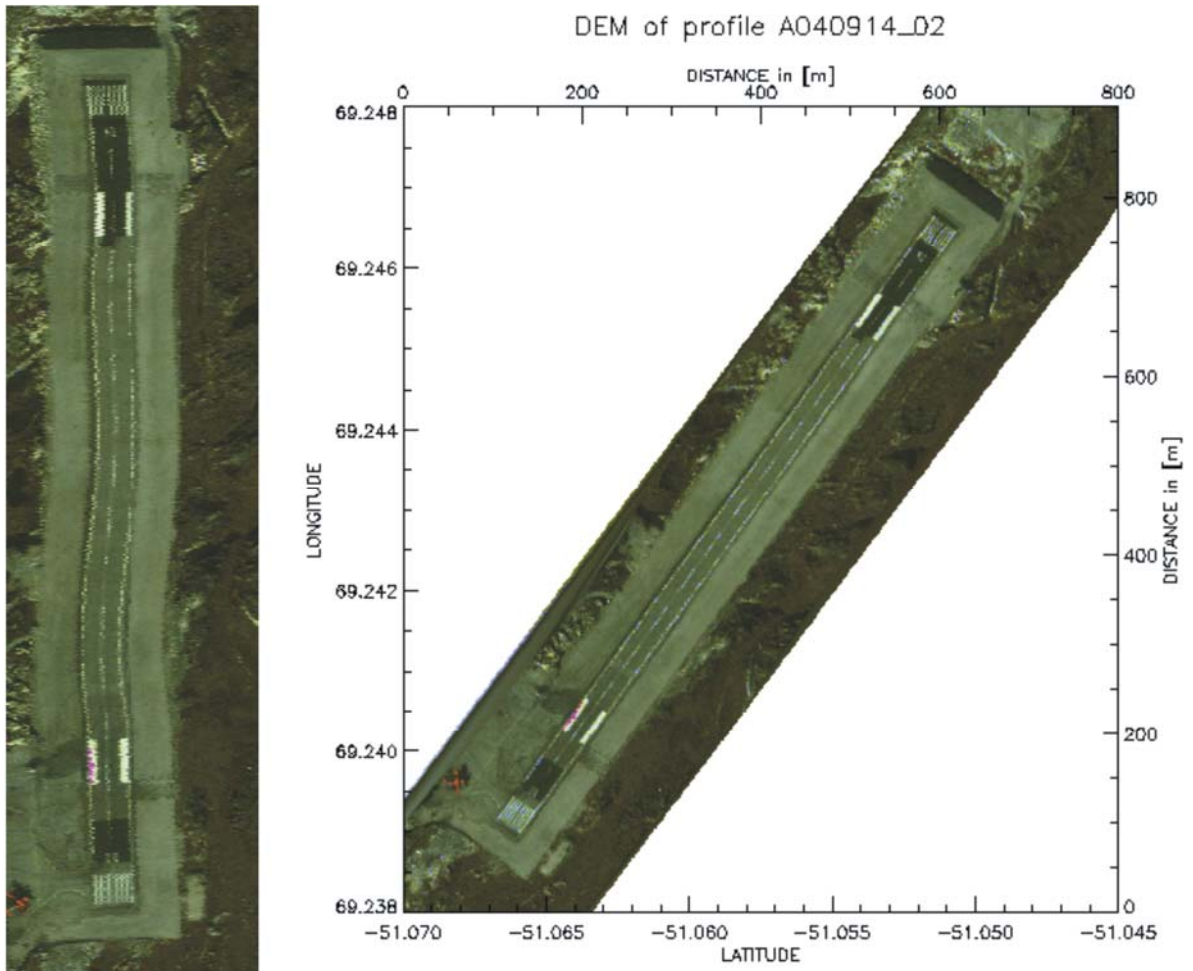
Figure 5.4-2 Runway Ilulissat before and after time shift correction. Map projection is UTM with respect to WGS 84.

5.5 Determination of Laser squinting angles

The laser scanner and LD90 have an inherent unknown orientation when installed in the aircraft. These squinting angles are determined by following the method shown in Figure 5.5-1.
Edge points of a hangar building obtained twice in two cross flights are compared. A least square Newton approximation is used when computing the ALS squint angles.
LD90 squint angles are calculated similar as LD90 time shifts while comparing a ALS-DEM (corrected by time shift and squint) with part of a LD90 profile.
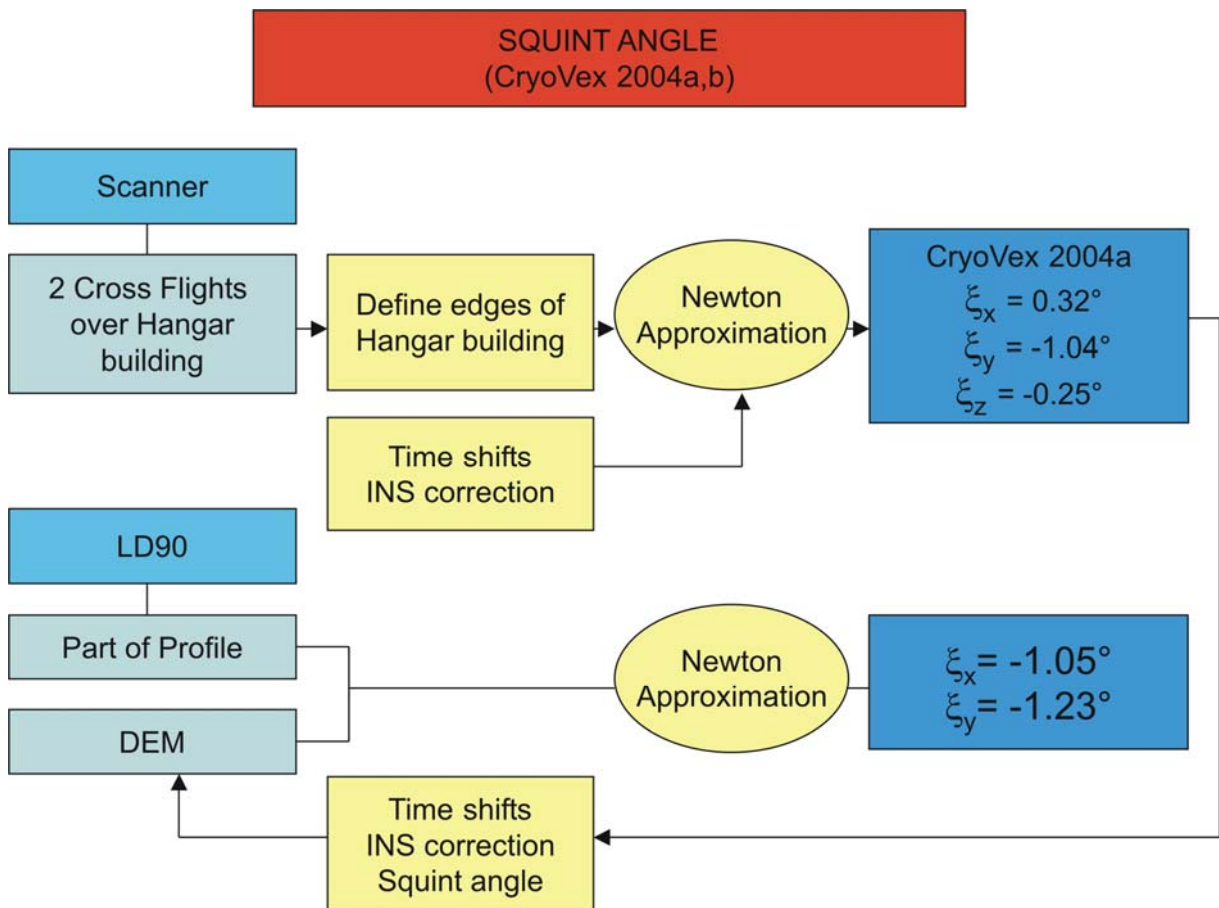
Figure 5.5-1 Concept to determine squint angles
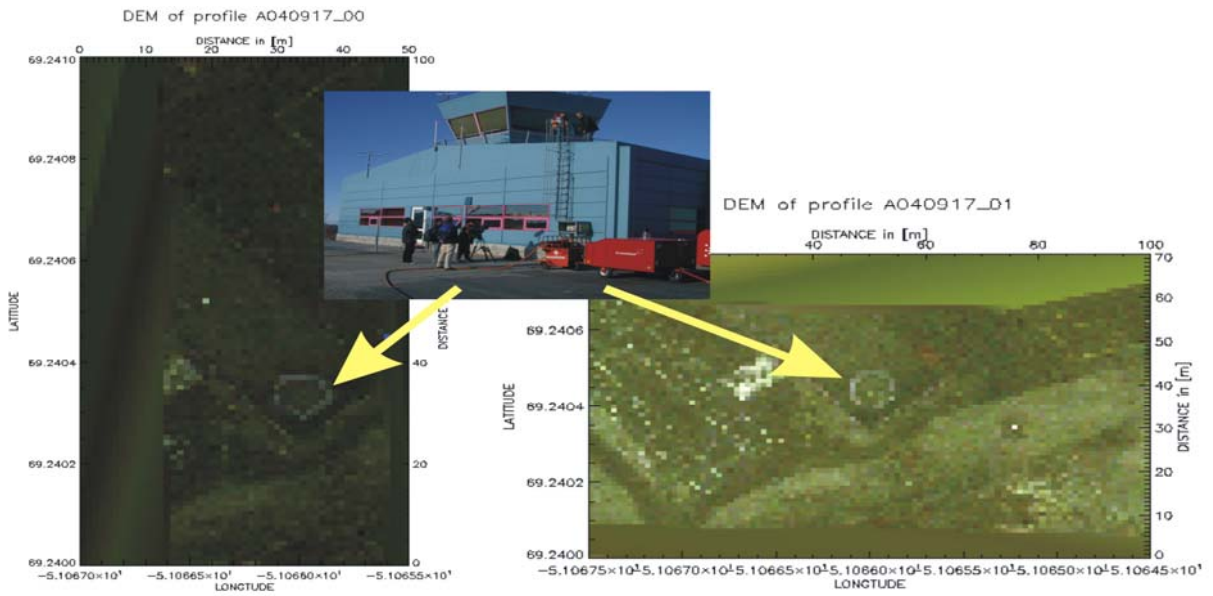
Figure 5.5-2 True color image of hangar building Ilulissat. Yellow arrows pointing towards the tower.
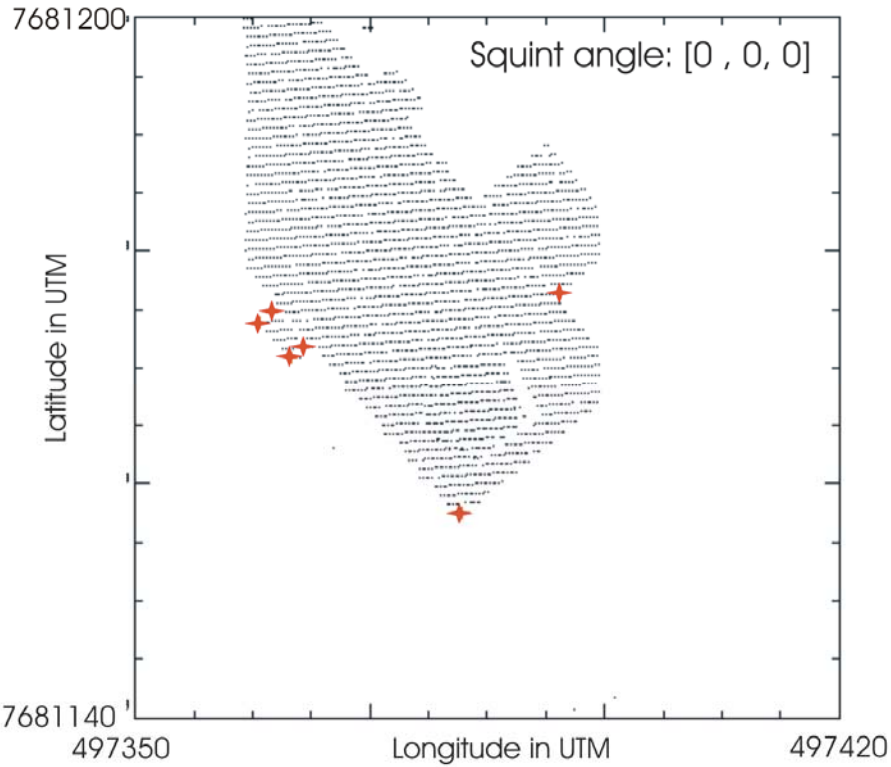
Figure 5.5-3 Determine the edges of the hangar building – cross flight 1.
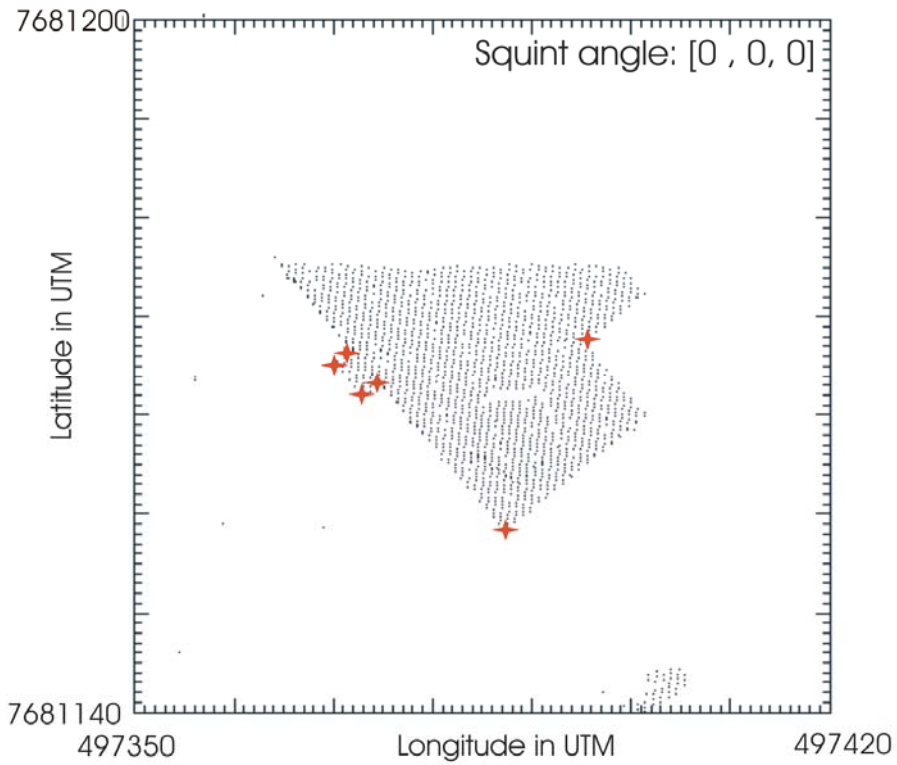
Figure 5.5-4 Determine the edges of the hangar building – cross flight 2
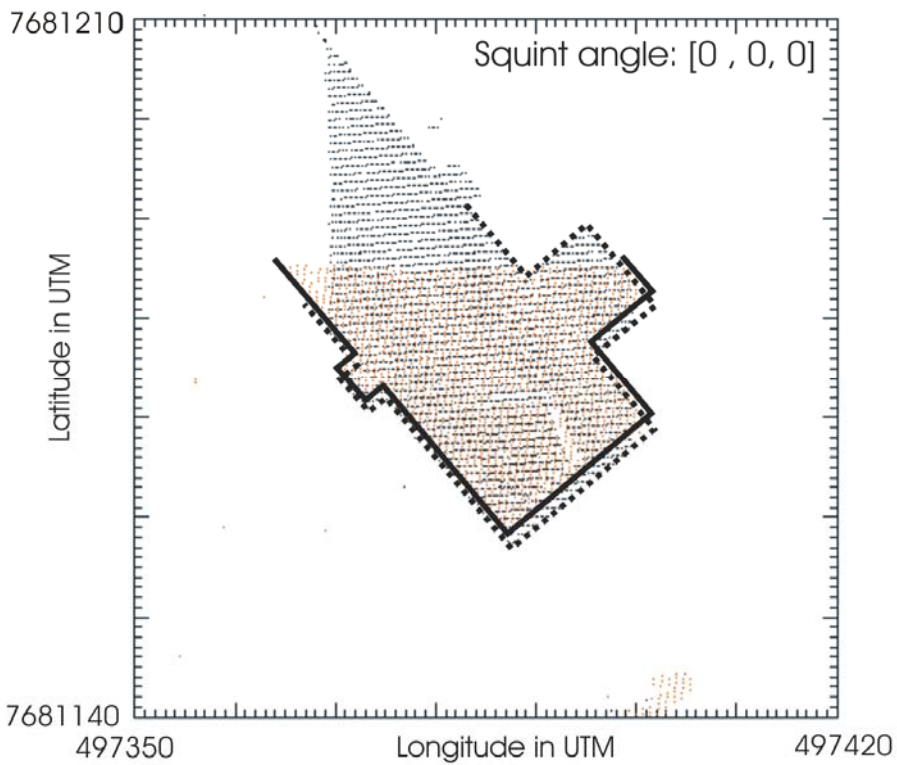
Figure 5.5-5 Hangar building before squint angle correction
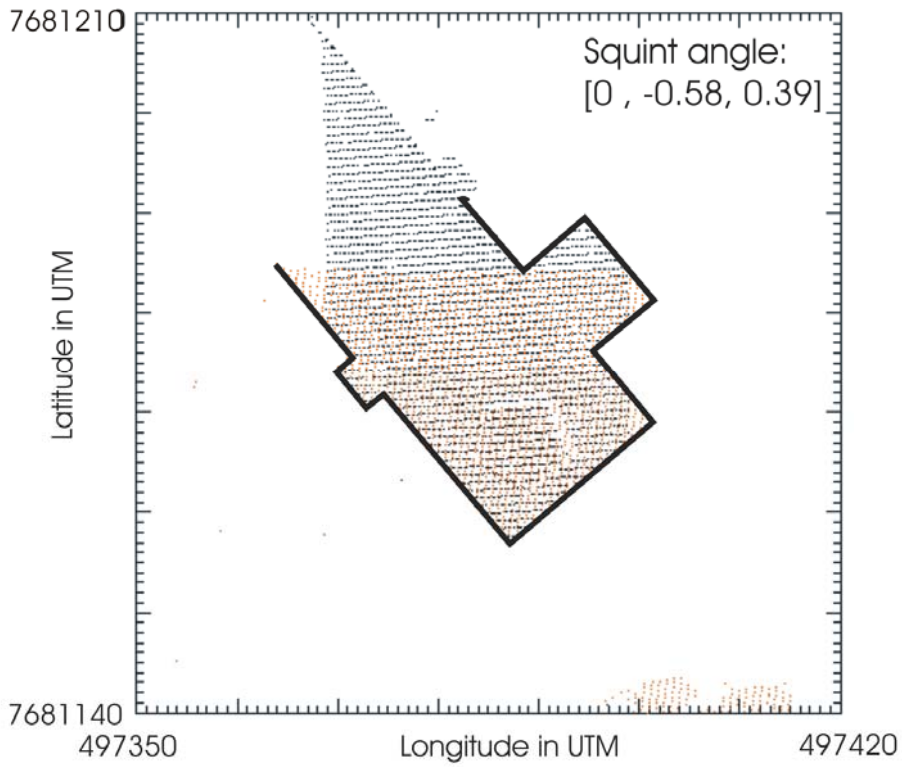
Figure 5.5-6 Hangar building after squint angle correction
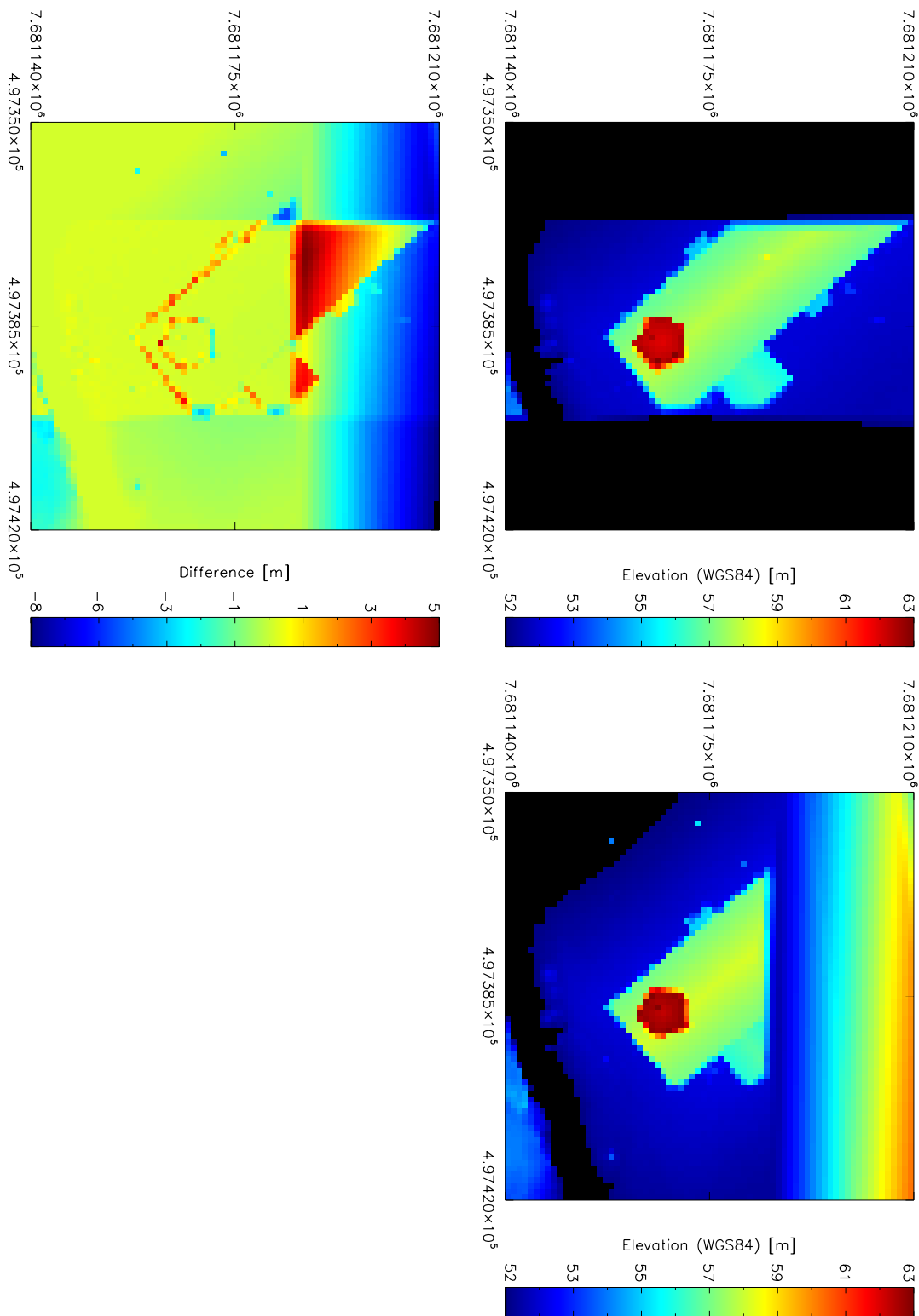
Figure 5.5-7 CryoVex2004B ALS-DEM images of the runway over flights at 17th Sep. 2004. Left figure presents the difference between both ALS-DEM's after application of squint angle correction.
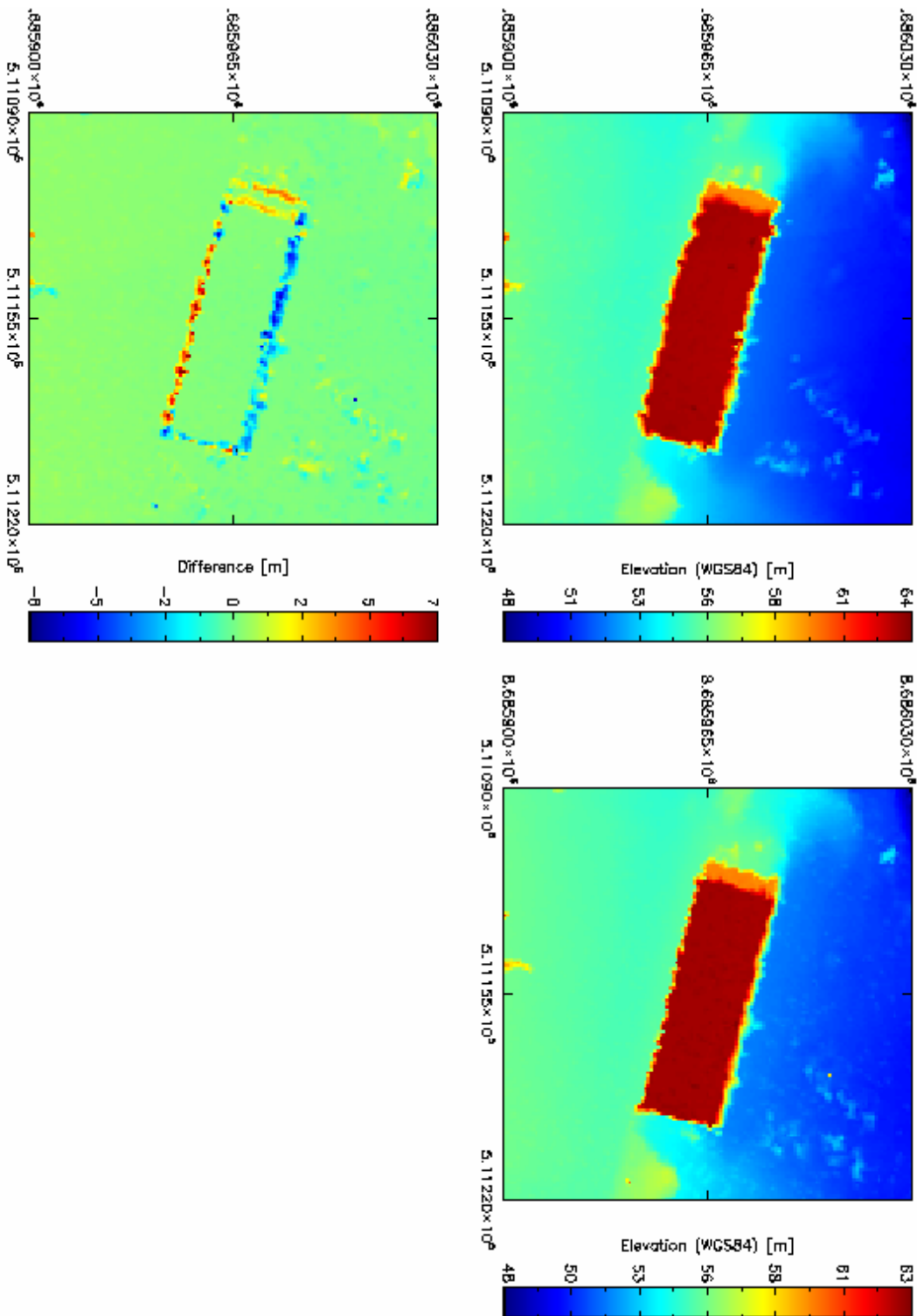
Figure 5.5-8 CryoVex2004A ALS-DEM images of the runway over flights at 2nd of May 2004. Left figure presents the difference between both ALS-DEM's after application of squint angle correction.

5.6 INS Correction

Implementation of the aircraft attitude correction (roll, pitch and heading) with respect to the instrument reference points in the aircraft mechanical reference frame (AMR) is one major point in processing ASIRAS, ALS and LD90 data. A detailed description for ESA's ASIRAS processor is included [R.1].
AWI is using a similar procedure which is described in the following sections. We copied great parts of [R.1] and added some minor points.
In general instrument positions are defined in the aircraft mechanical reference frame (AMR). In this frame, range measurements taking place. As a result we are interested in the position of the ground reflection point within an global earth fixed geodetic reference frame (GEF). Therefore a transformation from the AMR to GEF is necessary which considers attitude behavior of the aircraft, instrument positions defined in the AMR (see section 2.1) and a reference ellipsoid (WGS-84).
First we will define all reference frames used in the calculation and then we describe stepwise the determination of AMR origin in the GEF (section 5.6.11) and surface reflection points in the GEF (sections 5.6.11 and 5.6.12).

5.6.1 World Geodetic System (WGS-84)

Ellipsoidal parameters for the WGS-84 are:

Semi major axis, $a_e = 6378137.0$ metres

Semi minor axis, $b_e = 6356752.3142755$ metres

Eccentricity:

$$e = \frac{\left(a_e^2 - b_e^2\right)}{a_e^2}$$

Equation 5.6-1

Ellipsoidal flattening:

$$f = 1 - \sqrt{1-e}$$

Equation 5.6-2

East-West curvature:

$$\nu = \frac{a_e}{\sqrt{1 - e \cdot \sin^2(\phi)}}$$

Equation 5.6-3

,where ϕ is the geodetic latitude.

GPS, ASIRAS Level 1 and Level 1b, Scanner Level_L1B and processed LD90 positions are all described within this reference frame.

5.6.2 Global Earth Fixed Frame (GEF)

The GEF is related to the ITRF and WGS-84 and is used for processing ASIRAS, LD90 and scanner data. The origin of the reference frame is as defined by the ITRF. In the equatorial plane, the x-axis, $\vec{x}_{ge}$, is fixed with longitude $\lambda = 0$ degrees. The y-axis, $\vec{y}_{ge}$, is also in the equatorial plane, orthogonal to $\vec{x}_{ge}$ and is in the direction of $\lambda = 90$ degrees. The z-axis, $\vec{z}_{ge}$, forms the triple and is defined as,
$\vec{z}_{ge} = \vec{x}_{ge} \times \vec{y}_{ge}$.

The GEF axes have the following values:

$$\vec{x}_{ge} = \{1, 0, 0\}, \vec{y}_{ge} = \{0, 1, 0\}, \vec{z}_{ge} = \{0, 0, 1\}$$

Equation 5.6-4

5.6.3 Aircraft Mechanical Reference Frame (AMR)

This fixed aircraft mechanical reference (AMR) frame is used to describe instrument reference point positions within. The origin of the AMR is different for each aircraft hosting the instruments and is described in section 2.1. In all cases the x-axis, $\vec{x}_{am}$ is directed through the front nominal pointing of the aircraft, the y-axis, $\vec{y}_{am}$, is directed orthogonal to the x-axis in the direction of the right hand wing. The triple is completed via the cross product $\vec{z}_{am} = \vec{x}_{am} \times \vec{y}_{am}$.

The aircraft mechanical frame axes have the following values:

$$\vec{x}_{am} = \{1, 0, 0\}, \vec{y}_{am} = \{0, 1, 0\}, \vec{z}_{am} = \{0, 0, 1\}$$

Equation 5.6-5

It should be noted that the origin of the AMR will not be that of the moment of inertia of the aircraft. This ultimately will result in an error in the processing.
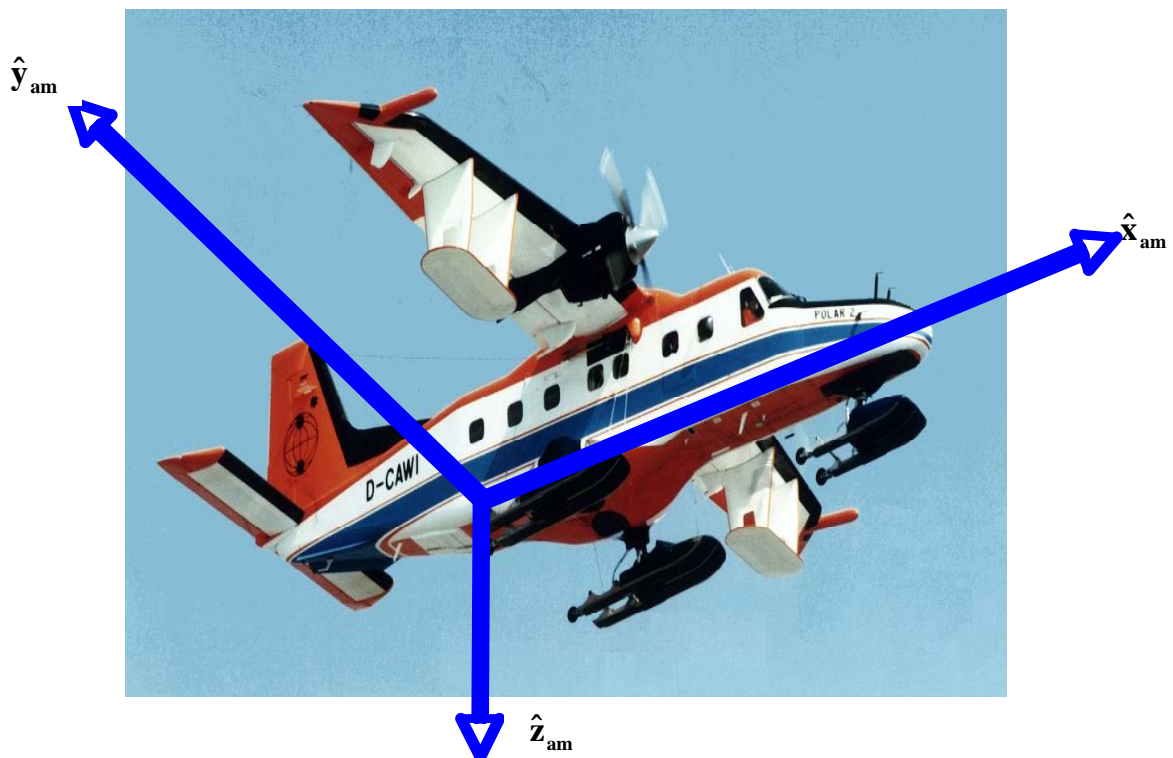
Figure 5.6-1 Aircraft mechanical reference frame diagram
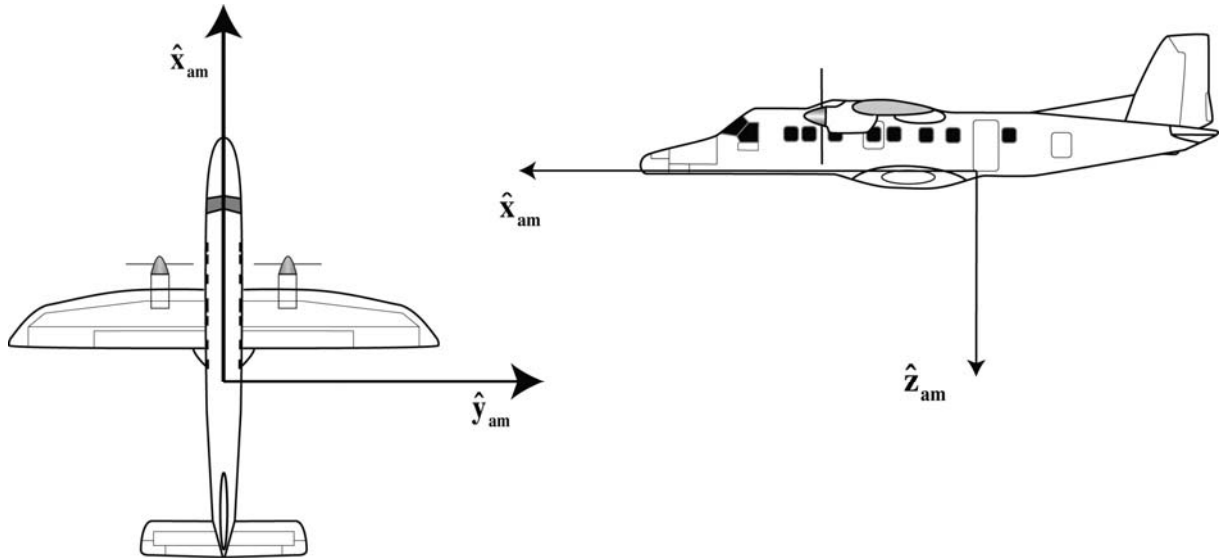
Figure 5.6-2 Aircraft mechanical reference frame diagram

5.6.4 Front GPS Reference Frame (GPS_F)

Note: GPS here refers to differentially processed GPS.
This aircraft fixed reference frame concerns the front GPS when it is available. This reference frame is time-variant, described with respect to the GEF and its origin is at the GPS antenna bottom (an Optimare term).

The z-axis, $\vec{z}_{gf}(t)$ is zenith to the ellipsoid (in the opposite direction to the ellipsoidal normal). This can be calculated by taking the GPS location described in the WGS-84 system, $\Phi_{WGS-84\_front}(\lambda, \phi, h, t)$, where, λ, is the longitude in degrees, ϕ, is the geodetic latitude in degrees, h, is the geodetic height and t is the time of the measurement in UTC.

The vector, $\vec{r}_{gf}(\vec{x}_{gf}, \vec{y}_{gf}, \vec{z}_{gf}, t)$, is determined by first computing the GEF Cartesian locations of $\Phi_{WGS-84\_front}(\lambda, \phi, h, t)$ and $\Phi'_{WGS-84\_front}(\lambda, \phi, 0, t)$ using the geodetic to GEF conversion described in section 1.1.1. This provides 2 vectors, the ellipsoid surface position, $\vec{r}'_{ge\_front}(x, y, z, t)$ and the position of GPS_F, $\vec{r}_{ge\_front}(x, y, z, t)$. Note that $\vec{r}_{ge\_front}(x, y, z, t)$ is ellipsoidal normal to $\vec{r}'_{ge\_front}(x, y, z, t)$.

The axes are now computed:

$$\vec{z}_{gf} = \frac{\vec{r}'_{ge\_front}(t) - \vec{r}_{ge\_front}(t)}{|\vec{r}'_{ge\_front}(t) - \vec{r}_{ge\_front}(t)|}$$

Equation 5.6-6

$$\vec{y}_{gf}(t) = \begin{pmatrix} -\sin\left(\dfrac{\lambda\pi}{180}\right) \\ \cos\left(\dfrac{\lambda\pi}{180}\right) \\ 0 \end{pmatrix}$$

Equation 5.6-7

$$\vec{x}_{gf}(t) = \vec{y}_{gf}(t) \times \vec{z}_{gf}(t)$$

Equation 5.6-8

5.6.5 Rear GPS Reference Fame (GPS_R)

This aircraft reference frame concerns the rear GPS when it is available. This reference frame is time-variant, described with respect to the GEF and its origin is at the GPS antenna bottom (an Optimare term).

The method of determining this reference frame vector $\vec{r}_{gr}\left(\vec{x}_{gr}, \vec{y}_{gr}, \vec{z}_{gr}, t\right)$ is identical to that of GPS_F with the exception the WGS-84 coordinates of GPS_R are described by $\Phi_{WGS-84\_rear}(\lambda, \phi, h, t)$.

5.6.6 Nominal Aircraft Reference Frame (NAR)

It is not known which of the front or rear GPS is available. Since there will be differences in the GPS_F and GPS_R reference frames due to DGPS processing and also due to operation of the aircraft at low altitude an assumption has to be made regarding the NAR. We assume at low altitude this assumption is valid and $\left\{\vec{x}_{gr}(t),\ \vec{y}_{gr}(t),\ \vec{z}_{gr}(t)\right\} = \left\{\vec{x}_{gf}(t),\ \vec{y}_{gf}(t),\ \vec{z}_{gf}(t)\right\}$ and we take the NAR to be equal which ever of the front or rear GPS is available. In other words:

If GPS_F is available,

$$\begin{pmatrix} \vec{x}_{na}(t) \\ \vec{y}_{na}(t) \\ \vec{z}_{na}(t) \end{pmatrix} = \begin{pmatrix} \vec{x}_{gf}(t) \\ \vec{y}_{gf}(t) \\ \vec{z}_{gf}(t) \end{pmatrix}$$

Equation 5.6-9

If GPS_R is available,

$$\begin{pmatrix} \vec{x}_{na}(t) \\ \vec{y}_{na}(t) \\ \vec{z}_{na}(t) \end{pmatrix} = \begin{pmatrix} \vec{x}_{gr}(t) \\ \vec{y}_{gr}(t) \\ \vec{z}_{gr}(t) \end{pmatrix}$$

Equation 5.6-10

Writing this into a matrix we get

$$R_{na}(t) = \begin{bmatrix} a_{11} & a_{12} & a_{13} \\ a_{21} & a_{22} & a_{23} \\ a_{31} & a_{32} & a_{33} \end{bmatrix}$$

Equation 5.6-11

, with $\vec{a} = \vec{r}_{na}\left(\vec{x}_{na}, \vec{y}_{na}, \vec{z}_{na}, t\right)$

The origin of this reference frame can be determined by first determining the AAR (described in the next section). However, since this reference frame is used entirely for its axes definition and not the origin we do not determine it here.

5.6.7 Actual Aircraft Reference Frame (AAR)

The AAR is defined as the AMR rotated about 3 axes using time-variant true heading, $\zeta(t)$, pitch, $\xi(t)$ and roll, $\eta(t)$, angles as determined from the time-shift corrected inertial navigation system (INS) data.

We take the AMR and rotate about the three angles (in units of radian) of rotation, $\zeta(t)$, $\xi(t)$ and $\eta(t)$ using the convention of application of rotations.

$$\begin{pmatrix} \vec{x}_{aa}(t) \\ \vec{y}_{aa}(t) \\ \vec{z}_{aa}(t) \end{pmatrix} = \left[R_{aa\_to\_am}(\eta,\xi,\zeta,t) \right]^{T} \begin{pmatrix} \vec{x}_{am}(t) \\ \vec{y}_{am}(t) \\ \vec{z}_{am}(t) \end{pmatrix}$$

Equation 5.6-12

,where

$$R_{aa\_to\_am} = R_1(\eta(t)) \cdot R_2(\xi(t)) \cdot R_3(\zeta(t))$$

Equation 5.6-13

Rotation matrices R_1, R_2, R_3 are defined in section 5.6.8

5.6.8 Rotation Matrices

Rotation matrices about axes 1, 2 and 3 (x,y,z) are provide the following rotations.

$$R_1(\alpha) = \begin{bmatrix} 1 & 0 & 0 \\ 0 & \cos\alpha & \sin\alpha \\ 0 & -\sin\alpha & \cos\alpha \end{bmatrix}$$

Equation 5.6-14

$$R_y(\alpha) = \begin{bmatrix} \cos\alpha & 0 & -\sin\alpha \\ 0 & 1 & \sin\alpha \\ \sin\alpha & 0 & \cos\alpha \end{bmatrix}$$

Equation 5.6-15

$$R_z(\alpha) = \begin{bmatrix} \cos\alpha & \sin\alpha & 0 \\ -\sin\alpha & \cos\alpha & 0 \\ 0 & 0 & 1 \end{bmatrix}$$

Equation 5.6-16

5.6.9 Determination Cartesian GEF (ITRF) coordinates from WGS-84 geodetic coordinates

Considering Equation 4.6-1, Equation 5.6-2 and determine the GEF components:

Equation 5.6-3 we

$$\vec{r}_{ITRF} = \begin{pmatrix} (v+h)\cos(\phi)\cos(\lambda) \\ (v+h)\cos(\phi)\sin(\lambda) \\ \left(v\dfrac{b_e^2}{a_e^2} + h \right)\sin(\phi) \end{pmatrix}$$

Equation 5.6-17

, where λ, is the geodetic longitude in degrees, ϕ, is the geodetic latitude in degrees, h, is the geodetic height in metres.

5.6.10 Determination WGS-84 geodetic coordinates from cartesian GEF (ITRF) coordinates

Considering we determine the GPS location described in the WGS-84 system, $\Phi_{WGS-84}(\lambda,\phi,h,t)$:

$$\lambda = \sqrt{x^2 + y^2}$$

Equation 5.6-18

$$\phi = \arctan\left(\left(z + \left(\frac{ea_e^2 \sin^3(\varepsilon)}{b_e^2} \right) \right), \left(\vartheta - \left(ea_e \cos^3(\varepsilon) \right) \right) \right)$$

Equation 5.6-19

$$h = \frac{\vartheta}{\cos(\phi) - v}$$

Equation 5.6-20

, where $\vec{r}_{ITRF}(x,y,z)$ is the position vector described in cartesian ITRF, $\vartheta = \sqrt{x^2 + y^2}$ and $\varepsilon = \arctan(a_e \cdot z, b_e \cdot \vartheta)$.

5.6.11 Determination of AMR origin in ITRF and WGS-84 coordinates

Depending on which GPS is available we have two measured GPS locations ($\vec{r}_{am\_GPS}$) in the mechanical reference frames for e.g D-CODE:
$\vec{r}_{am\_front} = (4.836,\ 0.561,\ -1.996)$ and $\vec{r}_{am\_rear} = (0.018,\ 1.398,\ -1.819)$.

Going from this GPS locations defined in the AMR to the AMR origin we simply have to apply a translation:

$$T_{GPS\_to\_AMR-orig} = -\vec{r}_{am\_GPS}$$

Equation 5.6-21

If GPS_F is available then $\vec{r}_{am} = -\vec{r}_{am\_front}$ and with section 0 and 5.6.6 $\vec{r}_{na}(t) = \vec{r}_{gf}(t)$.

If GPS_R is available then $\vec{r}_{am} = -\vec{r}_{am\_rear}$ and with section 5.6.5 and 5.6.6 $\vec{r}_{na}(t) = \vec{r}_{gr}(t)$.

Determine $\vec{r}_{aa}$ rotated from AMR into the AAR (see section 1.1.1):

$$\vec{r}_{aa}(t) = \left[R_{aa\_to\_am}(t) \right]^T \vec{r}_{am}$$

Equation 5.6-22

The actual mechanical reference frame <u>origin</u> in the GEF (ITRF) is now given by:
If GPS_F is used

$$\vec{r}_{ge\_AMR-orig}(t) = R_{na}(t)\ \vec{r}_{aa}(t) + \vec{r}_{ge\_front}(x, y, z, t)$$

Equation 5.6-23

If GPS_R is used

$$\vec{r}_{ge\_AMR-orig}(t) = R_{na}(t)\vec{r}_{aa}(t) + \vec{r}_{ge\_rear}(x, y, z, t)$$

Equation 5.6-24

Summarizing all steps we get:

$$\vec{r}_{ge\_AMR-orig}(t) = \left(R_{na}(t) \cdot \left[R_{aa\_to\_am}(t) \right]^T \cdot T_{GPS\_to\_AMR-orig} \right) \cdot \vec{r}_{am\_GPS} + \vec{r}_{ge\_GPS}(x, y, z, t)$$

Equation 5.6-25

Actual mechanical reference frame <u>origin</u> described in WGS-84 coordinates, $\Phi_{WGS-84\_AMR-orig}(\lambda, \phi, h, t)$ is computed by using the function described in section 5.6.10

5.6.12   Determination of ground reflection points in ITRF and WGS-84 coordinates

In general we are interested in the ground reflection points ($\vec{r}_{ge\_surface\_pnt}(t)$) obtaining by range measurements of the instruments. Two cases have to differentiate between:

ASIRAS – nadir looking instrument
LD90 or Scanner – not stringent nadir looking and potentially squinting.

Considering case 1:

Taking
Equation 5.6-25 two points have to be added.

Translation from the AMR origin to the instrument location defined in the AMR ($\vec{r}_{am\_INSTR}$).

$$T_{AMR-orig\_to\_INSTR} = \vec{r}_{am\_INSTR}$$

Equation 5.6-26

Insert the range measurement. This can easily done by subtracting the measured range from the z-component (h-component) of the computed instrument position in the GEF (WGS-84).

Combining those two steps with

Equation 5.6-25:

$$\vec{r}_{ge\_surface\_pnt}(t) = \left(R_{na}(t) \cdot \left[R_{aa\_to\_am}(t) \right]^T \cdot T_{AMR-orig\_to\_INSTR} \cdot T_{GPS\_to\_AMR-orig} \right) \cdot \vec{r}_{am\_INSTR} +$$
$$+ \vec{r}_{ge\_GPS}(x,y,z,t) - \vec{r}_{range}(0,0,range,t)$$

Equation 5.6-27

Actual ground reflection points described in WGS-84 coordinates, $\Phi_{WGS-84\_surface\_pnt}(\lambda,\phi,h,t)$ is computed by using the function described in section 5.6.10

Considering case 2:

Taking

Equation 5.6-25 three points have to be added.

Squint angle correction. The AMR is defined as the instrument mechanical reference frame (IMR) rotated about 3 axes using the squint angles $\left(\xi_1,\xi_2,\xi_3\right)$ as determined in section 1.1.

$$\left(\vec{r}_{am}\right) = \left[R_{am\_to\_im}\left(\xi_1,\xi_2,\xi_3\right) \right]^T \left(\vec{r}_{im}\right) \qquad\qquad \textit{Equation 5.6-28}$$

, with

$$R_{am\_to\_im} = R_1(\xi_1) \cdot R_2(\xi_2) \cdot R_3(\xi_3) \qquad\qquad \textit{Equation 5.6-29}$$

Rotation matrices R_1, R_2, R_3 are defined in section 5.6.8

The origin of IMR is equal to the origin of measurement and IMR axes have the follwing values:

$$\vec{x}_{im} = \{1,0,0\}, \vec{y}_{im} = \{0,1,0\}, \vec{z}_{im} = \{0,0,1\} \qquad\qquad \textit{Equation 5.6-30}$$

Insert the range measurement. This has to be done in the very beginning for not nadir looking instruments such as scanner and LD90. The range vector $\vec{r}_{range}(range,\beta,t)$ is dependent from the beam angle β:

$$\vec{r}_{range}(t) = \begin{pmatrix} 0 \\ \sin(\beta)\,range \\ \cos(\beta)\,range \end{pmatrix} \qquad\qquad \textit{Equation 5.6-31}$$

Range measurement takes place in the IMR.

Translation from the AMR origin to the instrument location defined in the AMR ($\vec{r}_{am\_INSTR}$), see Equation 5.6-26.

Combining those three steps with
Equation 5.6-25:

$$\vec{r}_{ge\_surface\_pnt}(t) = \left(R_{na}(t) \cdot \left[R_{aa\_to\_am}(t) \right]^T \cdot T_{AMR-orig\_to\_INSTR} \cdot T_{GPS\_to\_AMR-orig} \cdot \left[R_{am\_to\_im} \right]^T \right) \cdot \vec{r}_{range}(t) + $$
$$+ \vec{r}_{ge\_GPS}(x, y, z, t)$$

Equation 5.6-32

Actual ground reflection points described in WGS-84 coordinates, $\Phi_{WGS-84\_surface\_pnt}(\lambda, \phi, h, t)$ is computed by using the function described in section 5.6.10

5.7 Calibration of ASIRAS and first validation results

In this section we present calibration results for the laser scanner and ASIRAS of both campaigns CryoVex 2004A and CryoVex 2004B. In section 5.7.1 we demonstrate the high quality of laser scanner measurements.
In section 5.7.2 we demonstrate the determination of a constant offset existing between ASIRAS and the ALS-DEM as a result of unknown instrument characteristics (e.g. cable length) by comparing runway over flights.
In section 5.7.3 we are showing validation results derived by comparing data of selected test sites. Here we concentrate on the derived penetrating depth of the radar echo at corner reflector locations. Last we present examples of waveform plots of selected profiles showing different behavior of the radar echo when scattered from various snow regimes. An OCOG (offset center of gravity) retrack-algorithm was used while processing the ASIRAS Level_1B data. The main advantage of an OCOG-retracker is its relative simplicity and short processing time [R.1, R.5].

5.7.1 Quality of laser scanner measurements

As described in section 0 additional to the laser scanner a single beam laser was installed in the aircraft. Although the data rate of 4 Hz is quite low, the output is useful to check the laser scanner accuracy. Figure 5.7-1 presents a 100 s section of Austfonna icecap overflight. In the top plot of Figure 5.7-1 the surface elevation of the ALS-DEM and the single beam laser subtrack are overplotted. Because the y-axis, which defines the surface elevation with respect to WGS 84 in meters, has a wide range, small offsets between single beam laser subtrack and the ALS-DEM are not visible. In the middle plot the difference of both measurements is shown. The standard deviation is down to only 2.5 cm, which lies within the error range of the instrument.
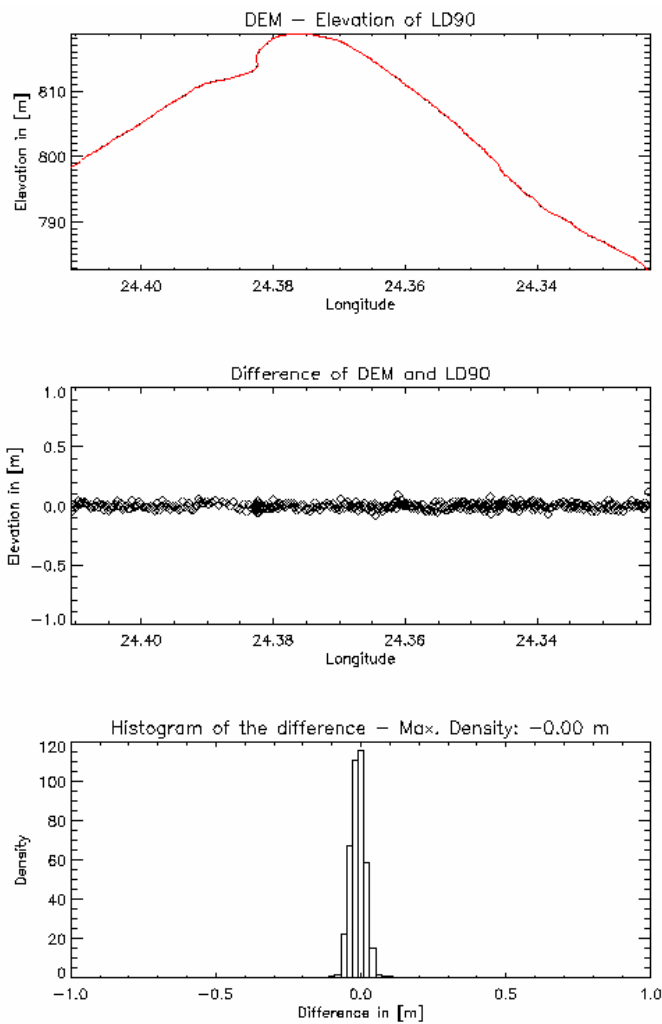
Figure 5.7-1 Quality check of laser scanner measurements over Austfonna Icecap at 20th April 2004.

5.7.2 Calibration of ASIRAS over runways

In order to calibrate the ASIRAS instrument runways were chosen as target assuming no penetration for both the radar and the Laser. Figure 5.7-2 shows an overflight over the Ilulissat runway on 2nd of September 2004. The solid line in the true color plot at the right side of Figure 5.7-2 represents the antenna subtrack taken from the ASIRAS Level_1B data. The comparison on this subtrack between the surface elevation of ASIRAS and the DEM elevation is plotted on the left hand side of the same figure. The first box shows the elevation of ALS-DEM (black line) and ASIRAS (red line). Clearly visible are outliers which correspond to retracking failures. Therefore locations are chosen where 1) the runway was retracked in a suffcient way and 2) the roll angle of the aircraft was close to zero. From the parts which were used an offset of ~ 85 cm was derived, which is also shown in the histogram. A waveform plot in Figure 5.7-3 shows the radar echo. Retracking errors are due to echo jumping which is clearly shown in the waveform plot. It is likely that the energy of the radar return is affected by echos reflected from the rough gravel surface next to the asphaltic runway in the centre.
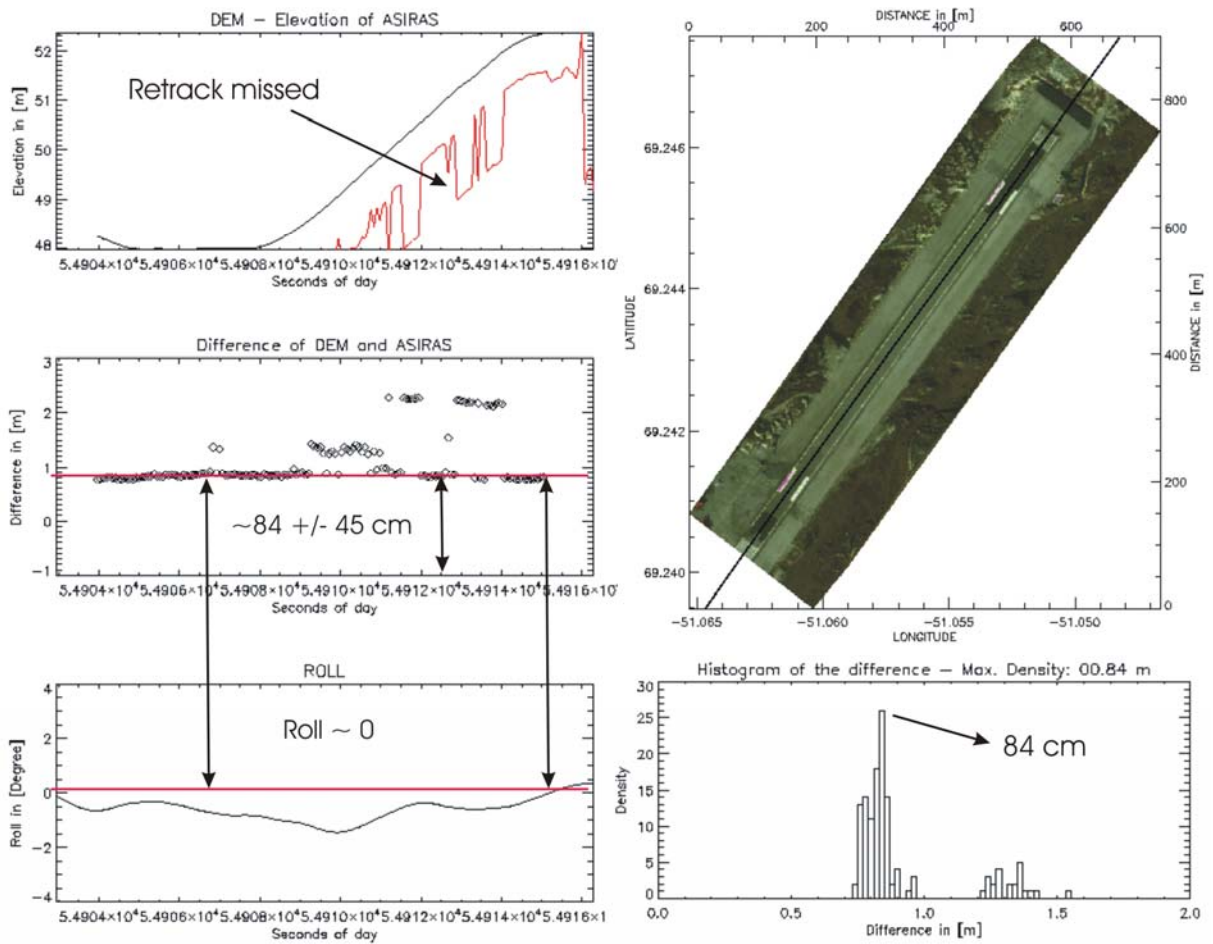
Figure 5.7-2 Runway over flight in Ilulissat. Comparison of ALS-DEM and ASIRAS subtrack showing a constant offset of 85 cm. Section was flown at 14th September 2004, profile A040914_01.
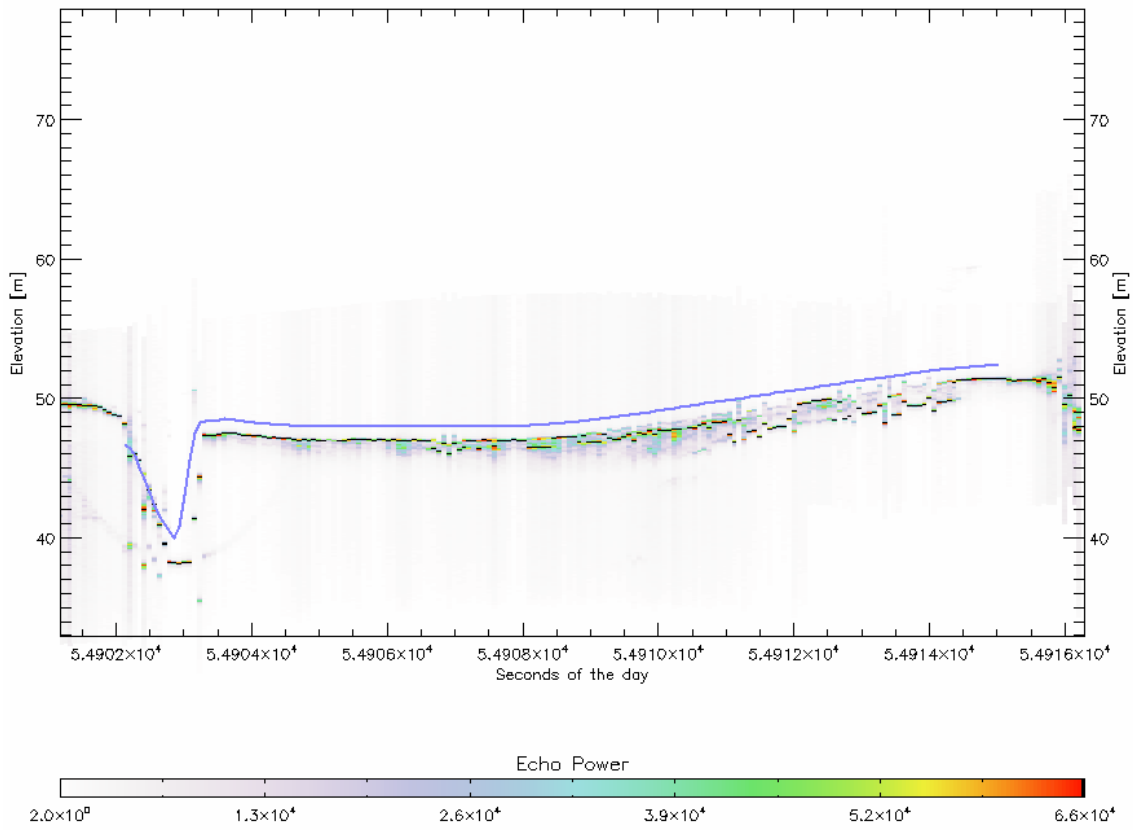
Figure 5.7-3 Waveform plot of the Ilulissat runway over flight. Blue line shows the ALS-DEM elevation. Echo power is normalized and scaling factors have not been applied.
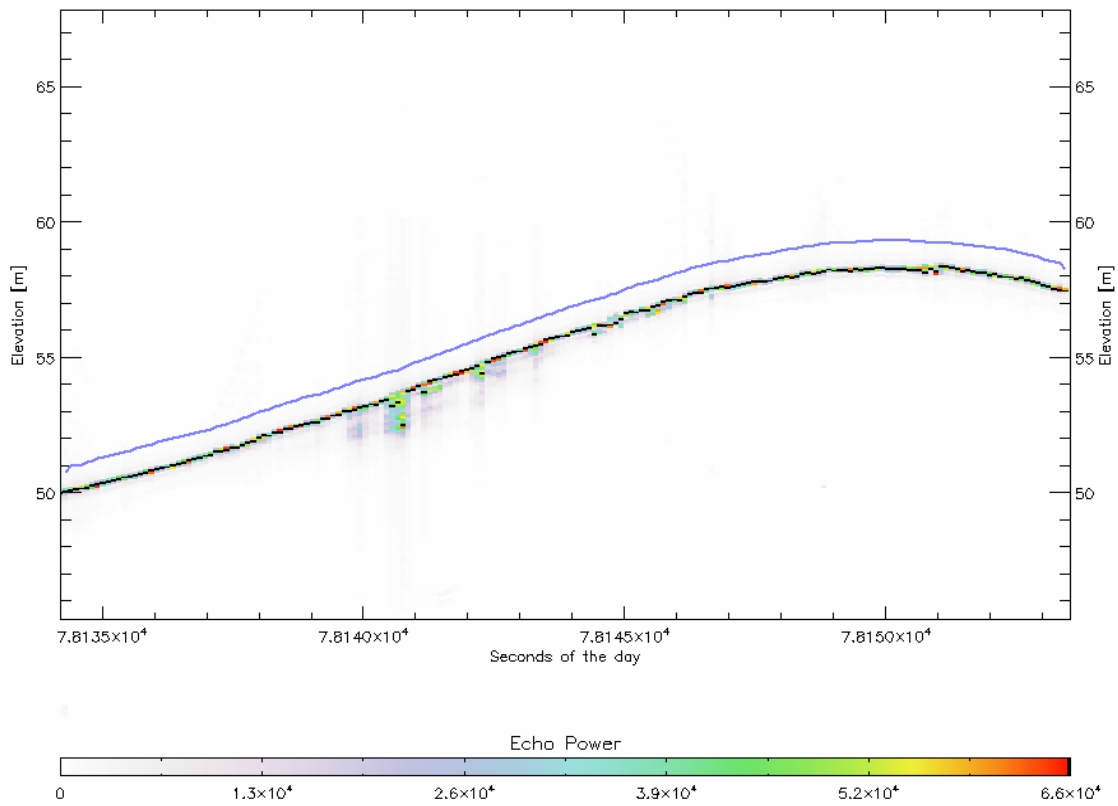
Figure 5.7-4 Waveform plot of the Resolute Bay runway over flight. Blue line shows the ALS-DEM elevation. Echo power is normalized and scaling factors have not been applied.
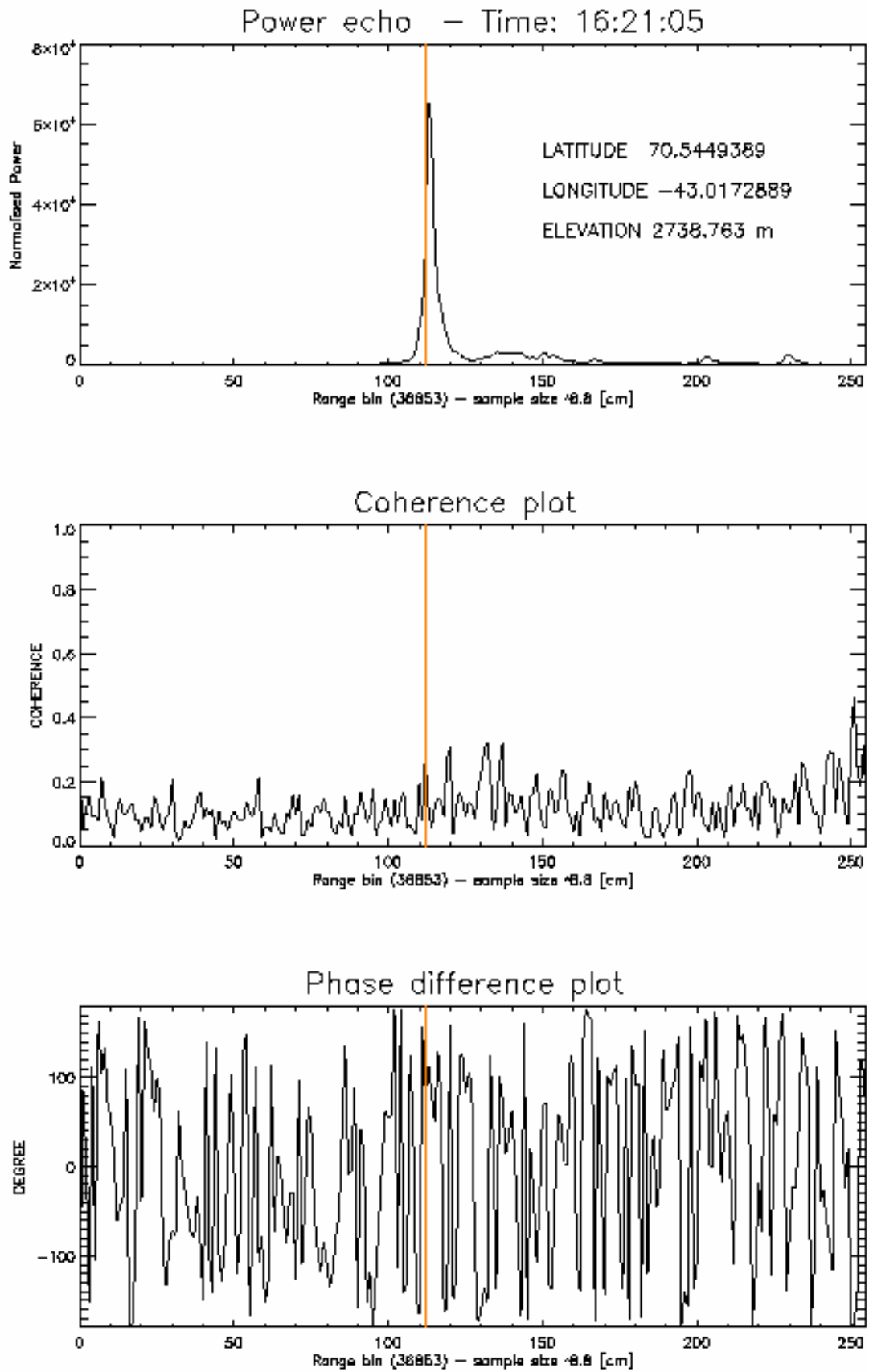
Figure 5.7-5 Power echo, coherence and phase difference plot over the EGIG line .The red line indicates the retracked range bin - 14th of Sep. 2004, profile A040914_02.

.
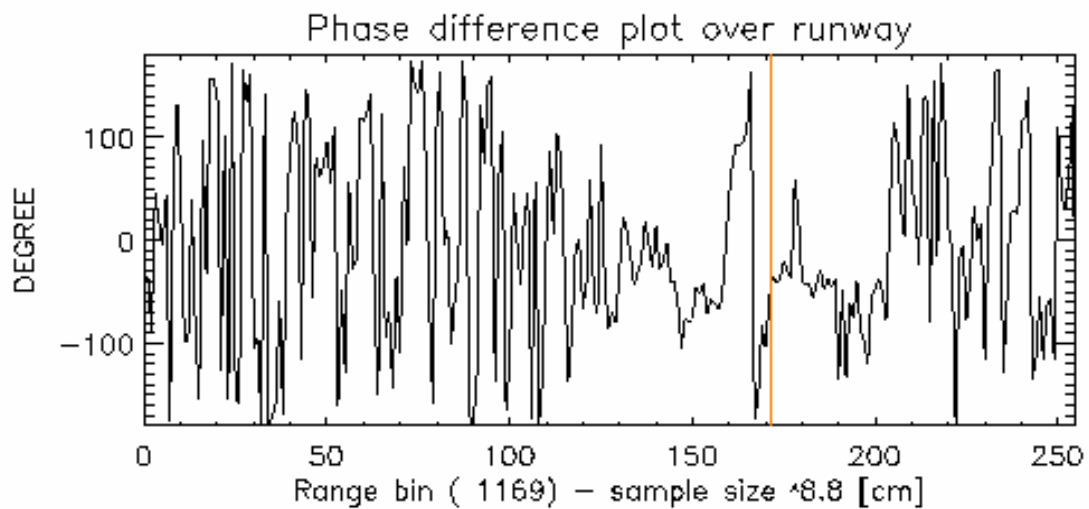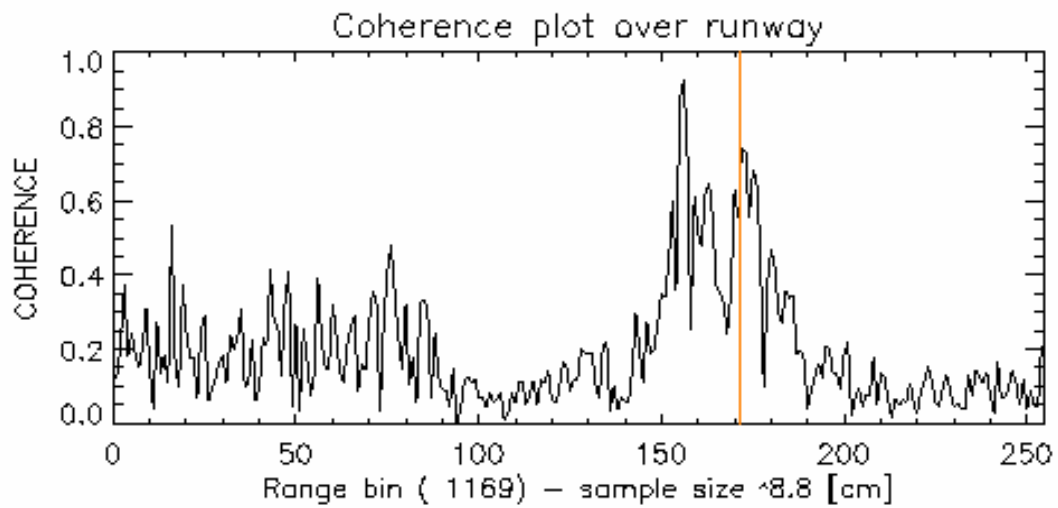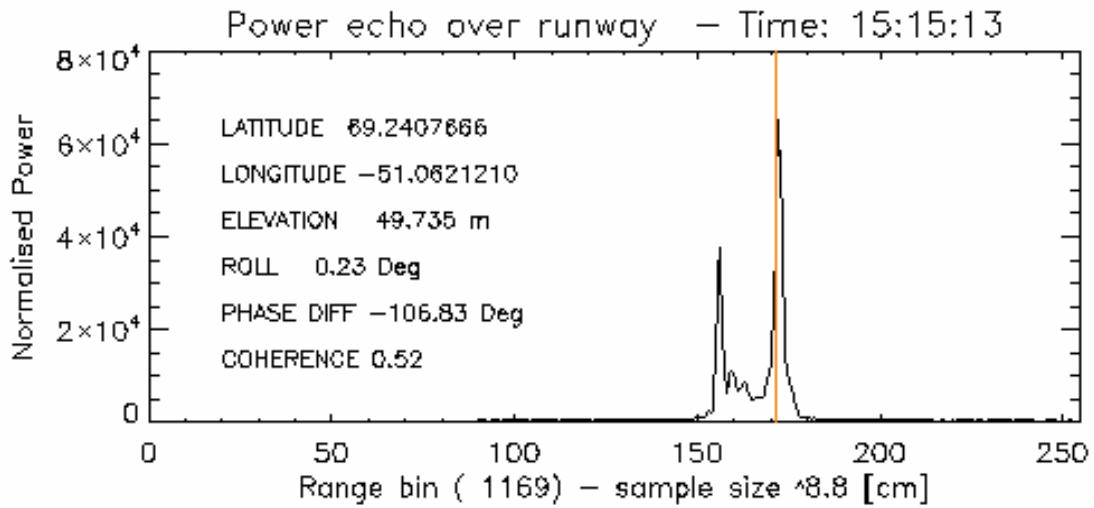
Figure 5.7-6 Power echo, coherence and phase difference plot over runway. The red line indicates the retracked range bin – 14th of Sep. 2004, profile A040914_01.

The true color image at the right hand side of Figure 5.7-7shows an overflight over the runway in Resolute Bay at May 2, 2004. Compared to Ilulissat the retracking quality is much better, but the difference plot of ASIRAS and ALS-DEM subtrack surface elevation (Figure 5.7-7, left hand side box 2) is noisy as well, probably due to the not perfect hit of the runway and the rough snow beside. In the histogram the offset of ~ 85 cm is clearly visible, which is the same value as determined for CryoVex 2004B. Figure 5.7-4 shows the more stable waveform of the echo, which results in a better retracking of the runway echo.
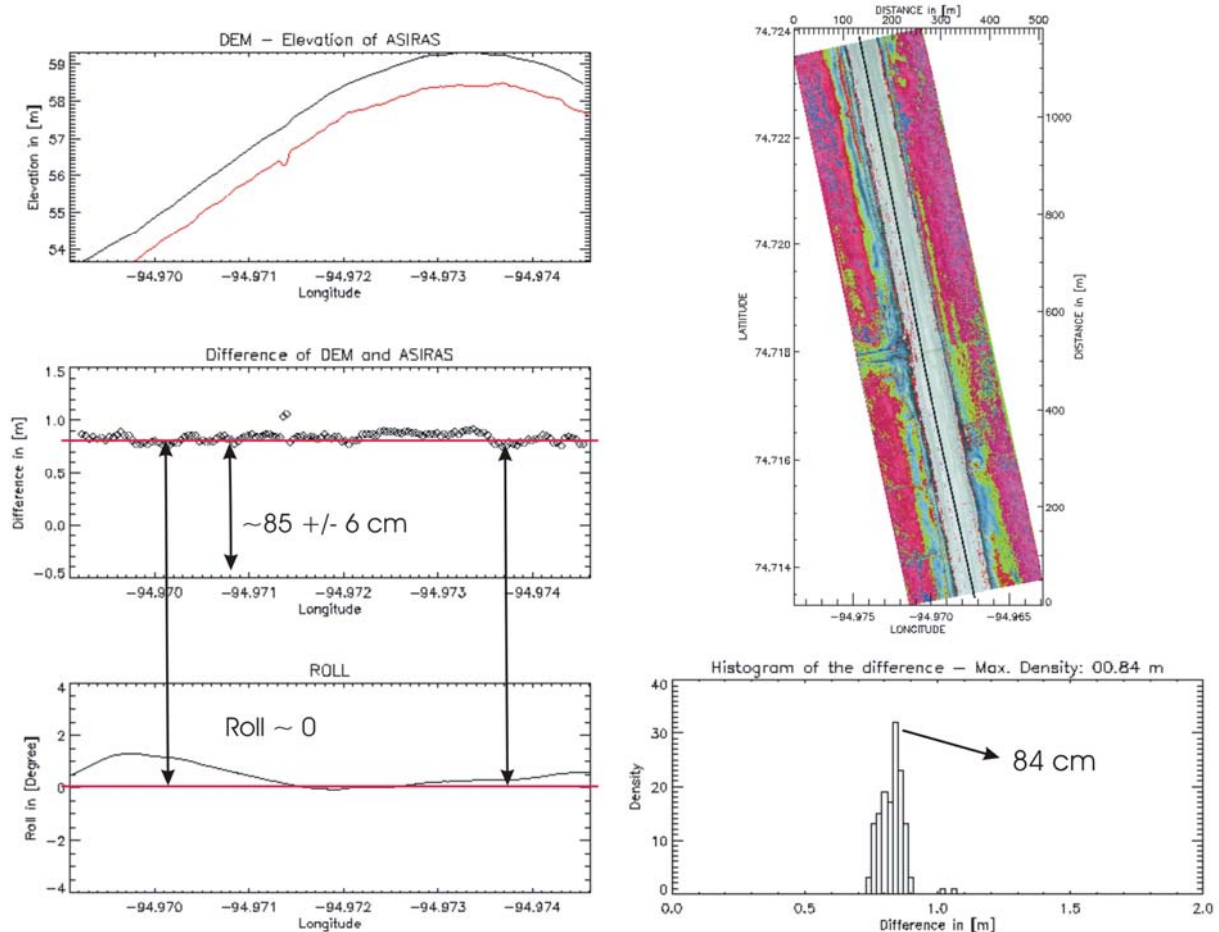
Figure 5.7-7 Runway over flight at Resolute Bay. Comparison of ALS-DEM and ASIRAS subtrack showing a constant offset of 85 cm. Section was flown at 2nd of May 2004, profile A040502_05.

Conclusion:

We conclude from the CryoVex 2004A and CryoVex 2004B runway overflights, that a calibration constant of 85 cm has to be applied to the ASIRAS data. A large deviation from this number over runways is primarily due to bad retracking result. The value should be checked in future activities by extensive runway overflights before and after each data recording flight. If possible the installation of corner reflectors above the runway during validation activity can be useful for improving the quality.

5.7.3 Validation of ASIRAS over test sites

Ground teams installed during their field measurements exactly up looking corner reflectors with the tip about 2 m above the snow surface. During the over flights precise navigation and sometimes a couple of runs were necessary in order to hit the target from an altitude of about 1100 m. Although some over flights were not successful, hits are available for both campaigns, which allow the height comparison of corner reflector and ground reflected ASIRAS data at most test sites. Figure 5.7-8 shows an example how corner reflectors were mounted on a wooden device, Table 5.8-5 and Table 5.8-6 summarizes ground and ASIRAS measurements.

Figure 5.7-8 Picture of corner reflector over sea ice, pre-campaign in March/April 2004.

5.7.3.1 CryoVex 2004B

A typical power echo for a corner reflector can be seen in Figure 5.7-10. Here the T21 corner reflector installed at the EGIG line on 14th of September 2004 (Figure 5.7-15) shows a clear peak followed by the surface reflection response. To estimate the distance between both peaks and therefore the distance between the tip of the corner reflector and the radar snow surface we have to consider the sample size of ~8.8 cm (see x- axis) in the echo plot. The peak to peak difference in both A040914_03 and A040914_02 over flights is determined to 26 samples or 2.28 m. By subtracting the true measured distance of 2,05 m from the peak to peak difference we determine the radar penetration to 23 cm. the plot in the mid of Figure 5.7-9 shows a maximum coherence over corner reflector T21 over flown in profile A040914_02.
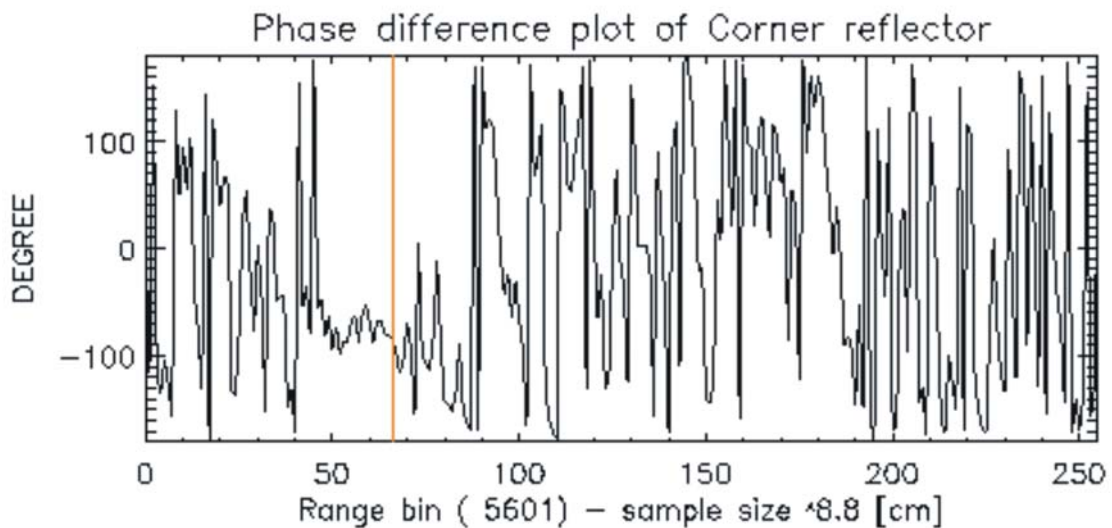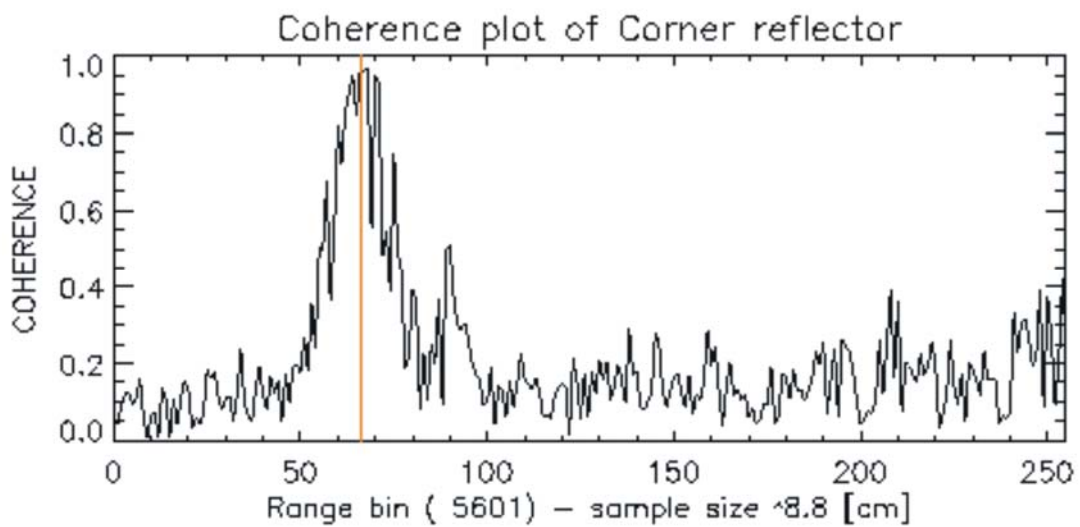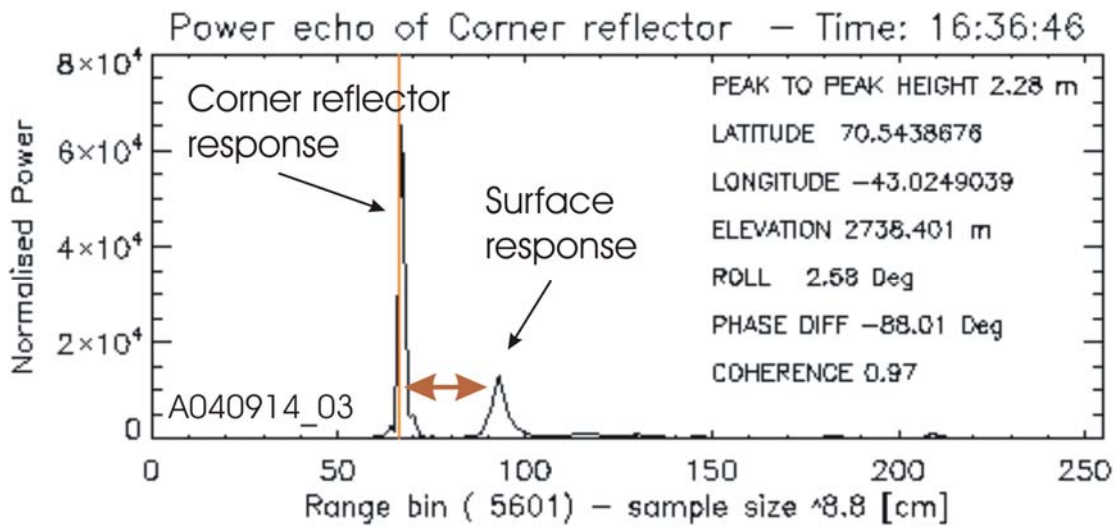
Figure 5.7-9 Power echo, coherence and phase difference for T21 corner reflector – A040914_03.
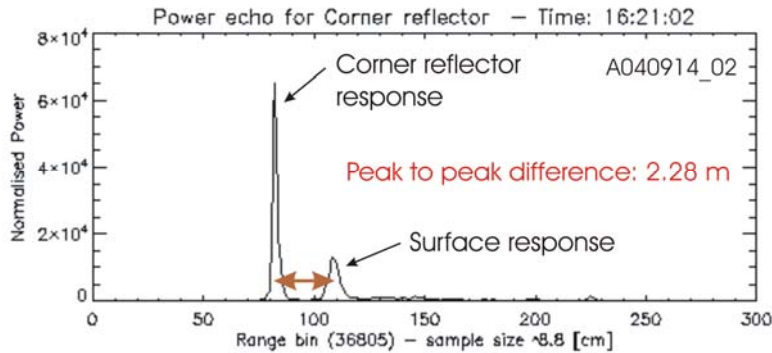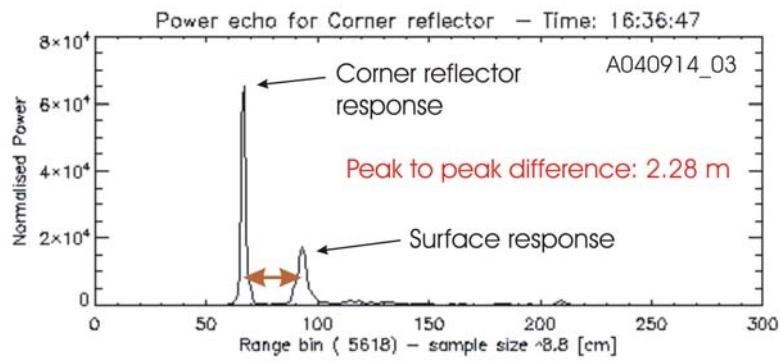
Figure 5.7-10 Power echo for T21 corner reflector – two overflights at 14th of Sep. 2004

Figure 5.7-12 is presenting three T05 corner reflectors over flights at 9th of September 2004. Similar to the T21 over flight in Figure 5.7-9 and Figure 5.7-10 a strong corner reflector response is visible in all of the three power echoes. The peak to peak difference is determined to 1.93 m and 2.11 m. This difference can be explained by the changing shape of the surface response and hence the uncertainty of tracking the surface in the maximum of the response peak. Although the surface is tracked a dilating echo increases the offset. Another reason for obtained differences in distance from corner to snow surface is a parabolic shape of the corner response seen from the aircraft with respect to time. Further analysis is necessary to determine the closest point of approach during the corner over flight. Ground team measured corner reflector height above the snow surface is 2.23 which gives a penetration depth of the radar echo at T05 of -12cm.
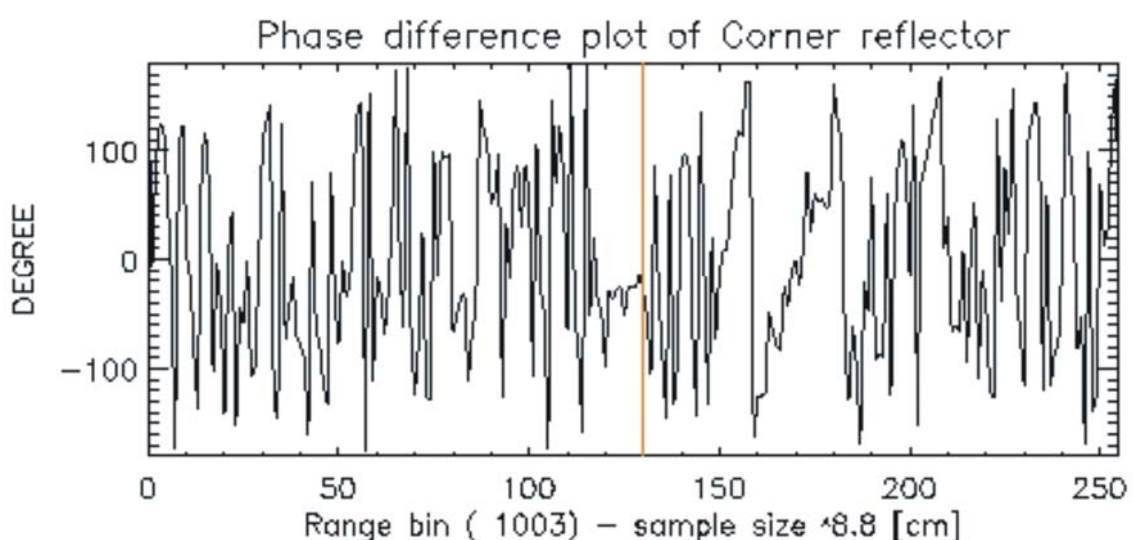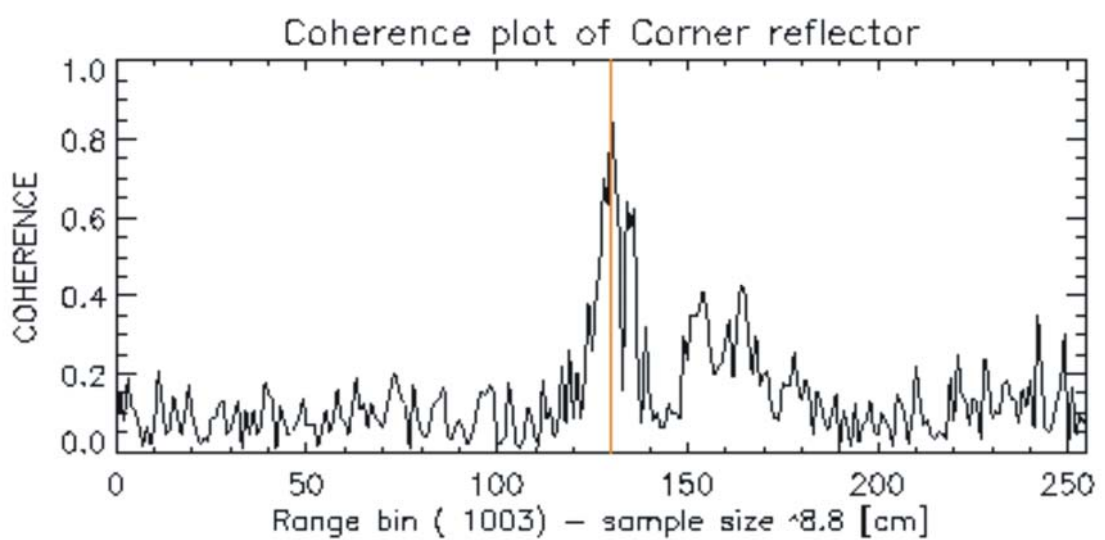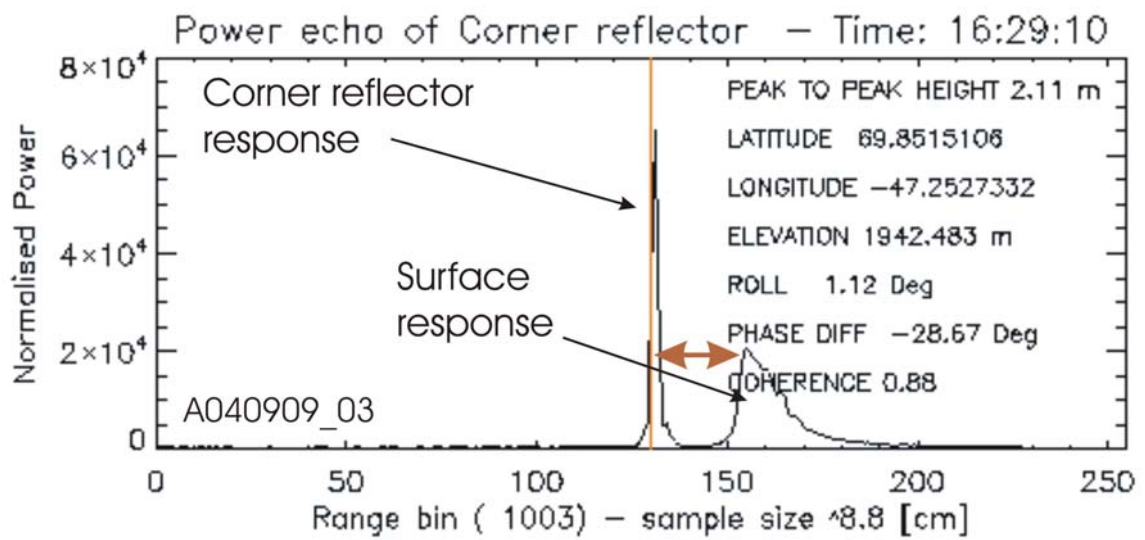
Figure 5.7-11 Power echo, coherence and phase difference for T05 corner reflector – A040909_03.
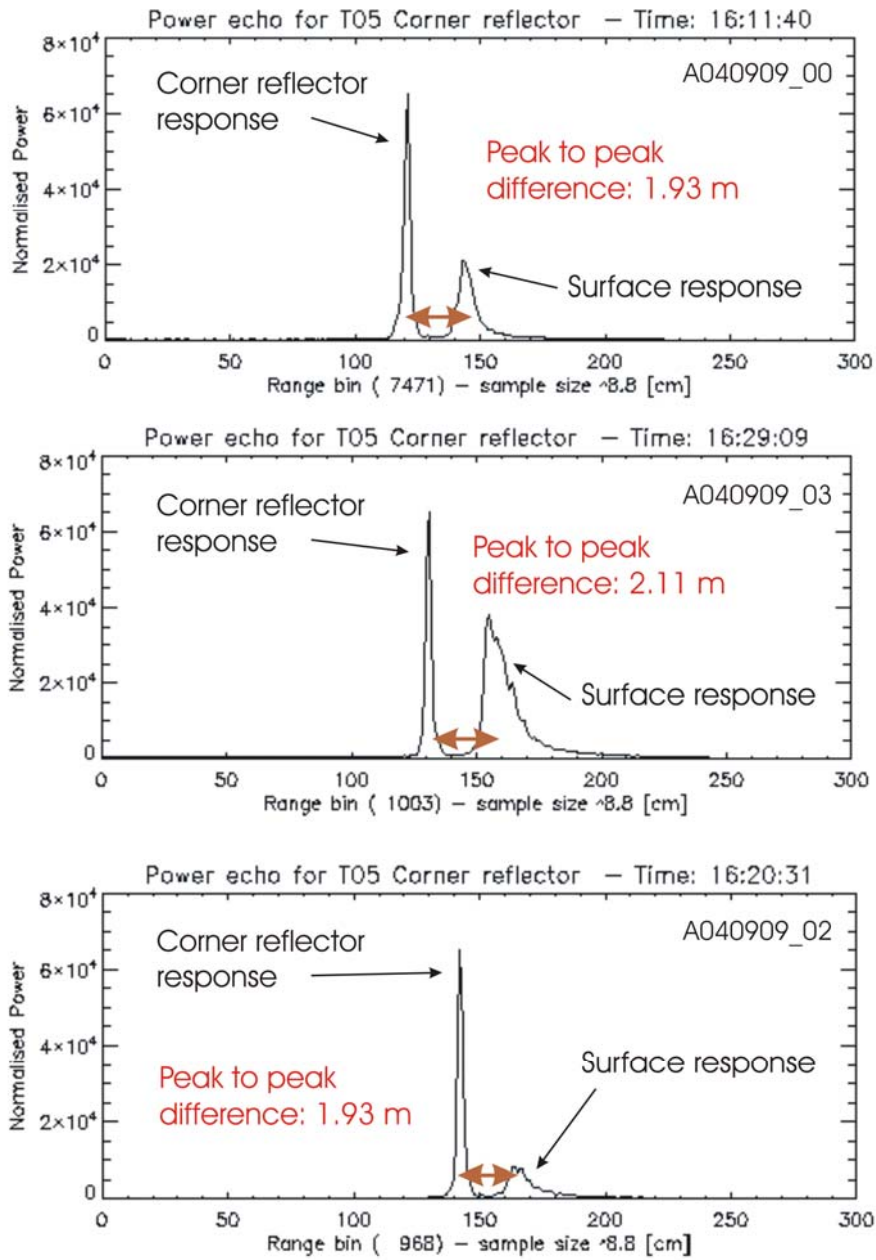
Figure 5.7-12 Power echo for T05 corner reflector – three over flights at 9th of Sep. 2004

EGIG–line CryoVex 2004B – 040909
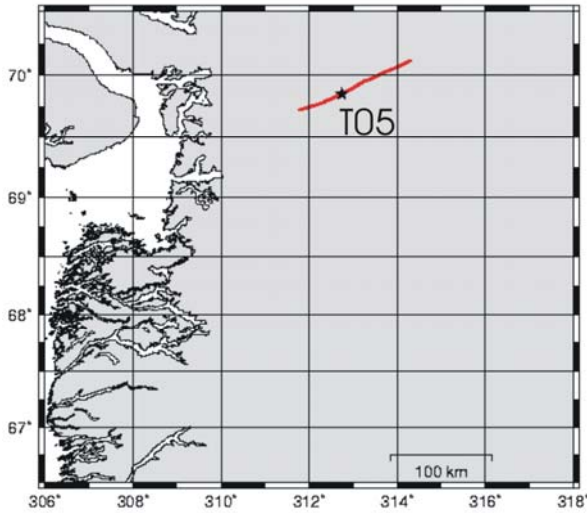
EGIG–line CryoVex 2004B – 040914
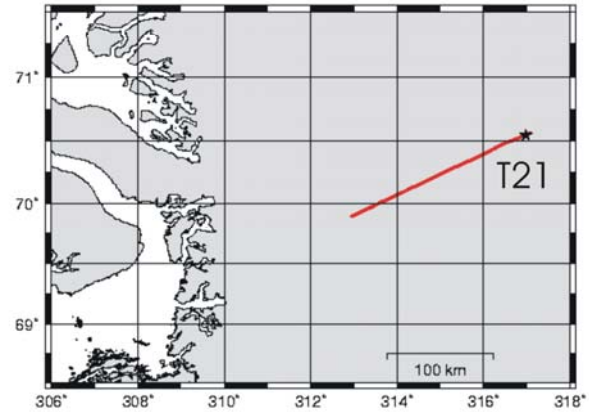
Figure 5.7-13 Corner reflectors (T05 and T21) over flight at 9th and 14th of September 2004

5.7.3.2 CryoVex 2004A

Flight activities during the CryoVex 2004A campaign included measurements across the Austfonna Icecap. Five corner reflectors were installed but only one (see Figure 5.7-15) could be hit. The result is shown in Figure 5.7-14. Like at T21 and T05 in CryoVex 2004B a strong corner reflector response is visible in the power echo. The surface response echo is strongly dilated and divided into two peaks, which results in a high uncertainty of tracking the surface. In this case the smaller, first peak was taken and the peak to peak difference is determined to 1.67 m. The ground team measured the corner reflector height above the snow surface with 1.56m, which yields a penetration depth of the radar echo at CRY-3 of 0.11 m.
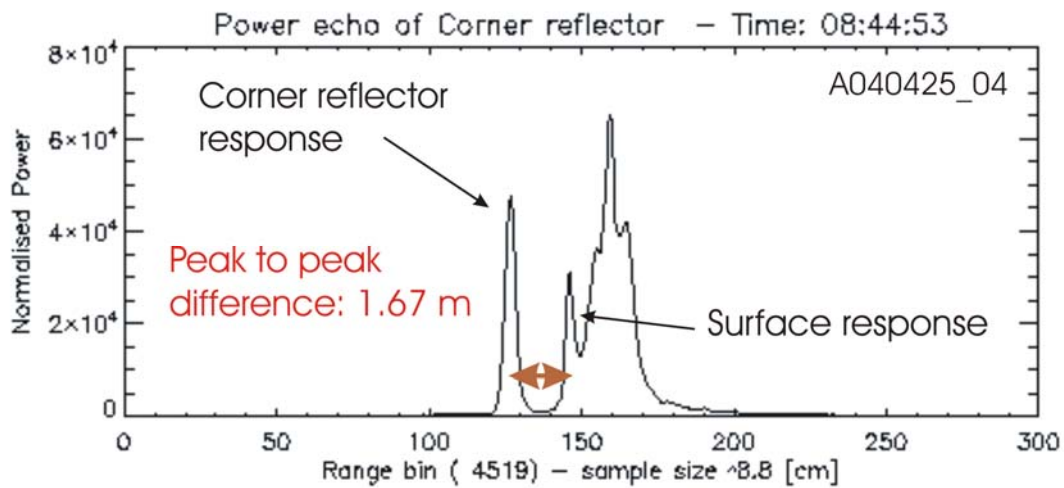
Figure 5.7-14 Power echo CRY-3 corner reflector – overflight at 25th of April 2004
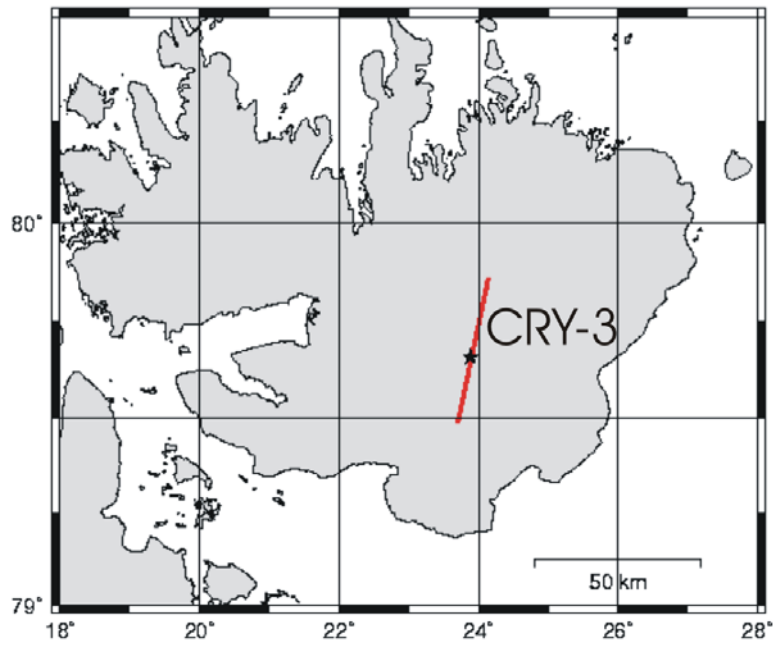
Figure 5.7-15 Corner reflector (CRY-3) over flight at 25th of April 2004
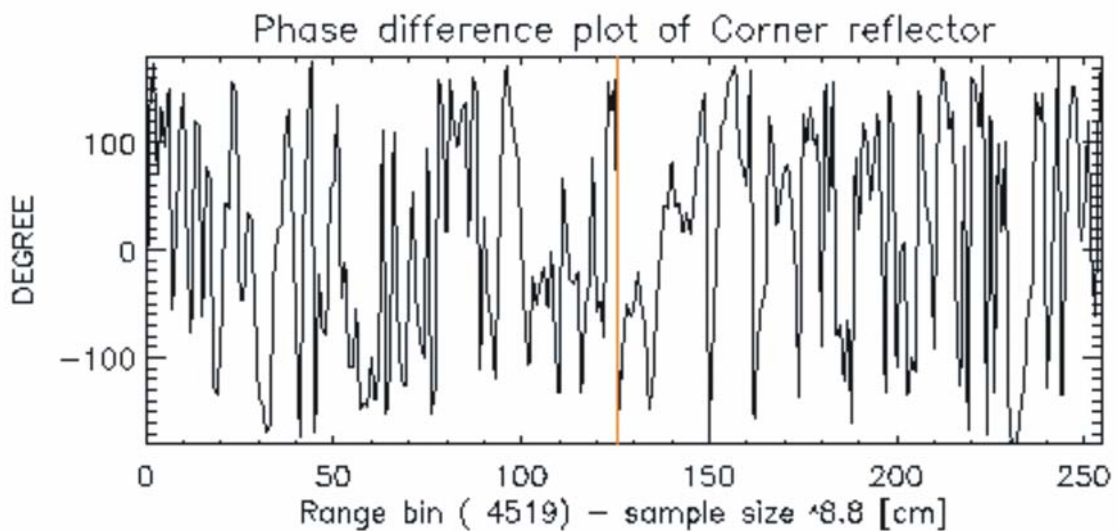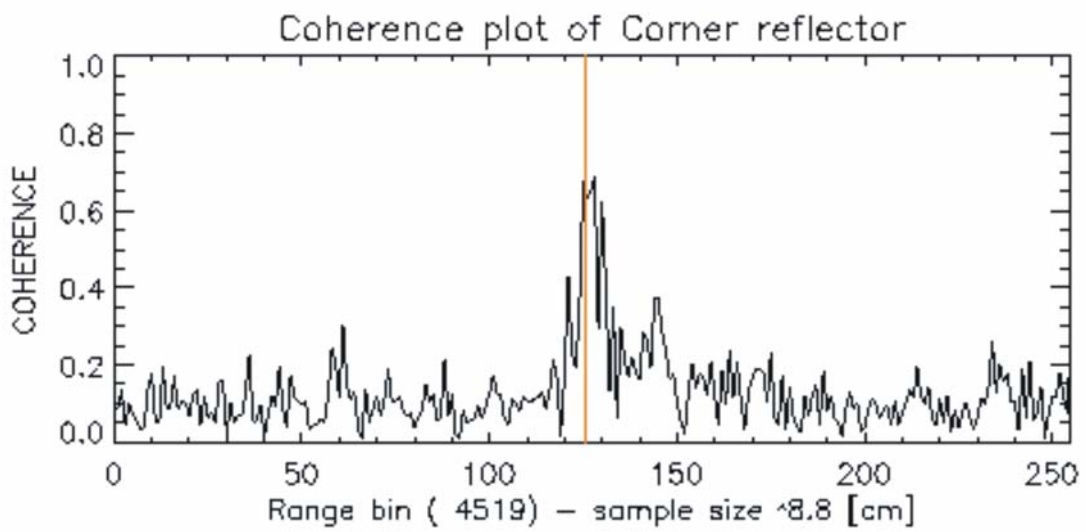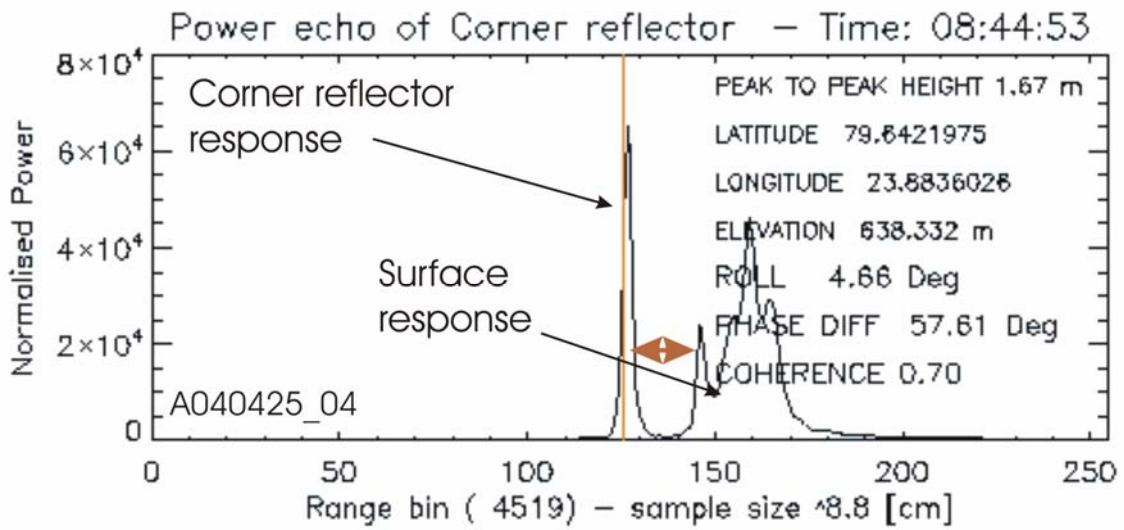
Figure 5.7-16 Power echo, coherence and phase difference for CRY-3 corner reflector – A040425_04.

5.7.4 ASIRAS radar penetration and sub layer detection

In this section we present a first analysis of surface and volume scattering behavior from different snow regimes. As example we show 100s sections of two profiles, EGIG-line profile A040914_03 and Austfonna Icecap profile A040420_01. In the top plot of Figure 5.7-17 the surface elevation of the ALS-DEM (solid black line) and the ASIRAS subtrack (red line) is shown. The middle plot at the left hand side shows the difference of both elevations and in the lower plot the roll of the aircraft is presented. A dominant feature in the first third of all three plots indicates the dependency of the retracked range from the roll. Obviously the echo is received through the tilted main beam and therefore Level_1B retracker is measuring not the range nadir to the aircraft. As a good estimation, proofed in several profiles, a roll between -1° to +1° is producing realistic surface elevation values. By looking closer in the middle to end of the profile also noisy data can be seen. We suggest that the retracker is missing the leading edge of the power echo due to an "unspiky" waveform as a consequence of a stronger volume scattering in the data. Nevertheless the quality is good and the penetration of the echo in the snow pack is estimated to 11 cm by subtracting the offset of 85 cm determined in section 5.7.2 from 96 cm seen in the histogram of Figure 5.7-17. This value corresponds quite well with the 11 cm penetration depth estimated in section 5.7.3. In contrast to the Austfonna profile part of the EGIG-line in western Greenland is presented in Figure 5.7-18. Here the retracking variation is much less due to more spiky echoes. Similar to Austfonna the penetration depth varies around 12 to 14 cm which is indicated in the histogram of Figure 5.7-18.

The waveform plot of both profile sections are shown in Figure 5.7-19 and Figure 5.7-20. Variant scattering characteristics due to different snow regimes are clearly visible when comparing both plots. The echo of the section of the EGIG line, which is situated in the dry snow zone, shows a clear and strong surface response and reflection patterns within the snow pack, see [R.3]. The power echo over the Austfonna Icecap shows small penetration and strong scattering at the surface. Due to strong surface scattering the waveform looses their spikiness and widens. The blue line in both plots shows the ALS-DEM surface elevation of the ASIRAS subtrack.
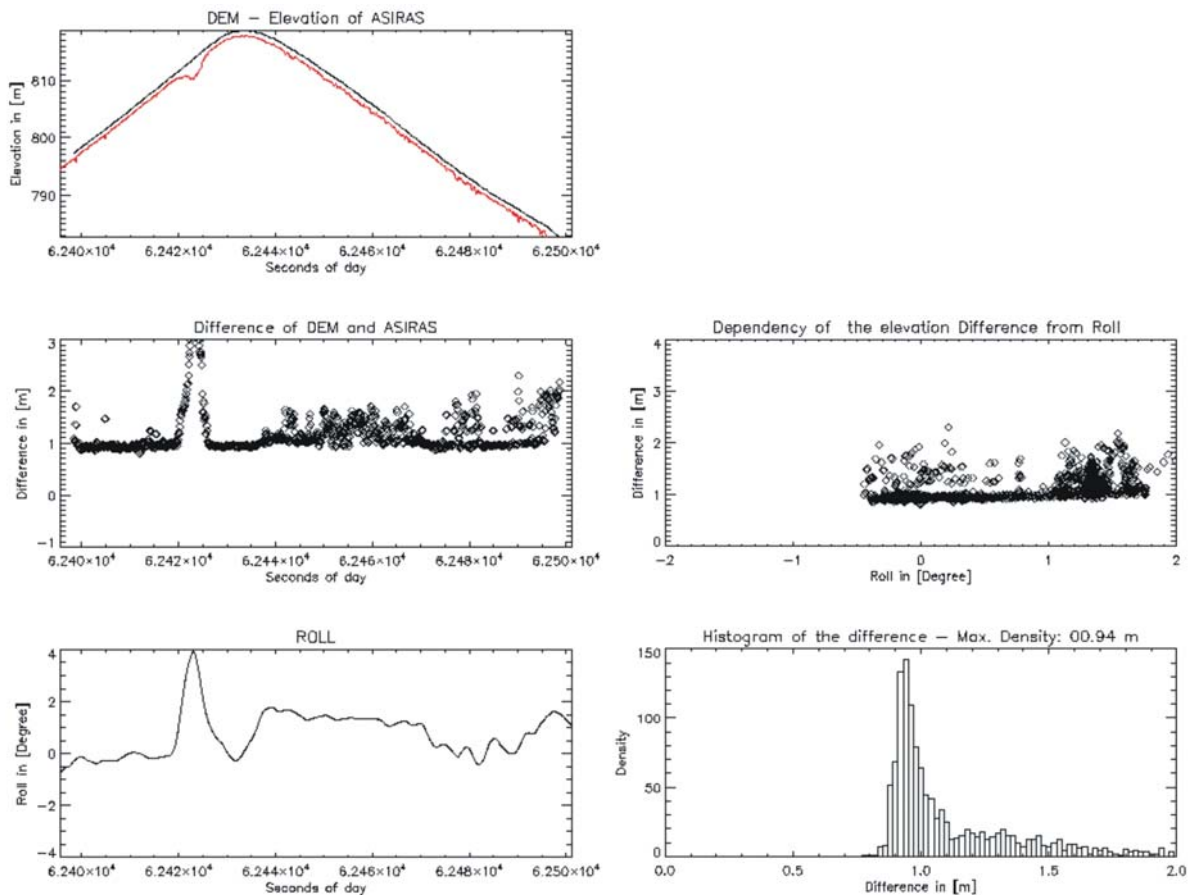
Figure 5.7-17 Section of a profile across the Austfonna Icecap of 100 s. Difference of ALS-DEM surface elevation and ASIRAS subtrack as well as a roll influence is visible.
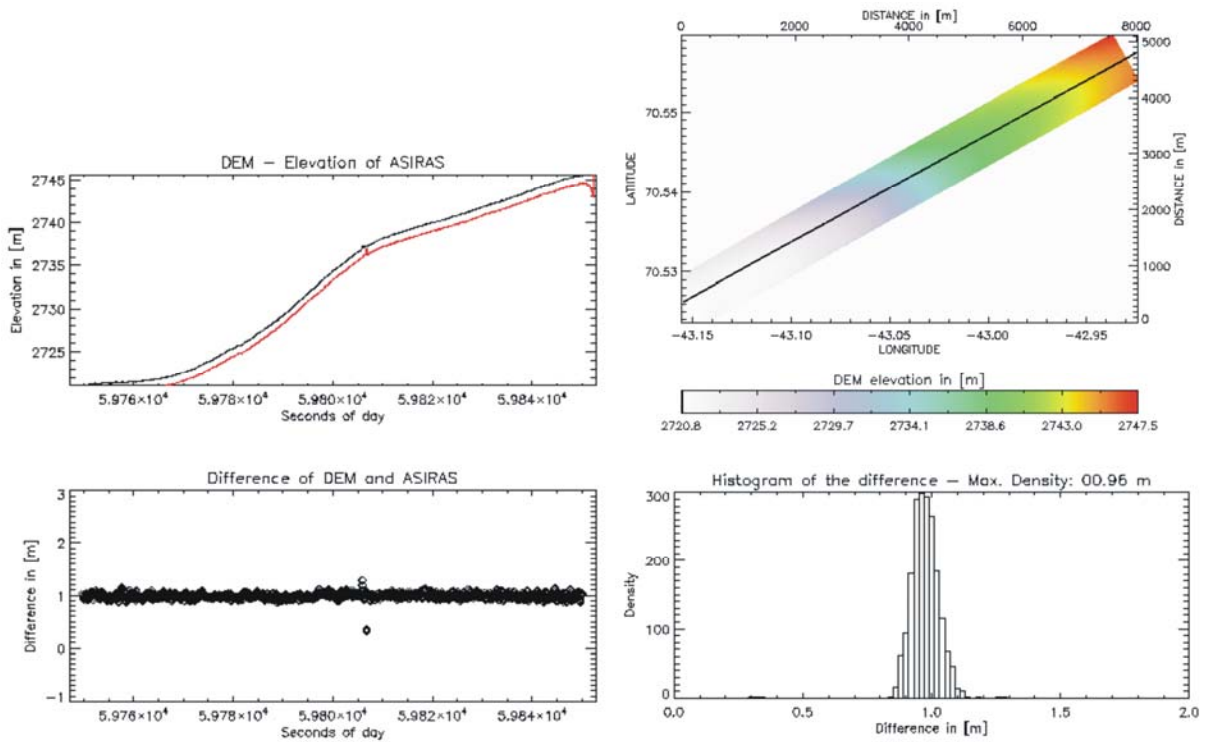
Figure 5.7-18 Section of a profile along the EGIG-line in western Greenland of 100 s. Difference of ALS-DEM surface elevation and ASIRAS subtrack as well a penetration depth of around 14 cm (96 – 82 cm) is shown.
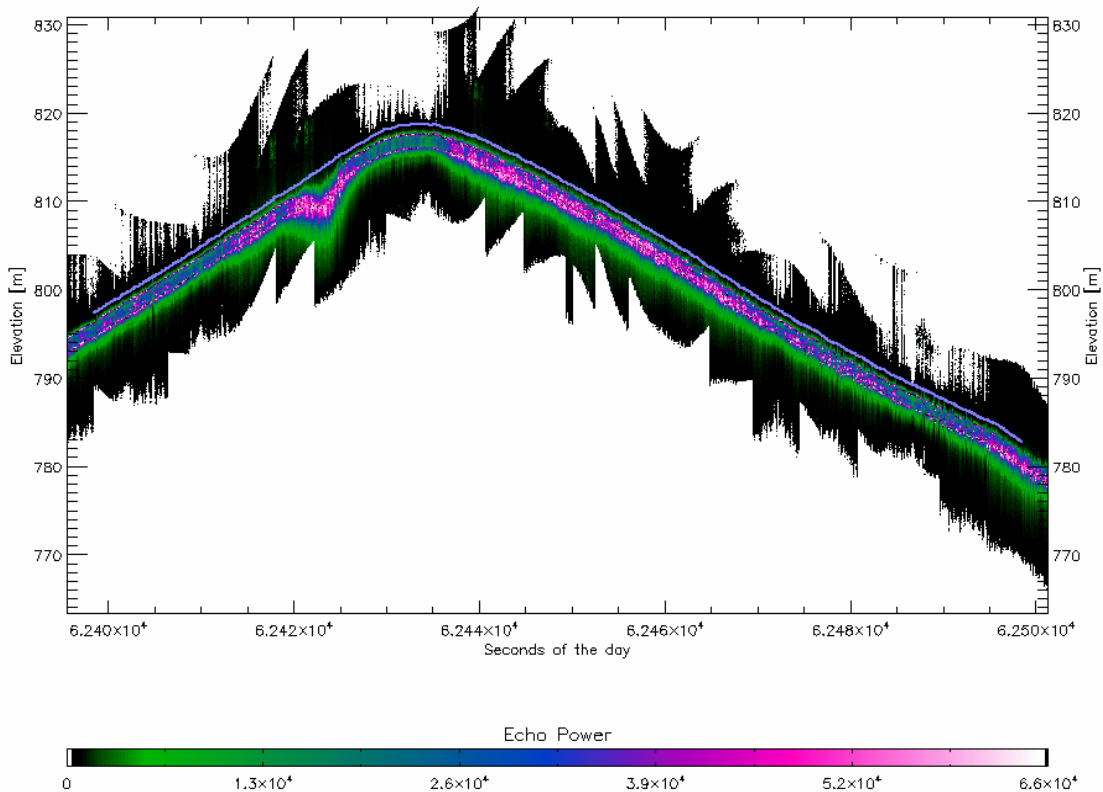
Figure 5.7-19 Waveform plot of a 100 s section of the Austfonna Icecap profile A040420_01. Blue line is indicating the ALS-DEM subtrack elevation. Echo power is normalized and scaling factors have not been applied.
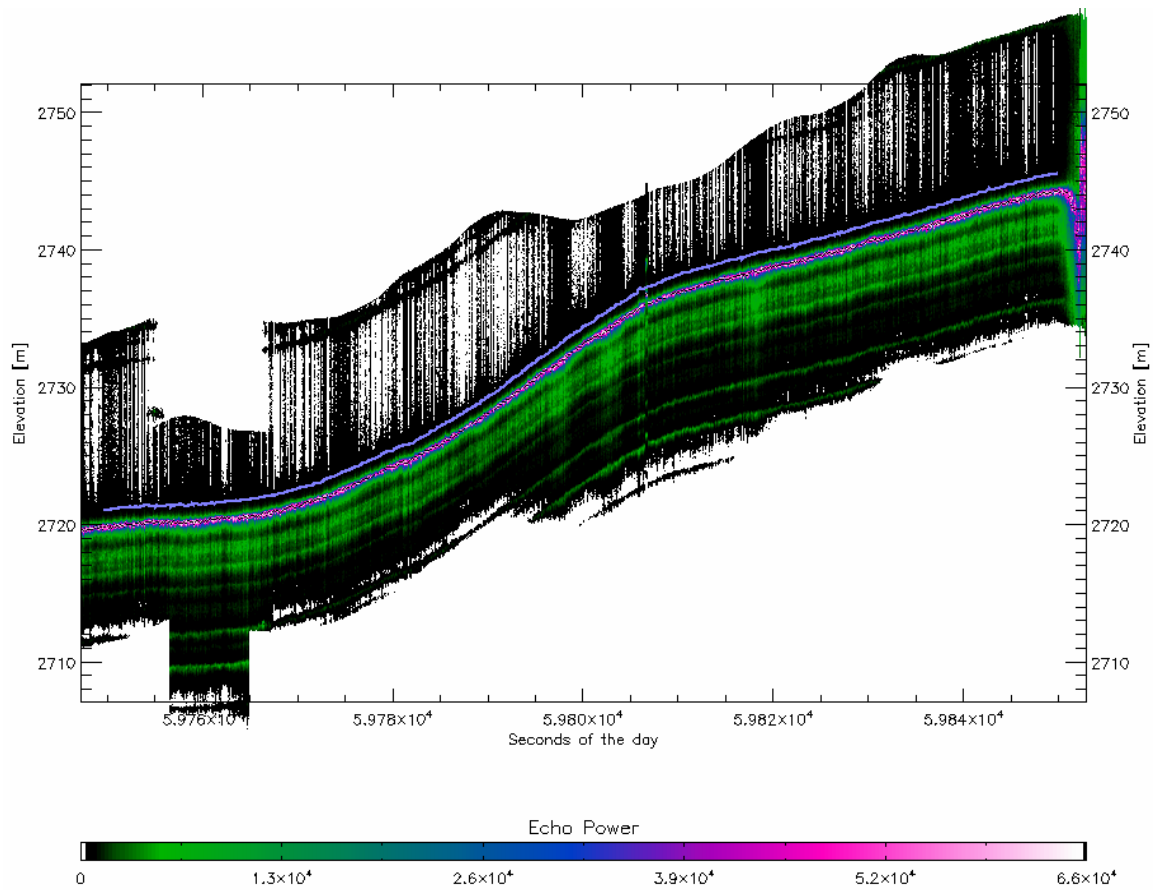
Figure 5.7-20 Waveform plot of a 100 s section along the EGIG-line profile A040914_03. Blue line is indicating the ALS-DEM subtrack elevation. Echo power is normalized and scaling factors have not been applied.

5.8 Tables of final processing results

Table 5.8-1 CryoVex2004A – Campaign solution of time shifts and squint angles

Timeshift INS	Timeshift LD90	Timeshift ALS	Timeshift ASIRAS	Squint Angle ALS	Squint Angle LD90
-1.04 s	-1.14 s	0 to -1 s	0.0 s to -2.2s	$\xi_x = 0.35$ $\xi_y = -0.94$ $\xi_z = -0.59$	$\xi_x = -0.17$ $\xi_y = -1.10$ $\xi_z = 0.0$

Table 5.8-2 CryoVex2004B – Campaign solution of time shifts and squint angles

Timeshift INS	Timeshift LD90	Timeshift ALS	Timeshift ASIRAS	Squint Angle ALS	Squint Angle LD90
-1.04 s	-1.14 s	0 to -1 s	0 s to -2.2 s	$\xi_x = 0.0$ $\xi_y = -0.58$ $\xi_z = 0.39$	$\xi_x = -0.12$ $\xi_y = -1.67$ $\xi_z = 0.0$

Table 5.8-3 CryoVex2004A runway calibration flights.

DAY	ASIRAS Logfile	ALS Start time	ALS Stop time	ASIRAS offset	STDDEV	COMMENT
0405020401	A040502_05	78550	78582	0,85	0,06	Runway hit, good quality
0405050501	A040505_03	72900	72913	/	/	No perfect hit, high roll, quality low

Table 5.8-4 CryoVex2004B runway calibration flights.

DAY	ASIRAS Logfile	ALS Start time	ALS Stop time	ASIRAS offset	STDDEV	COMMENT
0409040201	A040904_08	48700	48850	/	/	no perfect hit, no track over runway, bad quality
0409090401	A040909_05	67335	67385	/	/	Runway hit, bad tracking, low quality
0409140501	A040914_01	66105	66117	0,86	0,46	Perfect hit, tracking bad, medium quality

Table 5.8-5 Corner reflector position during CryoVex2004A. Last column shows the height above snow determined from the ASIRAS power echo over the corner reflector site.

Location	Corner	Latitude	Longitude	Altitude (WGS84)	Height above snow (real)	Height above snow (ASIRAS)
Austfonna	ETON	79,750418132	22,416823803	368,3	2,03	No hit
	CRY-1	79,959060470	24,243117837	684,9	1,77	No hit
	CRY-2	79,840846303	24,099046677	809,8	1,72	No hit
	CRY-3	79,659144461	23,883242674	637,0	1,56	1,67 m +/- 9cm
	CRY-4	79,599980402	24,671392375	468,3	1,49	No hit
EGIG	T05	69,851247809	-47,253459735	1939,8	2,235	
	T21	70,5438	-43,0253	2736,937	2,054	No hit
Devon		75,337867653	-82,67679824	1798,218	0	No hit

Table 5.8-6 Corner reflector position during CryoVex2004B. Last column shows the height above snow determined from the ASIRAS power echo over the corner reflector site.

Location	Corner	Latitude	Longitude	Altitude (WGS84)	Height above snow (real)	Height above snow (ASIRAS)
EGIG	T05	69,851247809	-47,253459735	1939,8	2,235	2,11 m +/- 9 cm
	T21	70,5438	-43,0253	2736,937	2,054	2,28 m +/- 9 cm
Devon		75,338147	-82,677368	1797,39	2,5	

Table 5.8-7 Detailed CryoVex2004A INS time shift results.

DAY	Time shift PITCH	STDDEV PITCH	Time shift vertical Velocity	STDDEV vvertical Velocity	Time shift Heading	STDDEV Heading
0404190101	-1,03	0,04	-1,05	0,07	-1,11	0,69
0404200201	-1,03	0,08	-1,04	0,07	-1,10	0,51
0404250301			-1,00	0,03	-1,10	0,03
0405020401	-1,02	0,06	-1,03	0,06	-1,10	0,39
0405050501	-1,02	0,04	-1,02	0,07	-1,08	0,15
0405060601	-1,02	0,1	-1,03	0,05	-1,10	0,61

Table 5.8-8 CryoVex2004B INS time shift results

DAY	Time shift PITCH	STDDEV PITCH	Time shift vertical Velocity	STDDEV vertical Velocity	Time shift Heading	STDDEV Heading
0409040201	-1,02	0,05	-1,02	0,05	-1,11	0,32
0409090301	-1,03	0,05	-1,01	0,04	-1,10	0,44
0409110401	-1,04	1,11	-1,00	0,18	-1,10	0,12
0409140501	-1,04	0,7	-1,02	0,06	-1,11	0,87
0409170701	-1,04	0,05	-1,03	0,04	-1,10	0,71

Table 5.8-9 CryoVex2004A ASIRAS processing status; processor version ASIRAS_03_03

Logfile	Number of PC1 files	Number of PC2 files	Original Logfile	Edited logfile	LINUX	MAC	number of processed records	COMMENTS
A040419_00	1	1	●			●	5000 of 5312	
A040419_01	1	1	●			●	8000 of 8272	
A040419_02	1	1	●			●	4500 of 4592	
A040419_03	2	2	●			●	16000 of 16272	
A040419_04	2	2	●			●	12500 of 12960	
A040419_05	2	2	●			●	14000 of 14280	
A040419_06	1	1	●			●	6000 of 6208	
A040419_07	1	1	●			●	8500 of 8784	
A040419_08	1	1	●			●	7500 of 7776	
A040420_00	1	1	●			●	3000 of 3248	
A040420_01	4	4	●			●	36000 of 36336	
A040420_02	4	4	●			●	28500 of 28880	

Logfile	Number of PC1 files	Number of PC2 files	Original logfile	Edited logfile	LINUX	MAC	number of processed records	COMMENTS
A040420_03	2	2	●		●		16500 of 16688	
A040420_04	5	5	●		●		44500 of 44864	
A040420_05	1	1	●		●		9000 of 9328	
A040425_00	3	3	●		●		19000 of 19200	
A040425_01	3	3	●		●		25000 of 25216	
A040425_02	2	2	●		●		12000 of 12208	
A040425_03	1	1	●		●		9000 of 9040	
A040425_04	2	3	●		●		18500 18656	
A040502_00	1	1	●		●		2500 of 2832	
A040502_01	3	3	●		●		19000 of 19488	
A040502_02	2	2	●		●		17500 of 17840	
A040502_03	1	1	●		●		6500 of 6992	
A040502_04	4	4	●		●		30500 of 30752	
A040502_05	1	1	●		●		8000 of 8208	
A040505_00	4	4	●		●		34500 of 34896	
A040505_01	2	2	●		●		13500 of 13808	
A040505_02	1	1	●		●		3000 of 3424	
A040505_03	1	1	●		●		2500 of 2560	
A040506_00	1	1	●		●		5500 of 5680	
A040506_01	9	6						file size PC1 and PC2 different
A040506_02	0	3						file size PC1 and PC2 different

Table 5.8-10 CryoVex2004B ASIRAS processing status; processor version ASIRAS_03_03

Logfile	Number of PC1 files	Number of PC2 files	Original logfile	Edited logfile	LINUX	MAC	number of processed records	COMMENTS
							as	
A040904_00	2	2	●		●		11500 of 11968	
A040904_01	1	1	●		●		6500 of 6688	
A040904_02	2	2	●		●		9500 of 9712	
A040904_03	1	1	●		●		6500 of 6624	
A040904_04	1	1	●		●		3000 of 3456	
A040904_05	1	1	●		●	●	5500 of 5904	SIGSEGV / MAC fine
A040904_06	1	1	●		●		7000 of 7488	
A040904_07	2	2	●	●	●	●	13500 of 13856	SIGSEGV / MAC fine
A040904_08	1	1	●		●	●	6500 of 6528	SIGSEGV / MAC fine
A040909_00	2	2	●		●		17500 of 17904	
A040909_01	1	1	●		●		4000 of 4096	
A040909_02	1	1	●		●		2500 of 2992	
A040909_03	4	4	●	●	●		29000 of 29120	
A040909_04	1	1	●		●		8000 of 8240	
A040909_05	1	1	●		●		5000 of 5088	
A040911_00	2	2	●		●		10000 of 10432	
A040911_01	4	4	●	●	●	●	7500 of 28240	SIGSEGV / MAC SIGSEGV

Logfile								
A040914_00	1	1	•		•		5500 of 5808	
A040914_01	1	1	•		•		3000 of 3136	
A040914_01	1	1	•		•		3000 of 3136	
A040914_01	1	1	•		•		3000 of 3136	
A040914_02	7	7	•		•	•	63000 of 63248	SIGSEGV / MAC fine
A040914_03	2	2	•		•		11000 of 11440	
A040914_04	1	1	•	•	•		2500 of 2864	
A040914_05	1	1	•	•	•		0	no surface locations
A040914_06	1	1	•	•	•		4500 of 4752	
A040914_07	1	1	•	•	•		3500 of 3616	
A040916_00	1	1	•					no GPS DATA available
A040916_01	1	1	•					no GPS DATA available
A040916_02	1	1	•					no GPS DATA available
A040917_00	17	17	•	•	•		155000 of 155072	

Table 5.8-11 CryoVex2004A - ASIRAS time shifts and difference to ALS-DEM

Logfile	STARTIME	STOPTIME	ASIRAS TSHIFT	DIFF MEDIAN	DIFF STDDEV	COMMENT
A040419_00	45300	45350	-1,20	1,01	0,75	BQ
A040419_01	45570	45640	-1,00	0,98	0,32	
A040419_02	56360	56420	-1,32	0,99	0,14	
A040419_03	57000	57100	-1,10	0,98	0,19	
A040419_04	57900	58000	-1,20	1,03	0,12	
A040419_05	58570	58660	-1,00	1,04	0,16	
A040419_06						
A040419_07	59800	59850	-1,10	0,85	0,88	BQ
A040419_08	60200	60300	-1,13	0,98	0,10	
A040420_00	/	/	/	/	/	BQ
A040420_01	62400	62500	-1,00	0,98	0,28	
A040420_02	63550	63650	-1,23	0,95	0,19	
A040420_03	65020	65060	/	/	/	BQ
A040420_04	66100	66200	-1,00	0,95	0,56	
A040420_05	68300	68400	-2,20	1,06	0,97	BQ
A040425_00	27300	27400				no DEM
A040425_01	28200	28300				no DEM
A040425_02	29350	29450				no DEM
A040425_03	30100	30200				no DEM
A040425_04	31200	31300				no DEM
A040502_00	/	/	/	/	/	BQ
A040502_01	69220	69320	-1,13	0,99	0,14	
A040502_02	69830	69930	-1,28	1,21	7423,00	noisy
A040502_03	70800	70900	-1,19	1,40	0,24	noisy
A040502_04	73790	73890	-1,41	0,88	0,12	
A040502_05	78565	78582	-1,06	0,85	0,06	RUNWAY LM
A040502_05	78133	78155	-1,06	0,86	0,07	RUNWAY HM
A040505_00	68100	68200	-1,01	2,88	0,37	BQ
A040505_01	70990	71060	-1,00	1,02	31767,00	BQ
A040505_02	/	/	/	/	/	BQ

A040505_03	72577	72584	-1,26	0,66	0,07	RUNWAY HM / BQ
A040505_03	72900	72913	-1,12	0,46	0,94	RUNWAY LM / BQ
A040506_00	47950	48050	-0,89	2,85	0,36	BQ
A040506_01						Missing data
A040506_02						Missing data

Table 5.8-12 CryoVex2004B - ASIRAS time shifts and difference to ALS-DEM

Logfile	STARTIME	STOPTIME	TIME SHIFT	MEDIAN	STDDEV	COMMENT
A040904_00	45300	45350	0,00	1,14	3284,55	BQ / + DEM
A040904_01	45570	45640	0,00	0,96	0,49	BQ / + DEM
A040904_02	45950	46050	0,00	1,08	133,00	BQ / + DEM
A040904_03	46300	46360	0,00	1,11	0,20	
A040904_04	/	/	/	/	/	BQ DEM
A040904_05	/	/	/	/	/	BQ
A040904_06	47220	47320	0,20	0,96	0,16	BQ
A040904_07	/	/	/	/	/	BQ / + DEM
A040904_08	/	/	/	/	/	RUNWAY BQ
A040909_00	57900	58000	-0,89	1,05	0,29	
A040909_01	/	/	/	/	/	BQ
A040909_02	58790	58850	-0,82	1,00	0,37	BQ / Roll
A040909_03	59800	59900	-0,06	0,92	0,17	
A040909_04	/	/	/	/	/	BQ / + DEM
A040909_05	/	/	/	/	/	RUNWAY BQ / + DEM
A040911_00	63970	64070	-1,00	0,77	0,16	BQ LD90
A040911_01	64700	64780	-1,00	0,84	0,16	BQ LD90
A040914_00	/	/	/	/	/	BQ
A040914_01	54905	54915	-1,30	0,70	0,46	RUNWAY HM / DEM BQ
A040914_01	66105	66117	-1,30	0,84	0,45	RUNWAY LM
A040914_02	58000	58100	-1,13	0,98	0,14	
A040914_03	59650	59750	-1,02	0,98	0,08	
A040914_04	/	/	/	/	/	BQ
A040914_05	/	/	/	/	/	BQ
A040914_06	/	/	/	/	/	BQ
A040914_07	/	/	/	/	/	BQ
A040916_00						GPS missing
A040916_01						GPS missing
A040916_02						GPS missing
A040917_00	53000	53100	-1,00	0,96		

Table 5.8-13 CryoVex2004A - LD90 time shifts, squint angles and difference to ALS-DEM. Solution for squint angles is printed in bold characters at the bottom.

Logfile	STARTIME	STOPTIME	LD90 TSHIFT	LD90 ROLL	LD90 PITCH	DIFF MEDIAN	DIFF STDDEV
A040419_00	45300	45350	-1,14	-0,07	-1,02	0,03	0,03
A040419_01	45570	45640	-1,14	-0,18	-0,99	0,02	0,02
A040419_02	56360	56420	-1,14	-0,22	-1,12	0,02	0,02
A040419_03	57000	57100	-1,14	-0,22	-1,10	0,02	0,02
A040419_04	57900	58000	-1,14	-0,17	-1,14	0,02	0,02
A040419_05	58570	58660	-1,14	-0,17	-1,11	0,02	0,02
A040419_06							
A040419_07	59800	59850	-1,14	-0,16	-1,10	0,03	0,03

A040419_08	60200	60300	-1,14	-0,19	-1,11	0,02	0,02
A040420_00	/	/					
A040420_01	62400	62500	-1,14	-0,18	-1,10	0,02	0,02
A040420_02	63550	63650	-1,14	-0,16	-1,12	0,02	0,02
A040420_03	65020	65060	-1,14	-0,19	-1,10	0,03	0,03
A040420_04	66100	66200	-1,14	-0,18	-1,11	0,03	0,02
A040420_05	68300	68400	-1,14	-0,18	-1,10	0,05	0,05
A040425_00	27300	27400					
A040425_01	28200	28300					
A040425_02	29350	29450					
A040425_03	30100	30200					
A040425_04	31200	31300					
A040502_00	/	/					
A040502_01	69220	69320	-1,14	-0,13	-1,11	0,03	0,03
A040502_02	69830	69930	-1,14	-0,19	-1,11	0,03	0,03
A040502_03	70800	70900	-1,14	-0,15	-1,09	0,04	0,03
A040502_04	73790	73890	-1,14	-0,21	-1,12	0,03	0,03
A040502_05	78100	78160	-1,14	-0,09	-1,10	0,04	0,08
A040505_00	68100	68200	-1,14	-0,15	-1,11	0,03	0,03
A040505_01	70990	71060	-1,14	-0,18	-1,10	0,03	0,02
A040505_02	/	/					
A040505_03	72900	72913	-1,14	-0,14	-1,04	0,02	0,02
A040506_00	47950	48050	-1,14	-0,04	-0,74	0,09	0,09
A040506_01							
A040506_02							
			MEAN	-0,16	-1,08	0,03	0,03
			MEDIAN	-0,17	-1,10	0,03	0,03
			STDDEV	0,043	0,078	0,015	0,018

Table 5.8-14 CryoVex2004B - LD90 time shifts, squint angles and computed difference to ALS-DEM. Solution for squint angles is printed in bold characters at the bottom.

Logfile	STARTIME	STOPTIME	LD90 TSHIFT	LD90 ROLL	LD90 PITCH	DIFF MEDIAN	DIFF STDDEV
A040904_00	45300	45350	-1,14	-0,10	-1,67	0,17	0,18
A040904_01	45570	45640	-1,14	-0,22	-1,50	0,18	0,18
A040904_02	45950	46050	-1,14	0,00	-1,61	0,13	
A040904_03	46300	46360	/	/	/	/	/
A040904_04	/	/	/	/	/	/	/
A040904_05	/	/	/	/	/	/	/
A040904_06	47220	47320	-1,14	-0,13	-1,57	0,14	0,11
A040904_07	/	/	-1,14	-0,22	-1,57	0,30	0,31
A040904_08	/	/	/	/	/	/	/
A040909_00	57900	58000	-1,14	-0,19	-1,64	0,15	0,11
A040909_01	/	/	/	/	/	/	/
A040909_02	58790	58850	-1,14	-0,11	-1,44	0,19	0,16
A040909_03	59800	59900	-1,14	-0,02	-1,61	0,11	0,09
A040909_04	/	/	/	/	/	/	/
A040909_05	/	/	/	/	/	/	/
A040911_00	63970	64070	/	/	/	/	/
A040911_01	64700	64780	/	/	/	/	/
A040914_00	/	/					
A040914_01	54905	54915					
A040914_01	66105	66117					
A040914_02	58000	58100	-1,14	-0,3	-1,83	0,12	0,17
A040914_03	59650	59750	-1,14	0,30	-1,92	0,11	0,10
A040914_04	/	/					

A040914_05	/	/					
A040914_06	/	/					
A040914_07	/	/					
A040916_00							
A040916_01							
A040916_02							
A040917_00	53000	53100	-1,14	-0,17	-1,89	0,09	29
				-0,03	-1,80	0,13	0,45
			MEAN	-0,10	-1,70	0,15	3,39
			MEDIAN	-0,12	-1,67	0,14	0,17
			STDDEV	0,148	0,143	0,054	8,243

5.9 Results, conclusions and recommendations

Results:

Both CryoVex2004a and CryoVex2004B were succesfully accomplished. AWI could show how to determine calibration values and delivers an almost complete data set of processed data.
AWI obtained calibration, validation results which are summarized in the following points:

- ASIRAS offset for both campaigns, determined by two runway over flights is ~85 cm
- Penetration depth of radar echo is ~10-15 cm
- Resolution of internal layering is very dependent on the snow regime and can be clearly identified over dry snow zone along EGIG-line
- OCOG retracker is sensitive to surface and volume scattering and needs improvement especially over refrozen snow and runways
- Aircraft roll above |1°| leads to wrong surface elevation heights after retracking
- ALS-DEM are of high quality over snow and introduced methodology is feasible
- ALS-DEM quality is low over runways when measured in high altitude (1100m)

Recommendations:

Data processing of the CryoVex2004A and CryoVex2004B data has revealed the importance of certain auxiliary measurements, which should be performed carefully during future campaigns:

- flight over runway at beginning and end of each flight in different altitudes in order to verify temporal stability of instruments and their cross calibration.
- once during each installation: overflight of individual building with known geodetic positions of corners to determine squinting angle (two altitudes).
- flights should be longer than 4 minutes to allow cross correlation between different sensors.
- deployment of corner reflectors on runways if possible.
- positions of corner reflectors should be determined more accurately than with a single hand held GPS measurement.

6 Part B.2 CryoVex2005 BoB processing results

6.1 Overview

The processing of the Bay of Bothnia 2005 (BoB 05) data is analogous to the concepts already presented for the CryoVex 2004 campaigns. Accordingly all steps, described in section 5, have been implemented and are not further described here. Instead we present the results of the data processing of the Bay of Bothnia (BoB) campaign and compare them with the in-situ measurements over the validation line.

6.2 Validation areas

Three areas have been selected for calibration and validation of the ASIRAS and laser data.
Buildings near Luneort airport, Germany. The hangar of OPTIMARE Sensorsystems at the airport in Bremerhaven was used to calculate the orientation of the Airborne Laser Scanner (ALS).
Runway of Oulu airport, Finland. The smooth surface of the runway was used to compare ALS data with altimeter data of the single beam laser (LD90) and ASIRAS
Validation line on landfast sea ice, near the island Hailuoto. Several overflights were used to validate the data in different altitudes
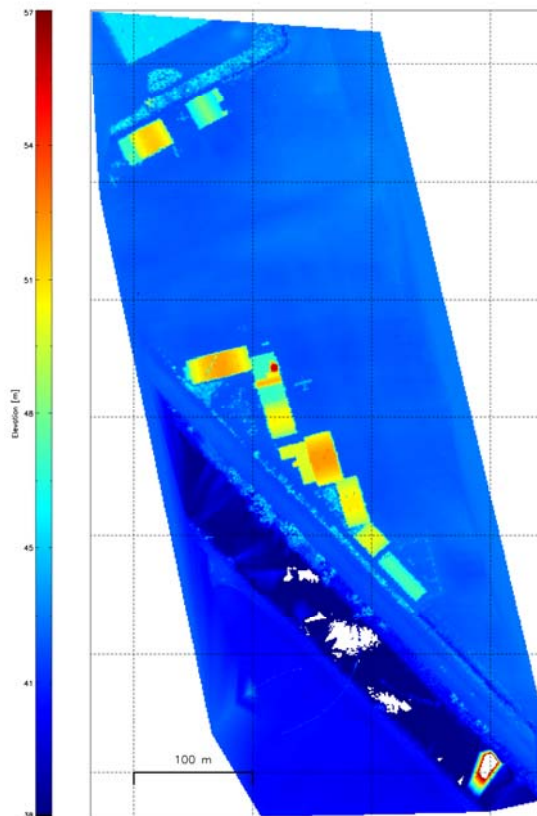
Figure 6.2-1 : Digital elevation model of the buildings at airport Luneort, (CalVal area 1)
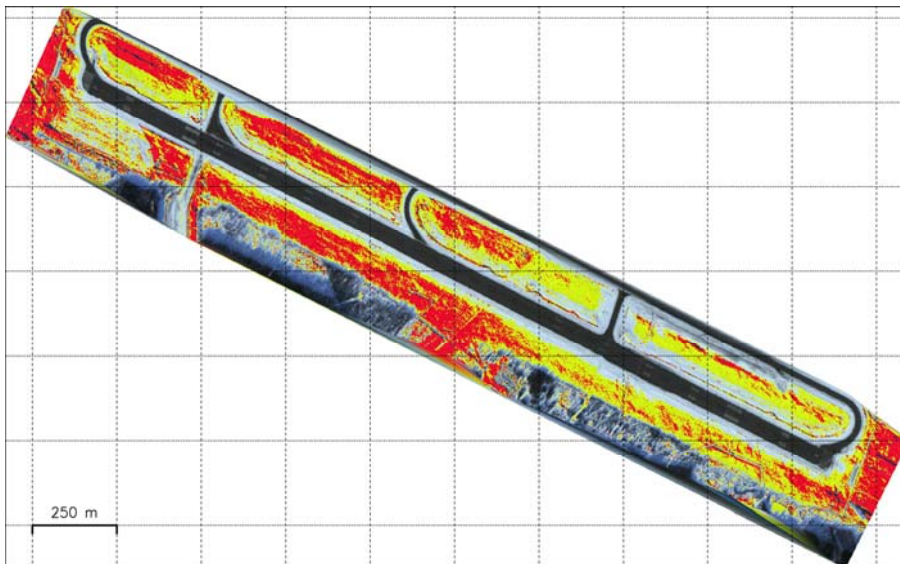
Figure 6.2-2 : True color image of the runway of Oulu airport (CalVal area 2)
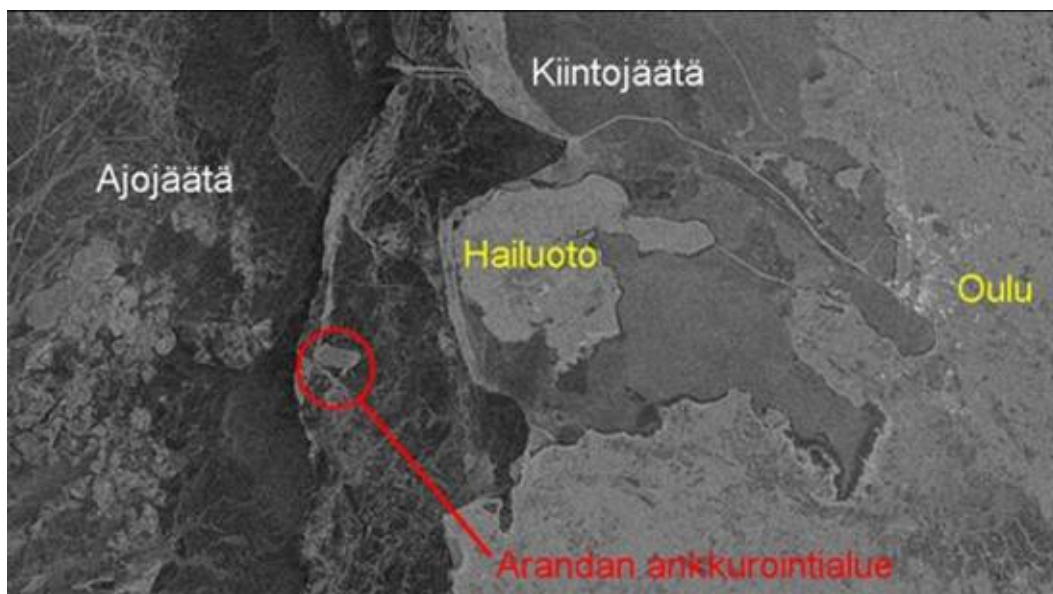
Figure 6.2-3 : SAR image of sea ice close to island Hailuoto. Red circle marks the position of the validation line (CalVal area 3)

While the regions 1 and 2 did not comprise any field work, a large dataset was collected on the ground of the validation area on the sea ice. From March 10 to March 15 the Finnish Research Ice Breaker Aranda anchored to an ice floe in the fast ice close to the island of Hailuoto in the Bay of Bothnia (see Figure 6.2-3).

On this ice floe, a 2200 meter long validation line was established, where snow thickness, ice thickness and freeboard were determined by drilling and surveying. Additionally the validation line was extensively surveyed by airborne EM. Two corner reflectors had been set up on the edges of the validation line. During the whole time the ice on the validation line was static, though a large polynya had opened close by in the later days of the campaign. After a mild winter season 2004/2005, the young first year ice of the validation line was almost snow free, as can be seen in Figure 6.2-8.

The thickness of the ice and the snow layer along the validation line is displayed in Figure 6.2-4. Several prominent pressure ridges can be seen at the center and the eastern end of the line. The drilling profile consists of measurements with irregular point spacing of 1 to 10 meters with higher resolution at the pressure ridges and lower resolution on the level ice and a total number of roughly 420 drill holes.
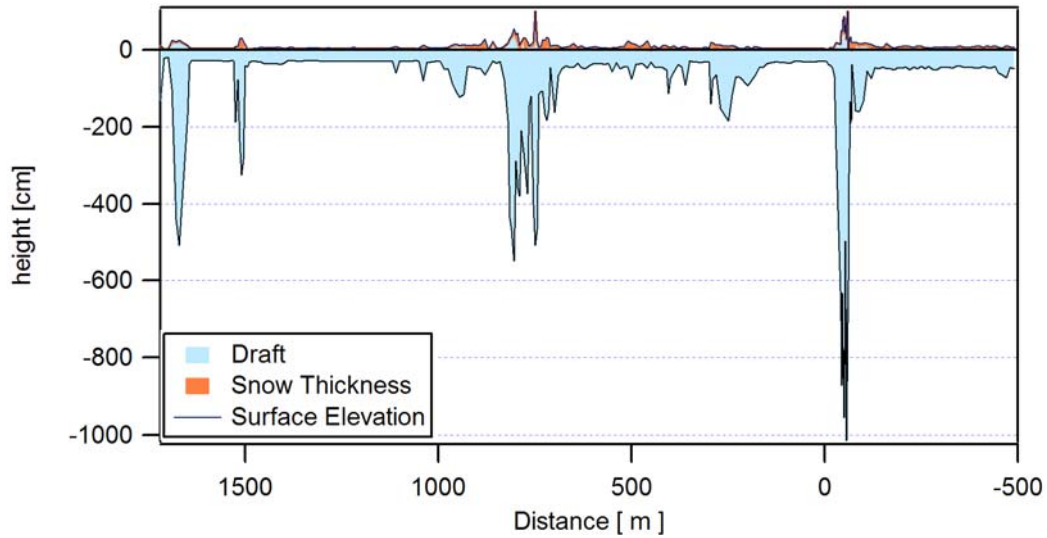
Figure 6.2-4 : Ice thickness and snow depths of the validation line obtained by drilling and levelling

The validation line was surveyed by airborne EM every time after takeoff from RV Aranda. An averaged surface elevation profile, obtained with the bird laser altimeter and a thickness profile is displayed along with the quantities obtained by drilling in Figure 6.2-5 and Figure 6.2-6, respectively. While the surface elevation profiles are in general good agreement, the EM thickness significantly underestimates the real thickness of deformed ice. This effect can be explained by the footprint of the EM signal with exceeds the ridge keel widths and by the keel porosity.
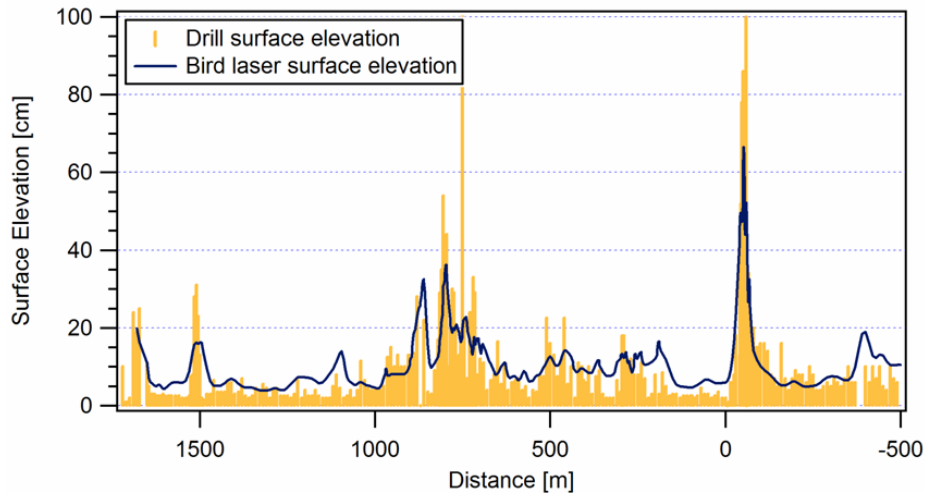
Figure 6.2-5 : Comparison of surface elevation from ground work and EM bird laser altimeter
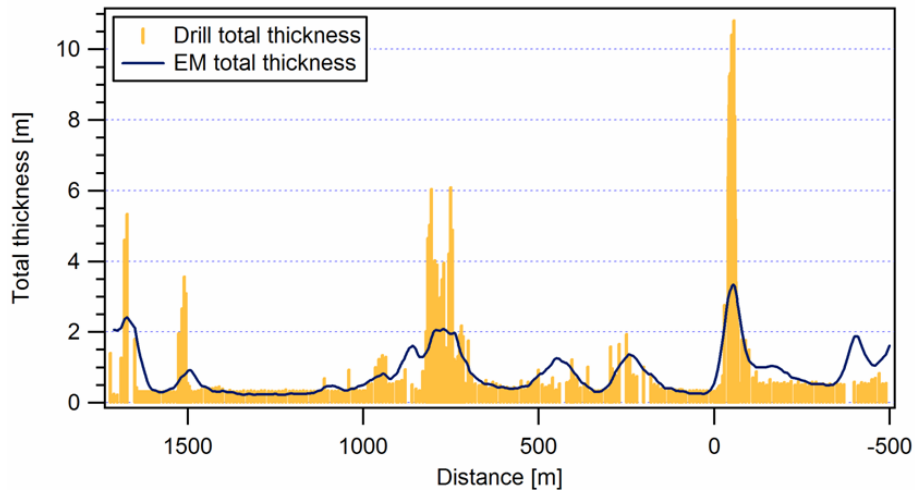
Figure 6.2-6 : Comparison of drilled total thickness and EM total thickness

The validation line was passed by the D-CODE aircraft in altitudes of 300, 500, 700 and 1100 meters (Table 6.9-4), starting with the lower altitudes. Because the laser scanner was not warmed up properly at the beginning of the measurements, a profile at the altitude of 300 meters was repeated.

Additional waypoints at extension points of the validation line were used to optimize the navigation of the aircraft. The flight track of the aircraft is shown in Figure 6.2-7. A second line south of the primary validation line was chosen to be surveyed were additional surface elevation information from levelling and EM ice thickness exist.
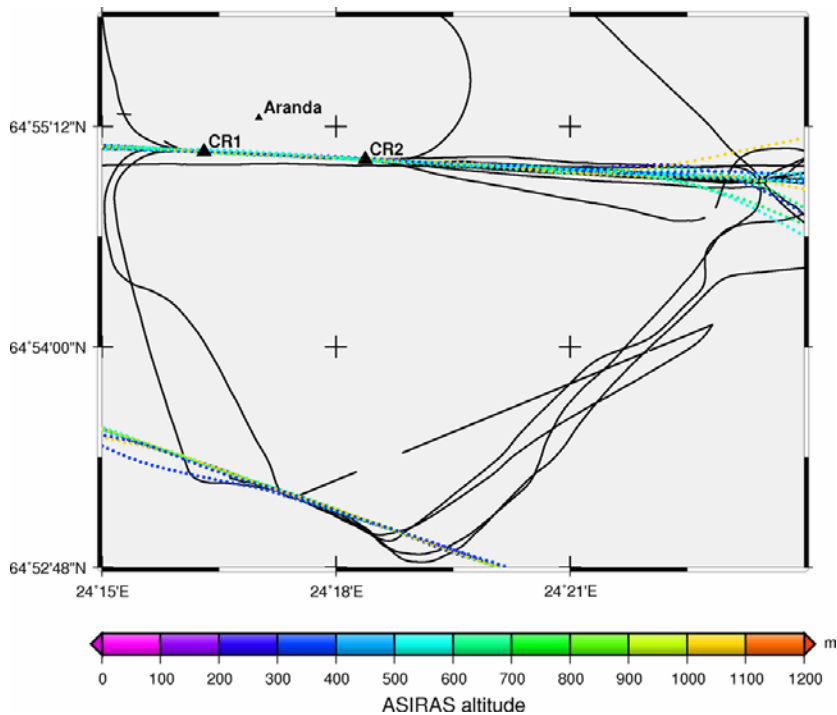
Figure 6.2-7 : Flight track of EM Bird (black) and aircraft (height : colorcoded). The primary validation line is positioned between both corner reflectors (CR1,CR2)

Figure 6.2-8 : Photo of the ice conditions at the validation line (CalVal area 3). The picture shows the eastern end with the eastern corner reflector with line of sight to the west

Two corner reflectors were installed on the ice at the edges of the validation line. Details are given in Table 6.2-1.

	Corner reflector (west)	Corner reflector (east)
Latitude	N 64º55.064	N 64º55.021
Longitude	E 24º16.307	E 24º18.372
Height	191 cm	188 cm

Table 6.2-1: Position of the corner reflectors and height above surface

Figure 6.2-9: Picture of a corner reflector deployment site (east reflector)

6.3 Airborne EM sea ice thickness data

In addition to the primary validation line, sea ice thickness along flight track of the D-CODE aircraft in the northern part of the Bay of Bothnia was surveyed with airborne EM. Both flights were planned for optimal spatial and temporal accordance. An overview is given in Figure 6.3-1.
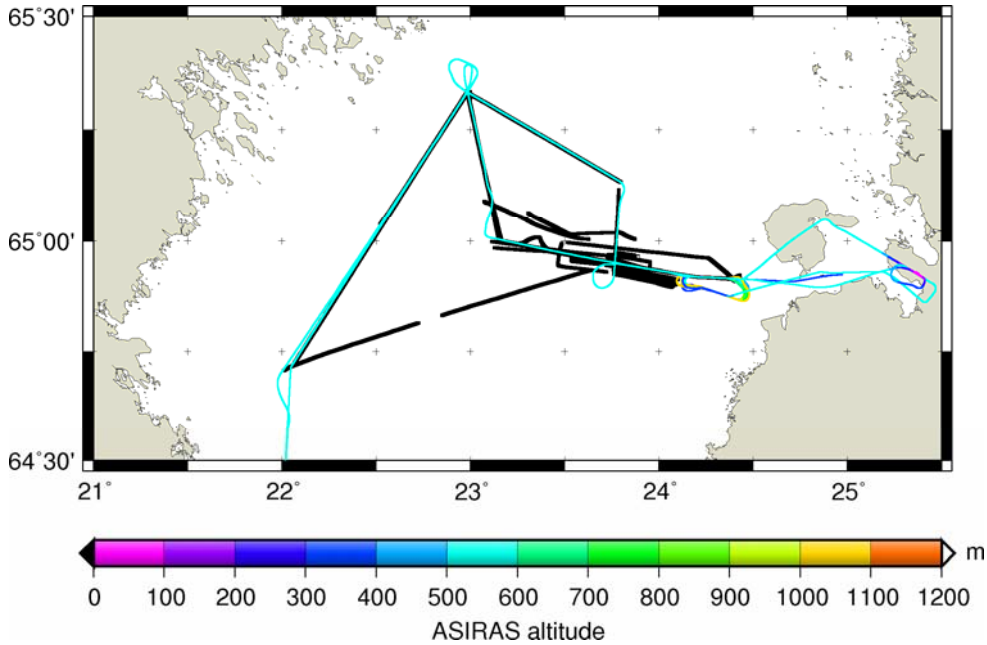
Figure 6.3-1 : Airborne EM flight tracks (black) and ASIRAS profiles in the northern part of the Bay of Bothnia

The aircraft was equipped with a GNS/IGI Navigation system, which allows an navigation accuracy of a few meters. The helicopter pilot used standard GPS navigation. The flight tracks were found to be in good agreement over the validation line, with deviation below 10 m, while some navigational errors of the helicopter lead to larger deviations on some segments of the transfer flights. But on the main part of the profiles good agreement was achieved. Two examples are shown in Figure 6.2-2 (validation line) and Figure 6.3-3 (transfer flight). All EM flights were therefore well within the footprints of the ALS and ASIRAS.
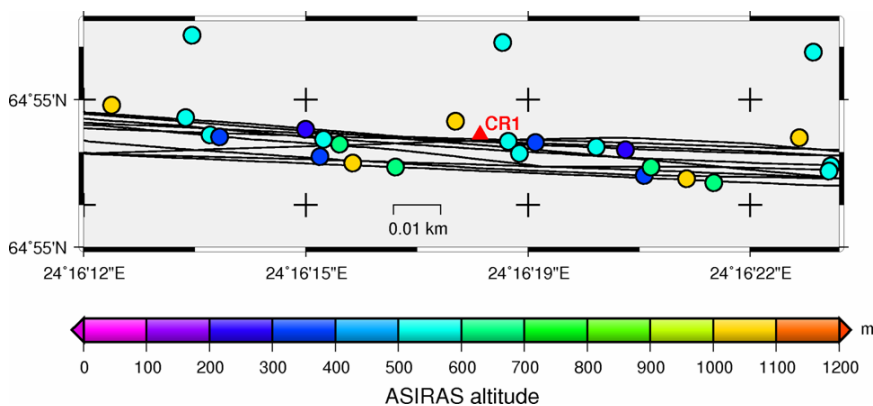
Figure 6.3-2 : Groundtracks of airborne EM (black) and aircraft (color coded circles) along primary validation line near western corner reflector
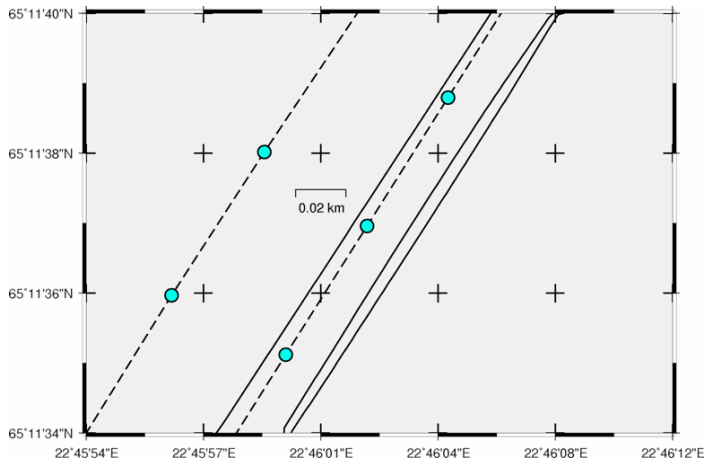
Figure 6.3-3 : Groundtracks of airborne EM (solid lines) and aircraft (dashed line) on transfer flight in western part of the Bay of Bothnia

6.4 Auxiliary data

6.4.1 GPS data

During the BoB 05 campaign no separate GPS receivers were used. Instead, the coordinates of fixed reference stations from the Swedish and Finnish network (see table xxx) were used for post-processing with Trimble Geomatics Office. Both networks refer to the same reference frame.

Table 6.4-1

Day	Reference	Latitude	Longitude	Height (m)
March 13, 14	Skelefton	64.879826167° N	21.048284792° E	58.893 m
	Kalajoki	64.257694128° N	23.948146087° E	24.308 m
March 14	Haukipudas	65.172665059° N	25.358598012° E	27.546 m
March 15	Helmstedt	53.865510675° N	8.701017543° E	33.374 m

Table 6.4-2 : Bay of Bothnia 2005, DGPS reference stations

6.4.2 INS data

The data of Inertial Navigation System (INS) needs to be corrected by a time shift relative to the GPS timestamps. The time shift can be found by a cross correlation of changes in the aircraft attitude, which can also be calculated by the two GPS antennas. Best results were obtained with the changes in pitch and roll angles. The cross correlation had been applied to three flights with different time windows. The result for the different intervals (example: Figure 6.4-1) has proven to be very stable except for aircraft manoeuvres and periods of a few minutes even after the manoeuvres. Therefore it can be concluded that the INS needs time to stabilize after larger pitch and roll angles. This is especially true for the repeated flights over the primary validation line were the aircraft performed full turns every 5 to 10 minutes. Therefore deviating results for the INS time shift after turns are neglected and the results are assumed to be constant for the whole campaign.

$t_{GPS} = t_{INS} - 1.04$ sec
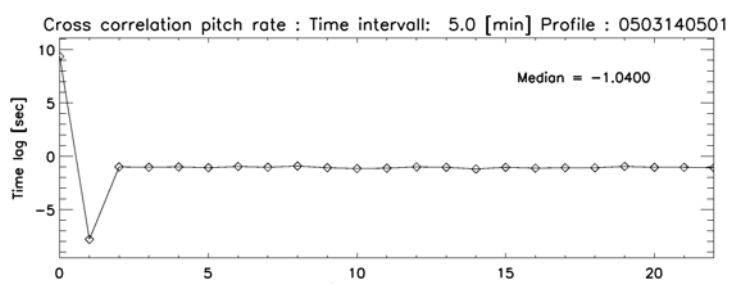
Figure 6.4-1 : Result of the cross correlation of INS and GPS pitch rate in transfer flight from Oulu to Stockholm. INS is heavily disturbed short after takeoff.

6.5 LMS – Q280 Airborne Laser Scanner

The data processing of the raw Airborne Laser Scanner (ALS) data requires knowledge of the time shift relative to GPS time, the positions of GPS and ALS and the instrument orientation. The

instrument position (summarized in section 2.1) was measured at the installation, while the orientation is initially unknown.

6.5.1 Time shift

From previous campaigns the time shift was found to be – 1.0 sec. This value has been found to be very suitable for the BoB 05 campaign for all flight days as well, because no INS artefact was observed in digital elevation models of each day.

6.5.2 Instrument orientation

The orientation of the laser scanner was obtained in the calibration- and validation area 2 in Luneort, Germany. Two perpendicular flights over the same building were used for an iterative approach for the calculation of three angles (squinting angles) which define the instrument orientation. The procedure is described in detail I section 5.5 and is shortly summarized here:

Create a digital elevation model for both overflights
Manual identification of the position of prominent features like corners of buildings in both DEM's
Finding the closest ground position of a laser beam to these features
Minimize the position between both DEM's with a Newton approximation
Designated squinting angle is represented by the convergence of the Newton approximation

Date	March, 15, 2005
1. overflight (North – South)	12:13:29 – 12:13:34
2. overflight (West – East)	12:15:50 – 12:15:54

Table 6.5-1 : Time window of building overflights at Luneort airport
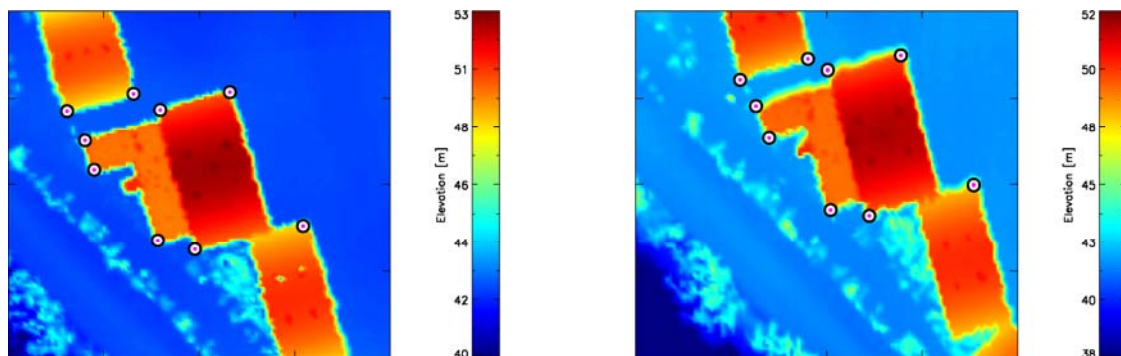
Figure 6.5-1 : Digital elevation models of both overflights (left: north - south, right: east - west). Circles mark the position of closest laser beam to the corners.

The Newton approximation allows only the simultaneous calculation of 3 corner positions. Therefore several runs with independent permutations of the 9 corners were performed. A "triangle" configuration was preferred to a "line" configuration of the selected corner positions. The resulting squinting angles are displayed in Table 6.5-2.

Squint Angle [deg]		± 1 σ
ξ_x	0.1182	0.0874
ξ_y	-2.2407	0.0609
ξ_z	-0.5032	0.7086

Table 6.5-2 : LMS - Q280 Airborne laser scanner: Instrument orientation (cf.Table 5.8-1)

The angles ξ_x and ξ_y describe the angular offset from the nadir direction, while ξ_z describes the tilt angle of the instrument. The tilt angle has the highest uncertainty. It can not be ruled out that inaccurate instrument positions lead to an ambiguous result of the Newton approximation. Additionally only one cross flight was performed, limiting the calibration process of the instrument orientation only to a single altitude. The erroneous of the tilt angle can also be observed in the difference of corrected digital elevations models of the building.
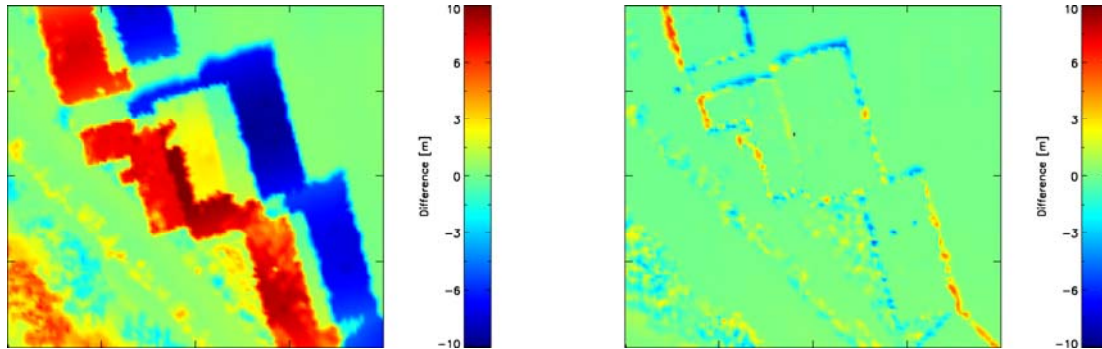
Figure 6.5-2 : Difference of DEM's of both overflight (left : uncorrected, right : corrected for instrument orientation)

Though the overall agreement of both digital elevation models is very good as can be seen in Table 6.5-3, a small systematic deviation remains. The positive and negative difference in the right part of Figure 6.5-2 may be removed with a slightly different tilt angle. But nevertheless the difference at the edges of the buildings is very close to the size of the laser beam offset and the elevation difference of the basement, which is represented by the median value in front of the hangar being almost zero.

DEM difference : Mean	1.3 ± 81.0 cm
DEM difference : Median	0.9 cm

Table 6.5-3 : Difference in digital elevation models of cross flights

Since the over flight in Luneort represents only a single altitude, a final test is applied at the validation area 3. This area had been surveyed in 4 different altitudes with the ALS on March 14. From these profiles 4 passes are selected and digital elevation models are created in a box with coverage at all altitudes. From these 4 digital elevation models a model is created with the mean values and the standard deviation of each grid point. The result is displayed in Figure 6.5-3:
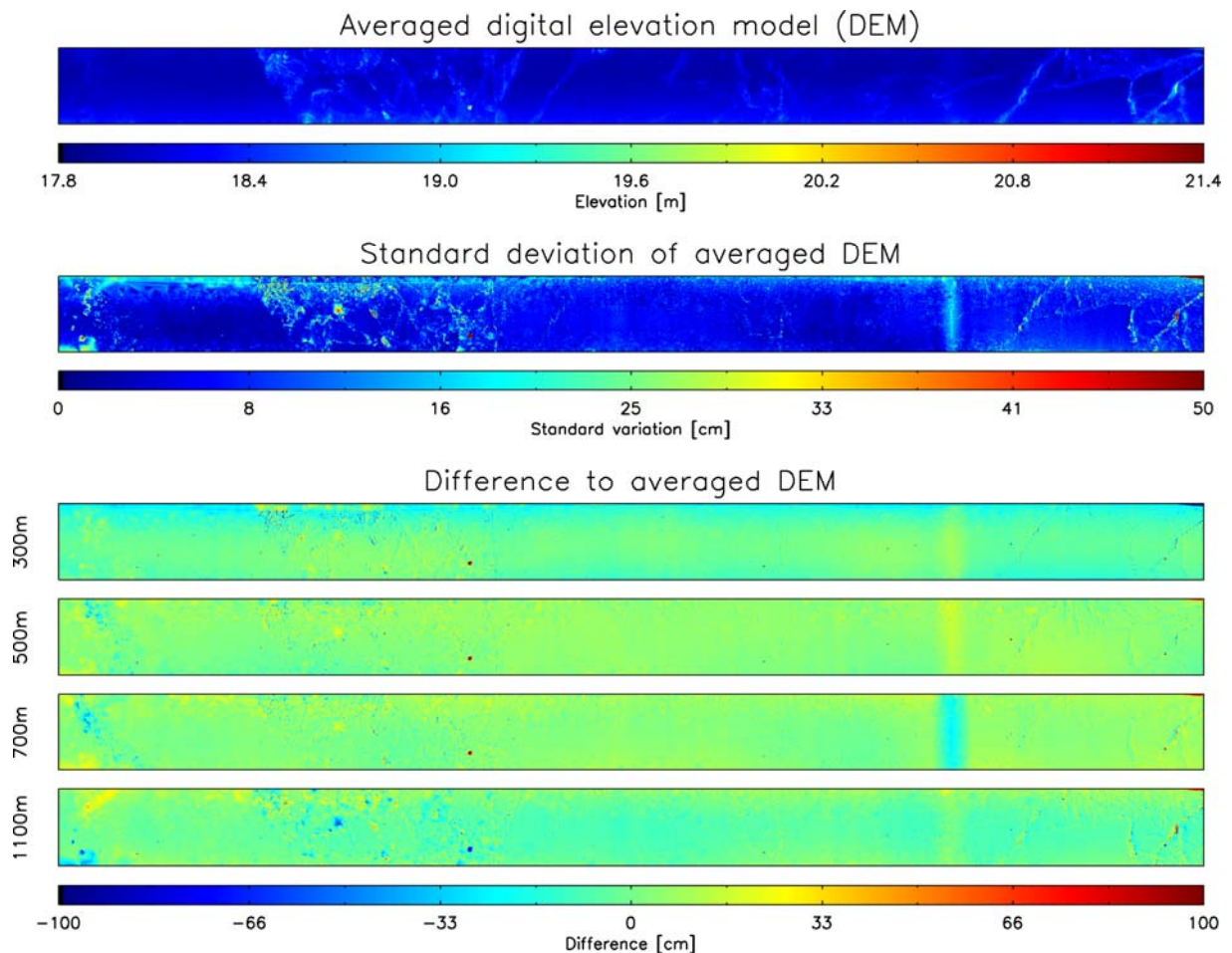
Figure 6.5-3 : Digital elevation model of the primary validation line (upper plot to lower plot: Mean DEM, Standard deviation of mean model, difference of model in different altitudes to mean model)

The mean digital elevation model shows mostly undeformed level ice, with some elevated deformed ice regions. The standard deviation of the mean model is, as expected, highest along the deformed ice and along the northern limit, which may be related to the laser return quality of a certain profile at higher scanner angles. For displaying convenience the maximal standard deviation is limited to 50 cm, with only a few spikes removed. The color coding of the difference between the original digital elevation models and the mean model reveal no large deviation. Therefore the mean elevation and the median of each model is calculated and plotted versus aircraft altitude in Figure 6.5-4. Though the deviations between the single models amount to 10 cm, no systematic error as a function of aircraft altitude can be observed. The difference may again be caused by the inaccurate instrument tilt angle, which may have different effects depending on the roll angle of the aircraft and the altitude.

As a final test the digital elevation models are validated with data from the laser altimeter onboard the airborne EM system. This dataset does not reveal the actual surface elevation because the elevations are related to level ice surface. However, the comparison is very useful to validate the position of some prominent pressure ridges (Figure 6.2-5). For the comparison, the ground track of laser roughness profile is extracted of each digital elevation model. The results can be found in the appendix (Figure 6.10-6 to Figure 6.10-9) . A very good agreement between the position of the prominent ridges is achieved for each altitude. The largest deviations are related to random laser returns over deformed ice and the fact that the EM laser profile is no real surface elevation profile.
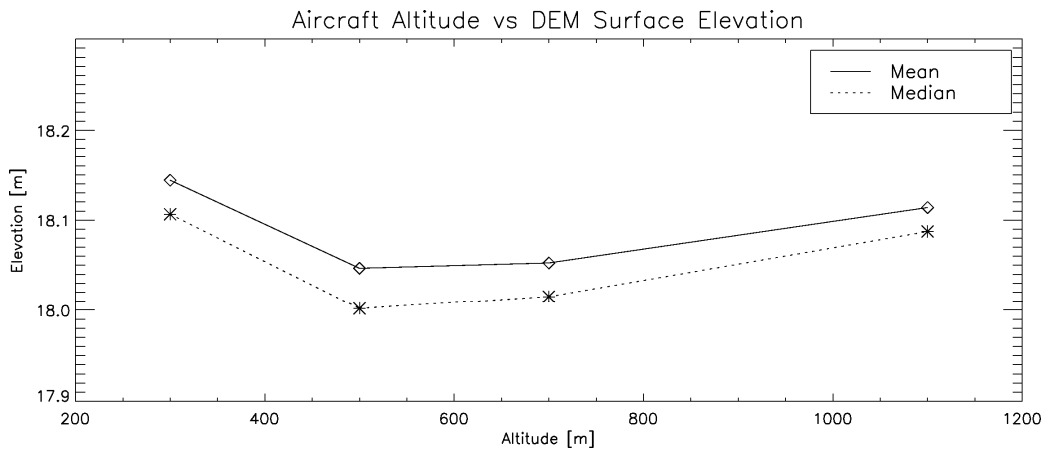
Figure 6.5-4 : Mean surface elevation and median for different digital elevation models versus aircraft altitude

From the comparisons it can be concluded, that the orientation of the laser scanner could be calculated with satisfactory accuracy, though more validation possibilities, e.g. several cross flight at different altitudes are highly desirable for future campaigns.

6.6 LD90 single beam laser altimeter

The calculation of the instrument orientation and time shift depends crucially on the quality of the digital elevation models. A calculation of the time shift by means of a cross correlation of the change in laser range with the change of aircraft GPS altitude is found to be unreliable because the results vary between +- 0.5 s. Therefore the time shift and orientation is calculated simultaneously with a Newton approximation, minimizing the difference between a digital elevation model and the single beam laser surface elevation.
Because of the ambiguity of time shift and squint angle a clearly defined profile is needed for a reliable result. The profiles over sea ice don't fulfil this requirement because of random backscatter along deformed ice, which leads to too high values for the difference of both profiles for the approximation. But the overpass over the runway at Oulu airport is very suitable. The results of the Newton approximation for both time shift and instrument orientation are summarized in Table 6.6-1. Because of the rotational symmetry of a single beam, only 2 angles, describing the offset from the nadir direction are needed.

ξ_x	- 0.1422 deg
ξ_y	0.1894 deg
Δt	-1.12 sec

Table 6.6-1 : Ld90 single beam laser altimeter : time shift relative to GPS time and instrument orientation (cf. Table 5.8-1).

6.7 Inter - laser comparison

As described in the previous section the quality of the single beam laser data depends already on the accuracy of the laser scanner. But nevertheless, a comparison of both data sets at different altitudes should reveal erroneous instrument orientations or time shifts. Therefore the difference in surface elevation for the 4 different altitudes between the digital elevation model and the single beam laser is calculated. The results are displayed in the appendix in Figure 6.10-1 to Figure 6.10-5 and summarized in Table 6.7-1.

Profile	Mean [cm]	1 [cm]	Median [cm]
#25 (300 m)	1.44	5.21	1.11
#15 (500 m)	-0.85	4.96	-0.57
#17 (700 m)	-1.18	6.08	-1.54
#25 (1100 m)	-0.35	8.89	-1.03

Table 6.7-1 : Statistical parameters of inter - laser comparison for different aircraft altitudes

The mean and median of the difference between both lasers are for all heights smaller than 2 cm. Only standard deviations are larger, which is mainly caused by deformed ice. The total variance with the altitude is also very small. The median value represents the difference in the level ice. It changes with roughly 2 cm at an altitude difference of 1000 m, which is assumed to be within the range of the instrument error.
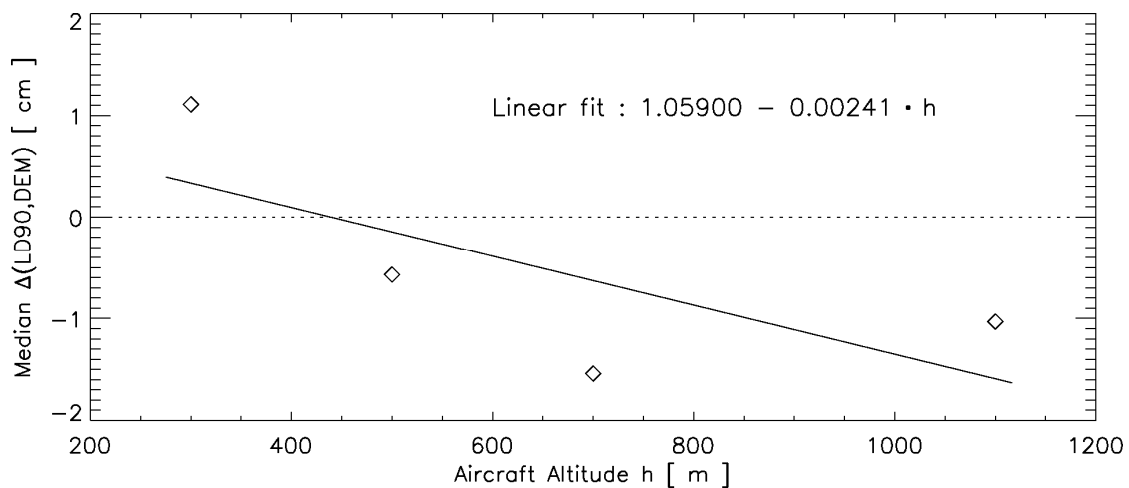
Figure 6.7-1 : Median of the difference of digital elevation model and single beam laser altimeter as a function of aircraft altitude

Over the runway in Oulu, the site of the instrument calibration, the median of the difference of LD90 and ALS amounts to -0.5 mm, which is a surprisingly small value (Figure 6.10-1). But while the statistical quantities compare very well, some local deviations between both instruments can be observed in the Figure 6.10-1 to Figure 6.10-5. These appear mostly random, but the digital elevation data seams to be more smoothed, while the elevation, retrieved from the single beam laser appear rougher. This may be related to the creation of the digital elevation model as a smoothing operation or the difference in instrument performance.

As a conclusion it can be highlighted from the inter – laser comparison, that the processed laser data can be used as a reliable source for the ASIRAS validation, though local deviations exists.

6.8 ASIRAS data

During BoB 2005 the Low Altitude Mode (LAM) was used for the first time in a field campaign. Therefore, the principal task was to prove the applicability of the instrument.

6.8.1 Processing

The ASIRAS data has been processed with software provided by ESA. The version of the processor used for this delivery is 3.03. Based on the large LAM data volume, the processor showed low performance on some profiles, needing up to 36 hours for a single profile (Used System : 2 CPUs XEON 2.4 GHz, 2 GB main memory [Linux]). All profiles are processed with an Offset Center Of Gravity (OCOG) retracker. This retracker proved to be very sensitive to roll manoeuvres, resulting in significantly large deviation from the actual surface elevation at roll angles > 1°. This leads to reduced data quality in most of the profiles.
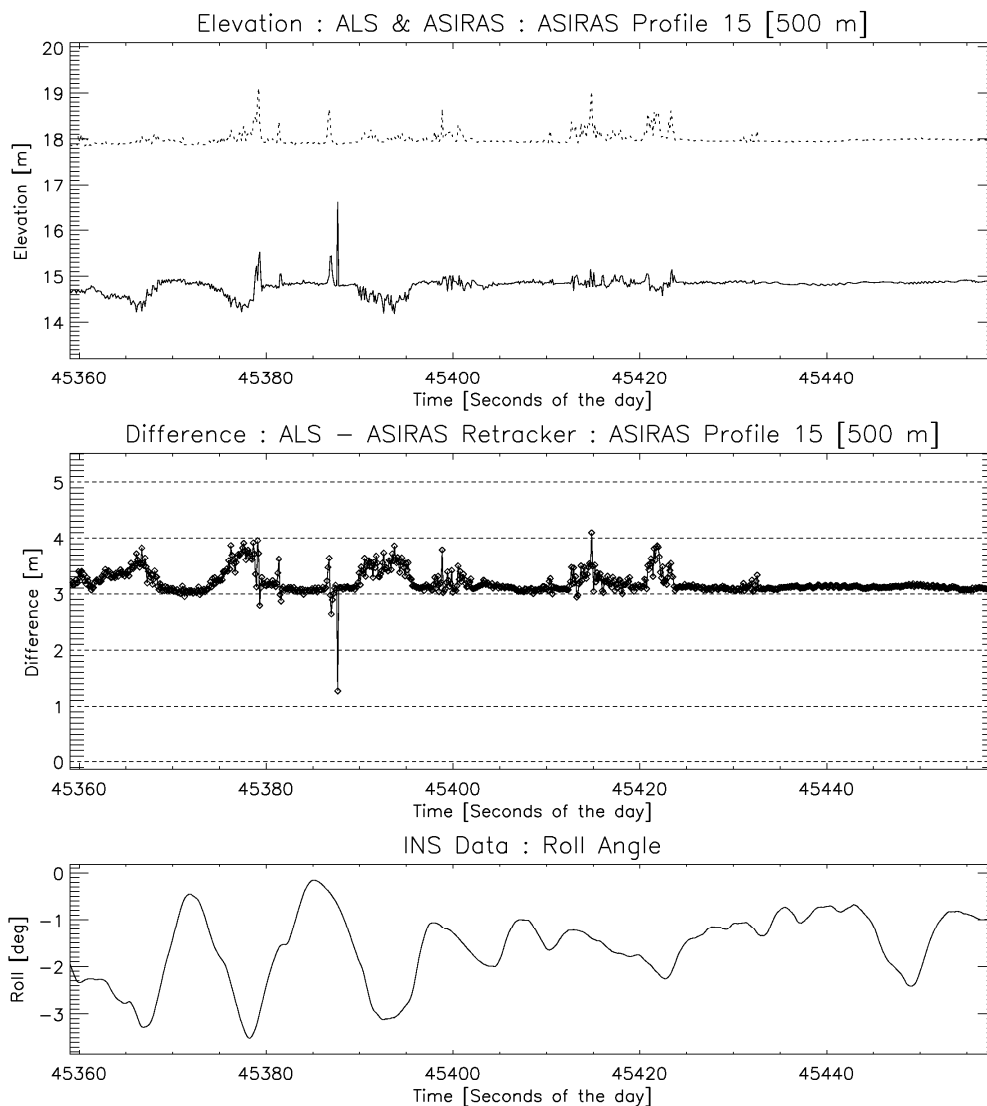
Figure 6.8-1 : Difference of digital elvation model and ASIRAS surface elevation and INS roll angle

Figure 6.8-1 shows an example of how the difference of an ASIRAS surface elevation profile deviates from a digital elevation model at roll events.
The processor failed for two profiles, because of unknown problems during data acquisition.

6.8.2 Time shift

The method of obtaining the time shift relative to GPS time is identical to the single beam laser. Unfortunately the retracker problem at larger roll angles leads to a significant deviation of the ASIRAS profile and the digital elevation model, which leads to a failure of the Newton approximation to converge over sea ice. An estimation of the time shift over the runway was successful, resulting in a value of

$t_{GPS} = t_{ASIRAS} - 1.12$ sec

It is known from the CryoVex 2004 campaigns that the ASIRAS time shift may vary for different profiles. Therefore the applicability of this value may be limited for the whole campaign. But the impact of a slightly wrong time shift is small compared to the deviation caused by the retracker problem.

6.8.3 Accuracy of corner reflector height retrievals

The relative accuracy of the retrieved surface elevation can be tested at the corner reflectors along the validation line. The height of both reflectors above the ice surface was measured with a ruler stick during the field campaign (Table 6.8-1). The corner reflectors are not clearly visible in all ASIRAS profiles, therefore one profile is selected representative of each reflector.

	Height [cm]	ASIRAS [cm]	Profile
Corner reflector (west)	191	190	#13
Corner reflector (east)	188	189	#9

Table 6.8-1 : Corner reflector height above ice surface

The example shows that a relative accuracy in centimetre range can be achieved with ASIRAS in the low altitude mode.
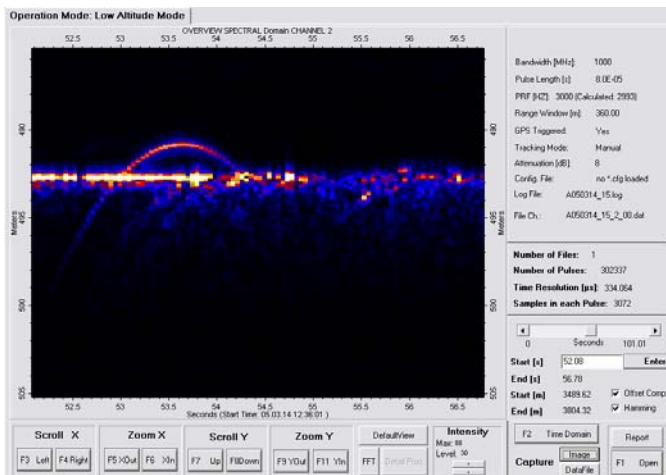
Figure 6.8-2: Corner reflector response in the ASIRAS raw data

6.8.4 ASIRAS - Laser comparison

The ASIRAS surface elevation profiles cannot be compared to a digital elevation model at all altitudes, because was only operational later during the measurements after it had warmed up. The result of three comparisons is presented in the following: #15 at 500m, #17 at 700 m and the calibration pass

over the Oulu runway (see Figure 6.10-10 to).

A characteristic feature of the comparisons is an offset of roughly 3.2 meters between the ASIRAS surface elevation and the digital elevation model. Because of the high accordance of the single beam laser and the laser scanner, it is assumed that this offset is caused by the ASIRAS instrument. The offset varies somewhat in the range of a few centimetres, but seems to be constant for each individual profile. However, the positions of the sea ice pressure ridges match very nicely, showing that the differences between ALS and ASIRAS surface elevations are not caused by time shift errors. For user convenience, the offset should be removed in the next version of the ASIRAS processor.

## 6.8.5 ASIRAS roll angle sensitivity

The roll angle sensitivity of the retrieved surface elevation, in particular in the LAM, has already been discussed in the previous sections. This effect has important implications for the data processing itself, which are discussed briefly in this section.

The processor (v3.03) raises a flag at roll angles greater than ± 1 degree, which happens very frequently throughout a profile (see bottom plot of Figure **6.8-3** as an example). The value of 1 degree is chosen arbitrarily and not based on any kind of analysis. Using the flagged out data leads to a great reduction in data volume and numerous discontinuities. This also strongly hampers calculations of the time shift for the ASIRAS profiles. This fact emphasises again the need for sufficiently long profiles and as few aircraft manoeuvres as possible.

The threshold value of ± 1 degree may need to be revised. As can be seen in figure Figure 6.8-1 differences arise between the ASIRAS and ALS elevations at roll angles < - 2 degree. Therefore it could be feasible to double the threshold value, which will increase the amount of usable data without inducing significant errors.

An example for the consequences of even larger roll angles is given on the right hand side of Figure 6.8-3. At the end of the pass over the runway in Oulu when the aircraft performed a quick turn, roll angles up to – 15 degree did occur. As to expected, the retracker fails in retrieving the surface elevation at this kind of manoeuvres and flags the data correctly, because of a blurry echo power (Figure 6.8-4 and Figure 6.8-5). But because these events are rather rare and the processor handling is working fine for this case, future efforts should concentrate on the range of relative small roll angles of about approximately 2 – 5 degree. A more robust retracker for this range will decrease the amount of work for the processing and significantly increase the scientifically useful data volume.
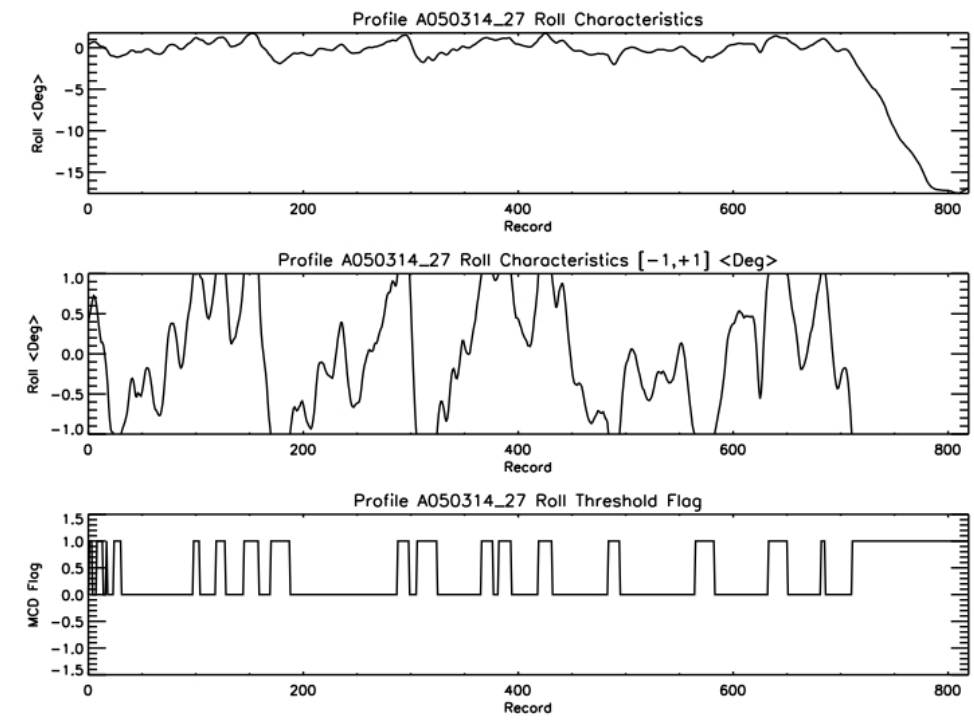
Figure 6.8-3 : Roll angle for ASIRAS profile #27 (Oulu runway). From top to bottom : roll angle, roll angle within processor limits, roll angle limit flag).
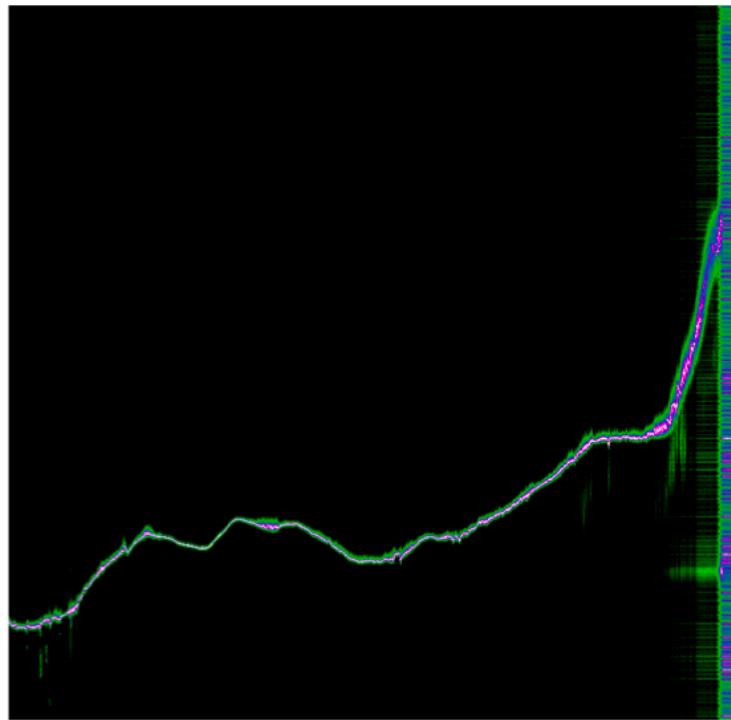
Figure 6.8-4 : Echoe power waveforms for ASIRAS profile #27 (Oulu runway).
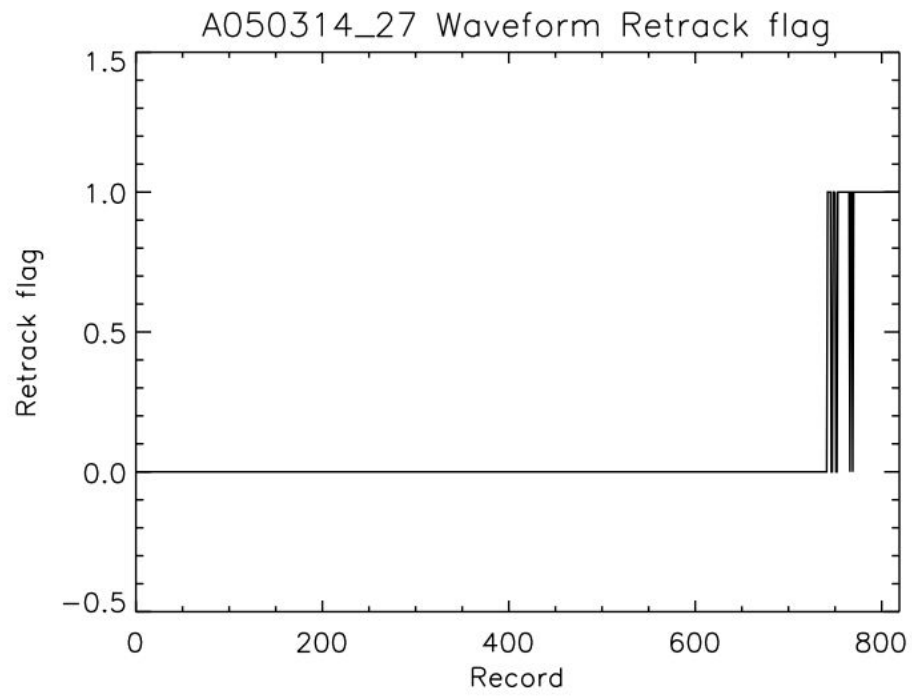
Figure 6.8-5 : Retracker flag for ASIRAS profile #27 (1 = no retracking possible; Oulu runway).

6.8.6 Summary

Significant progress has been made since the initial version of the processing software. But the main problem to be addressed in future campaigns for the low altitude mode data is the development of a less roll dependent retracker. The deviations caused by aircraft roll still prevent accurate comparisons of laser and radar surface elevation data over sea ice at the moment. If this problem is solved, the comparisons made with the digital elevation models show that the retrieval of detailed surface elevation profiles of sea ice is absolutely feasible in low altitude mode.
It is highly recommended for future campaigns that aircraft manoeuvres are reduced to an absolute minimum close to sites of great scientific interest. In addition, the cause of the offset in surface elevation between radar and laser should be identified, either in hardware or software, and should be considered with the ASIRAS processing software for processing convenience.

6.9 Processed data

This section gives an overview of the processed data and coverage of laser and radar for the Bay of Bothnia 2005 campaign. All times are in UTC. The tables also refer to the flights summarized in section 4.

Profile ID	Day	Start time [UTC]	Stop time [UTC]	Covered ASIRAS profile
0503130301	2005-03-13	17:00:25	18:11:38	#8 - #10
0503140403	2005-03-14	12:29:25	13:52:50	#15 - #27
0503140501	2005-03-14	15:10:11	17:38:15	#30 - #38
0503150601	2005-03-15	11:17:41	12:19:52	-

Table 6.9-1 : LMS Q280 airborne laser scanner level 1b products

Profile ID	Day	Start time [UTC]	Stop time [UTC]	Covered ASIRAS profile
0503130301	2005-03-13	14:53:02	18:08:49	#7 - #10
0503140403	2005-03-14	12:04:27	13:49:18	#9 - #27
0503140501	2005-03-14	15:25:43	17:37:56	#30 - #38
0503150601	2005-03-15	12:05:40	12:16:52	-

Table 6.9-2 : LD90 single beam laser altimeter level 1b products

Profile #	Start time	Stop time	Altitude [m]	Description
7	16:27:59	16:46:17	500	-
8	16:55:28	17:30:41	500	-
9	17:40:00	17:54:42	500	-
10	17:59:14	18:07:56	500	validation line

Table 6.9-3 : ASIRAS level 1b products. Transfer flight Stockholm – Oulu (Flight ID : 0503130301)

Profile #	Start time	Stop time	Altitude [m]	Description
8	11:59:05	12:02:00	300	2. line
9	12:06:58	12:07:58	300	validation line
10	12:07:58	12:13:32	300	2. line
11	12:16:04	12:18:48	300	validation line
12	12:21:34	12:22:14	300	2. line
13	12:27:19	12:28:32	500	validation line
14	12:31:30	12:32:39	500	2. line
15	12:35:59	12:37:39	500	validation line
16	12:40:14	12:41:57	500	2. line
17	12:45:54	12:47:40	700	validation line
18	12:50:19	12:52:03	700	2. line
19	12:55:09	12:57:16	700	validation line
20	12:59:37	13:01:35	700	2. line
21	13:04:58	13:07:14	1100	validation line
22	13:10:35	13:11:59	1100	2. line
23	13:15:06	13:17:20	1100	validation line
24	13:19:51	13:21:58	1100	2. line
25	13:24:39	13:27:10	300	validation line
26	13:29:30	13:30:42	300	2. line
27	13:45:30	13:47:06	500	Oulu runway

Table 6.9-4 : ASIRAS level 1b products. Flights over validation lines (Flight ID = 0503140403)

Profile #	Reason
25	Assumed : Incorrect instrument usage
26	Assumed : Incorrect instrument usage

Table 6.9-5 : List of non processible ASIRAS files

Profile #	Start time	Stop time	Altitude [m]	Description
30	15:29:05	15:30:51	500	-
31	15:31:14	15:39:16	500	-
32	15:41:31	15:42:59	500	-

Table 6.9-6 : ASIRAS level 1b products. Transfer flight Oulu - Stockholm (Flight ID: 0503140501)

Timeshift INS	Timeshift LD90	Timeshift LMS Q280	Timeshift ASIRAS
-1.04 sec	-1.12 sec	-1.00 sec	-1.12 sec

Table 6.9-7 : Overview : Instrument time shift

	LMS – Q280	LD90
$_x$ [°]	0.1182	- 0.1422
$_y$ [°]	-2.2407	0.1894
$_z$ [°]	-0.5032	0.0

Table 6.9-8 : Overview : Instrument angular orientation

6.10 Appendix : Bay of Bothnia 2005 Campaign

6.10.1 Inter – Laser comparisons
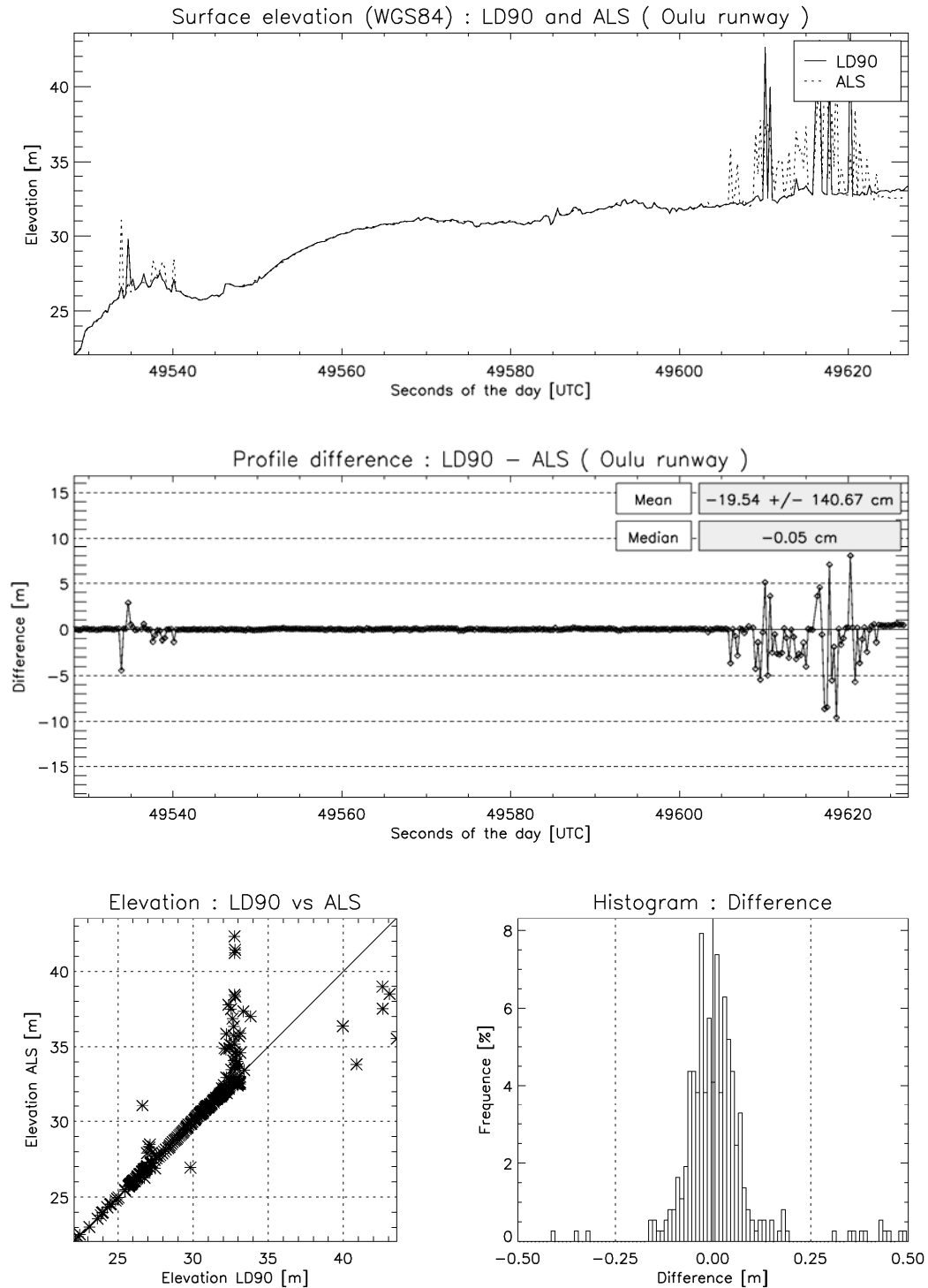
Figure 6.10-1 : Comparison of single beam laser and coincident ALS surface elevation profile (Oulu runway)
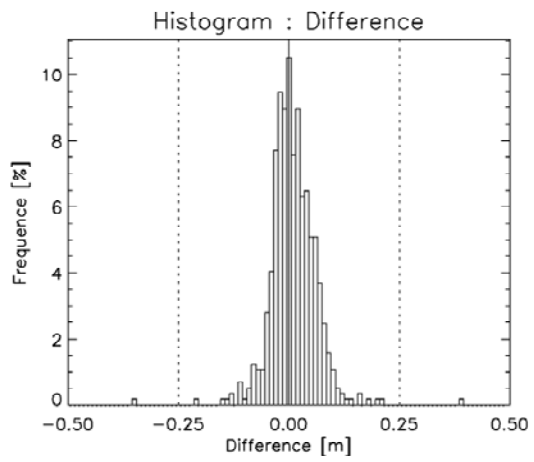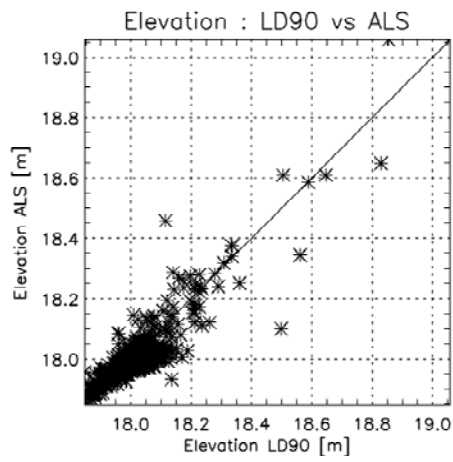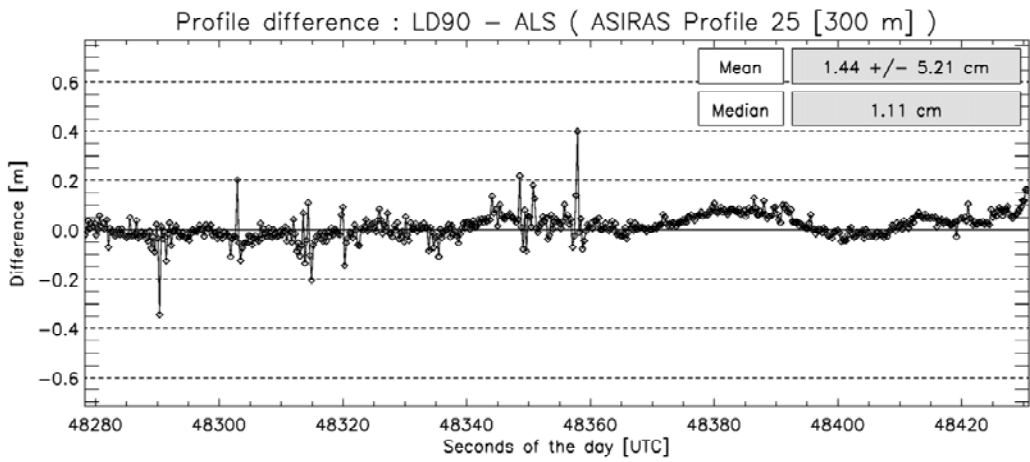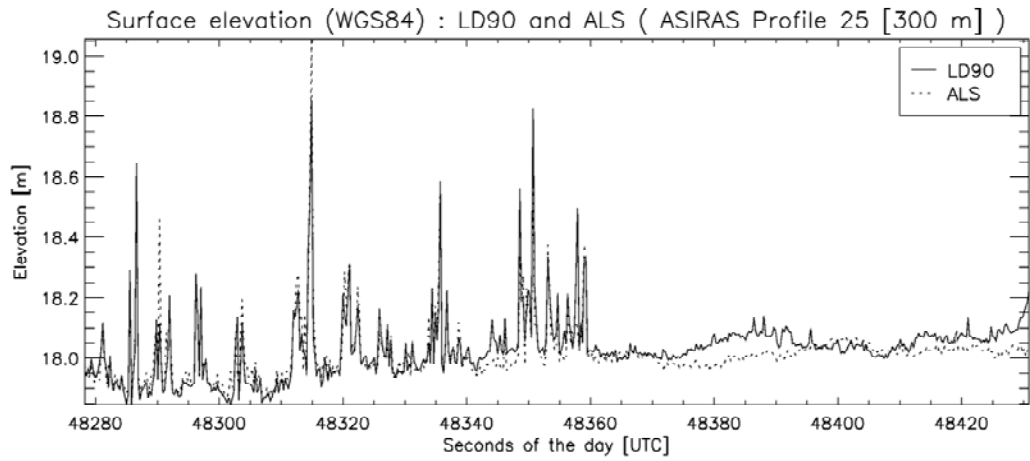
Figure 6.10-2 : Comparison of single beam laser and coincident ALS surface elevation profile (Validation line, 300 m)
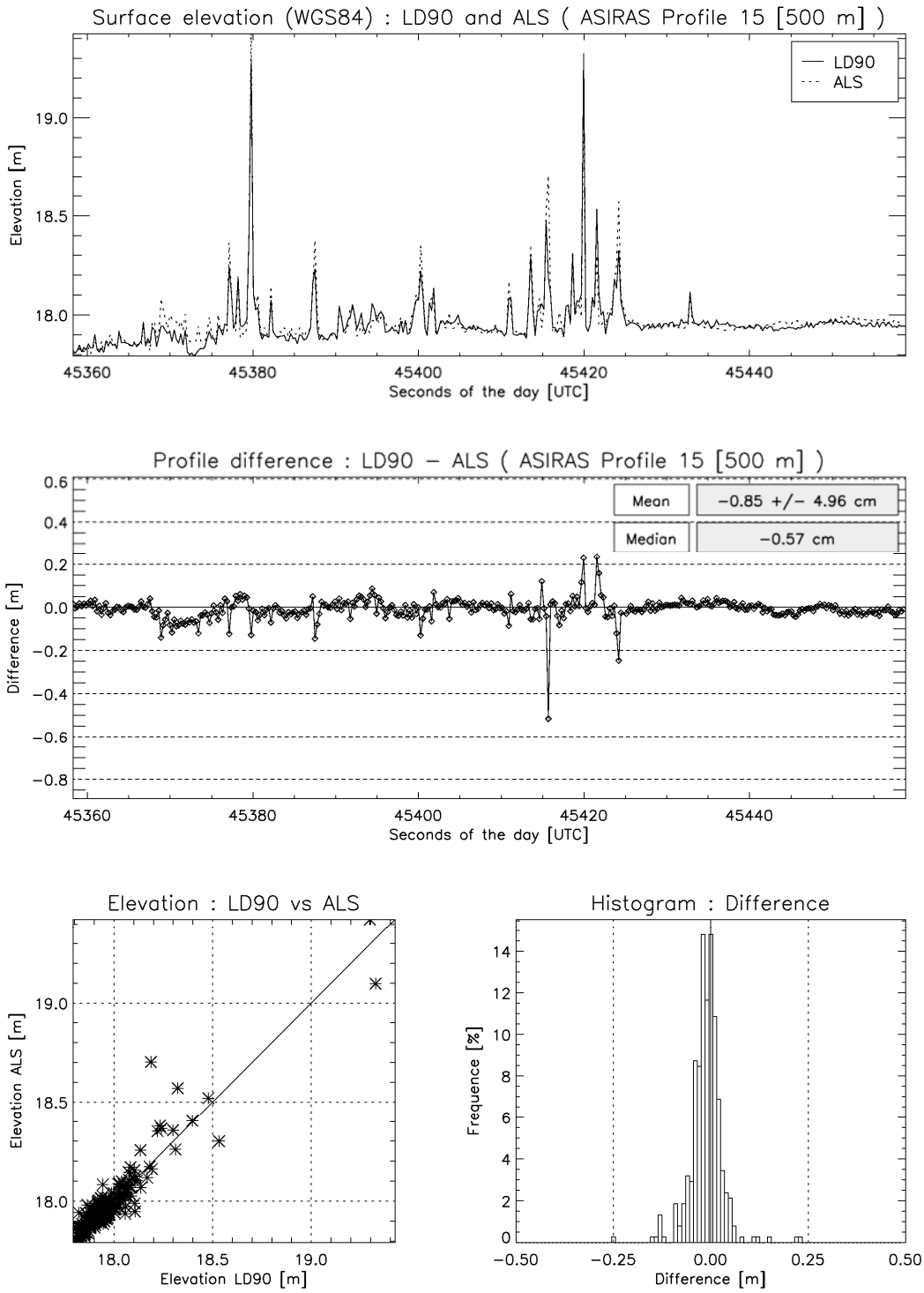
Figure 6.10-3 : Comparison of single beam laser and coincident ALS surface elevation profile (Validation line, 500 m)
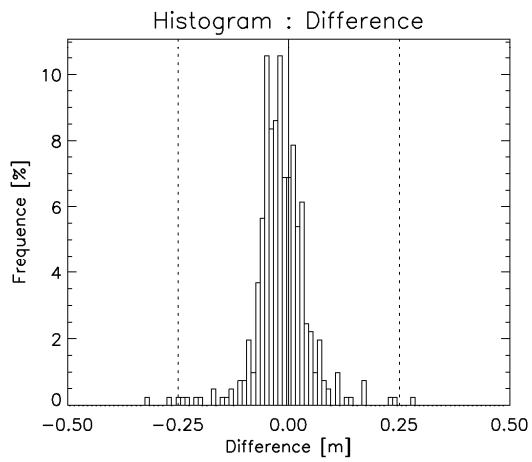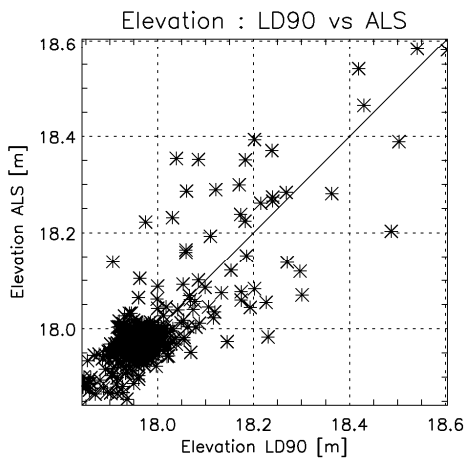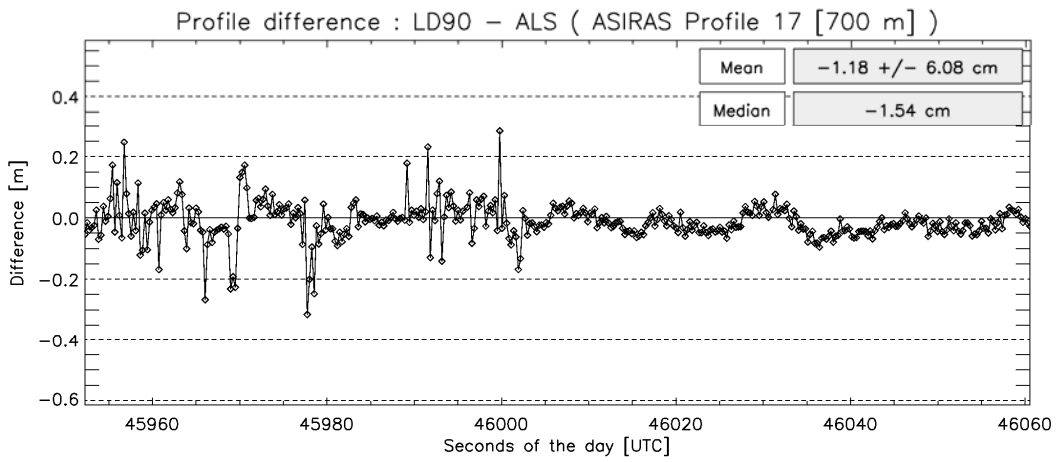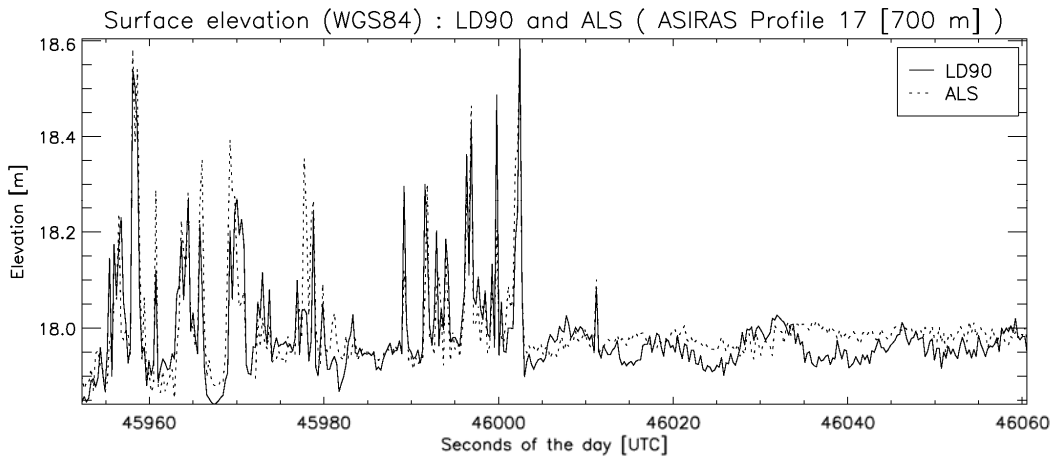
Figure 6.10-4 : Comparison of single beam laser and coincident ALS surface elevation profile (Validation line, 700 m)
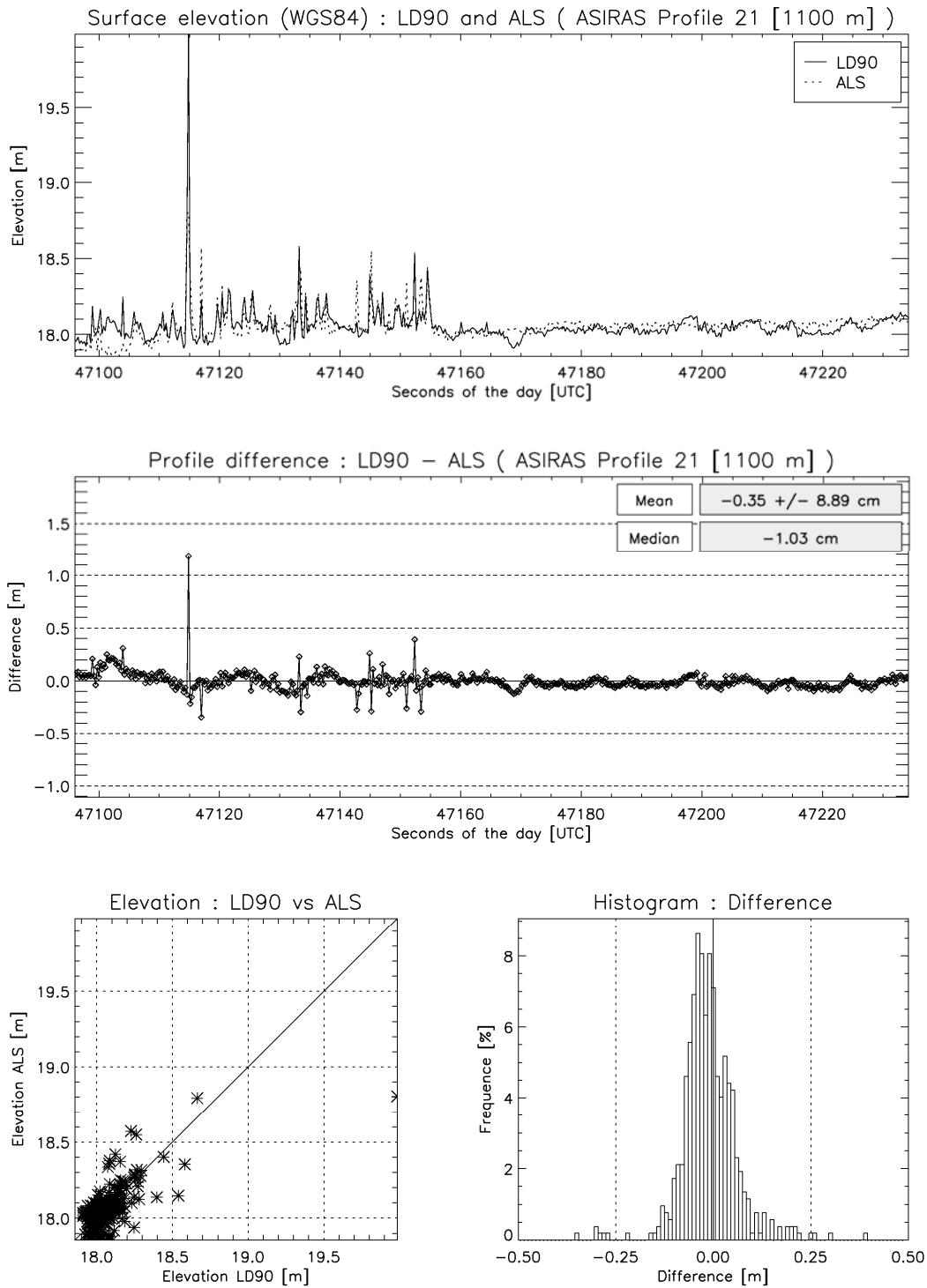
Figure 6.10-5 : Comparison of single beam laser and coincident ALS surface elevation profile (Validation line, 1100 m)

6.10.2   ALS surface elevation vs EM Bird surface roughness
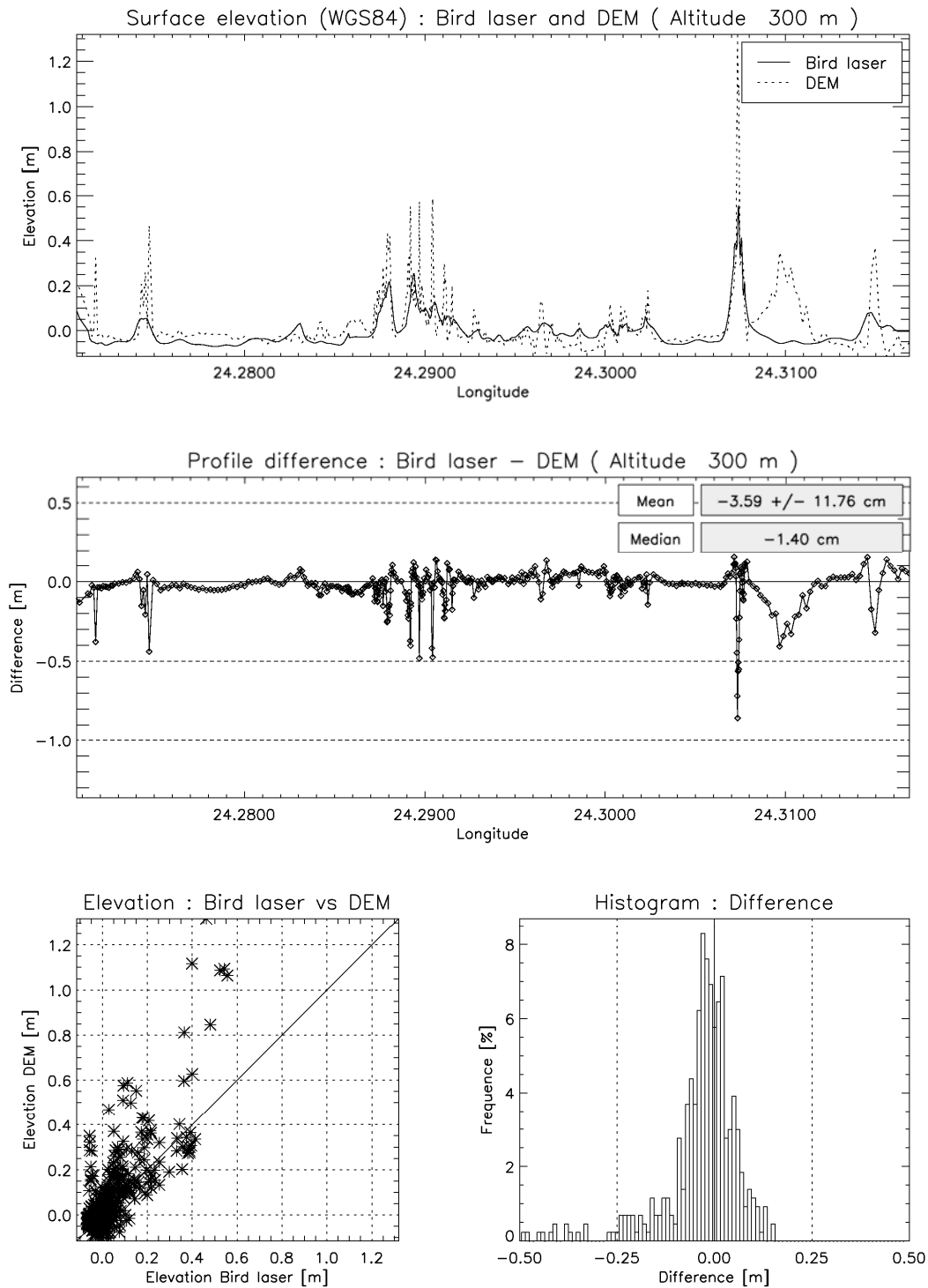
Figure 6.10-6 Comparison of ALS surface elevation profile and surface roughness profile obtained with EM Bird laser (300 m)
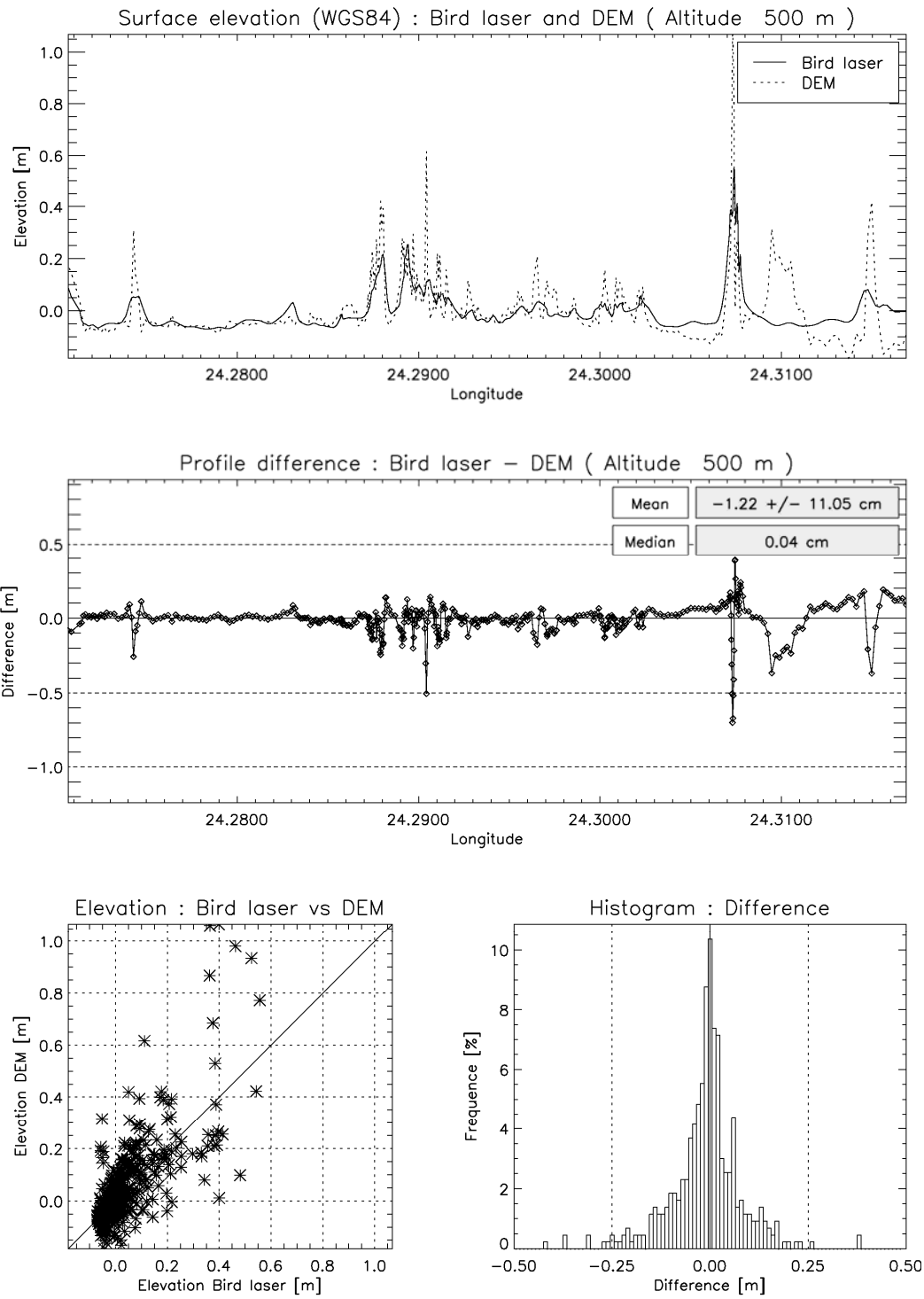
Figure 6.10-7 : Comparison of ALS surface elevation profile and surface roughness profile obtained
with EM Bird laser (500 m)

Surface elevation (WGS84) : Bird laser and DEM (Altitude   700 m)

Profile difference : Bird laser − DEM (Altitude   700 m)

Mean	−1.91 +/− 13.84 cm
Median	0.82 cm

Elevation : Bird laser vs DEM

Histogram : Difference
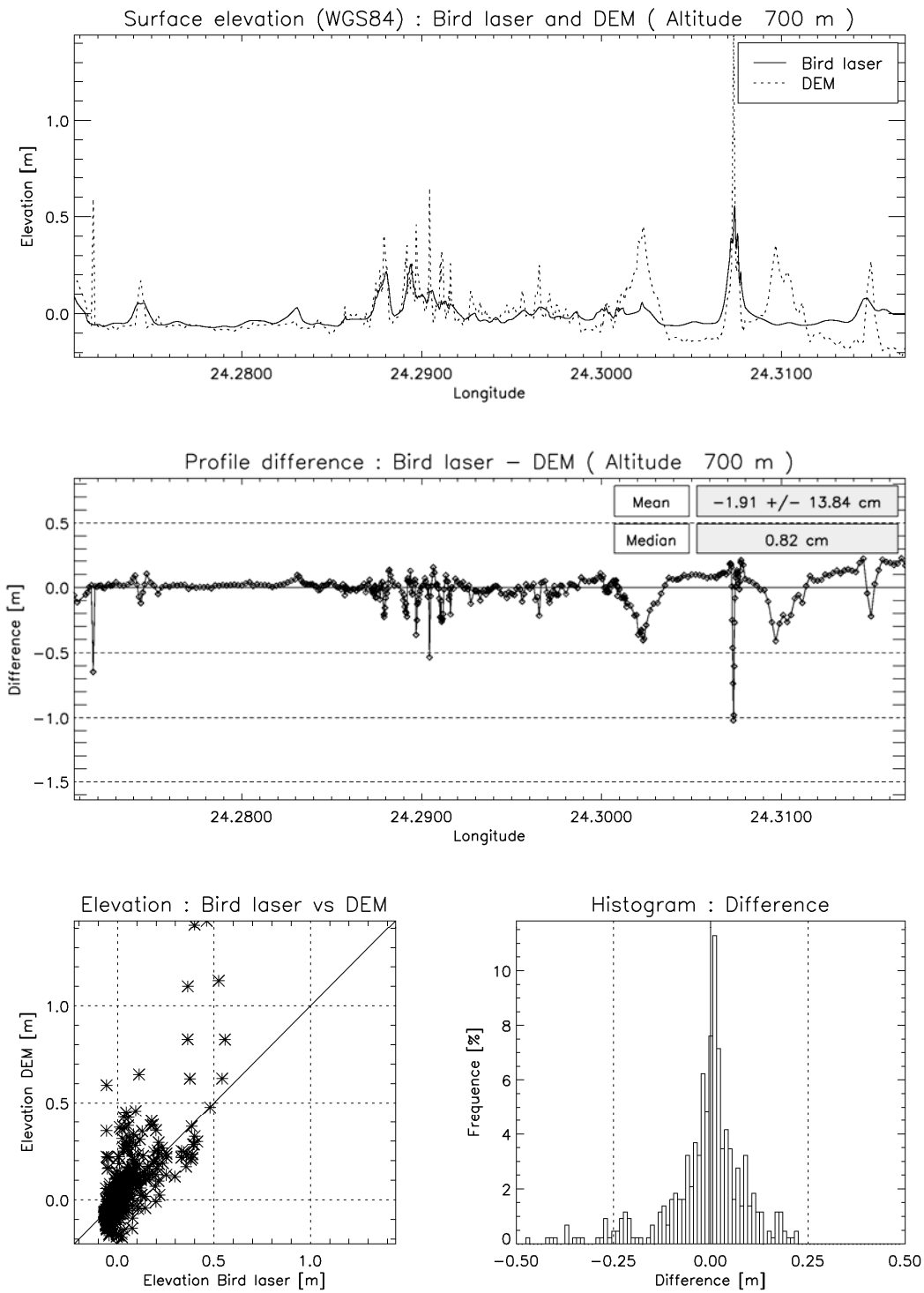
Figure 6.10-8 : Comparison of ALS surface elevation profile and surface roughness profile obtained with EM Bird laser (700 m)
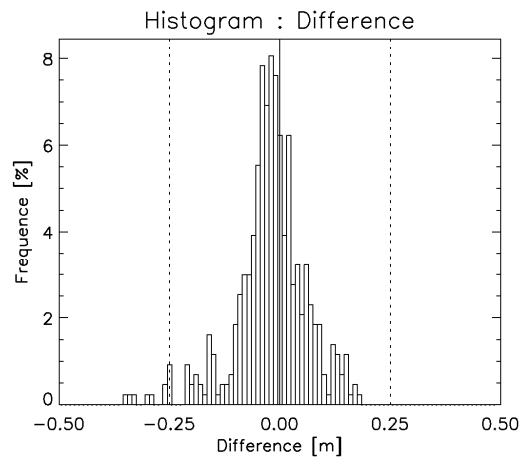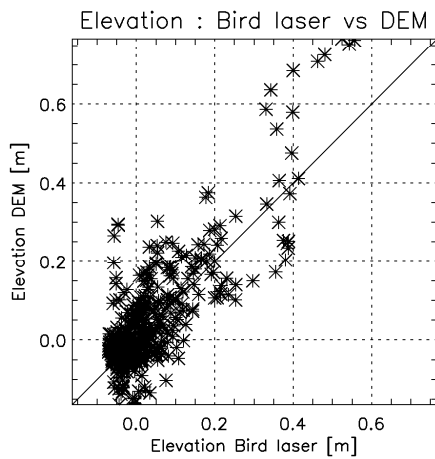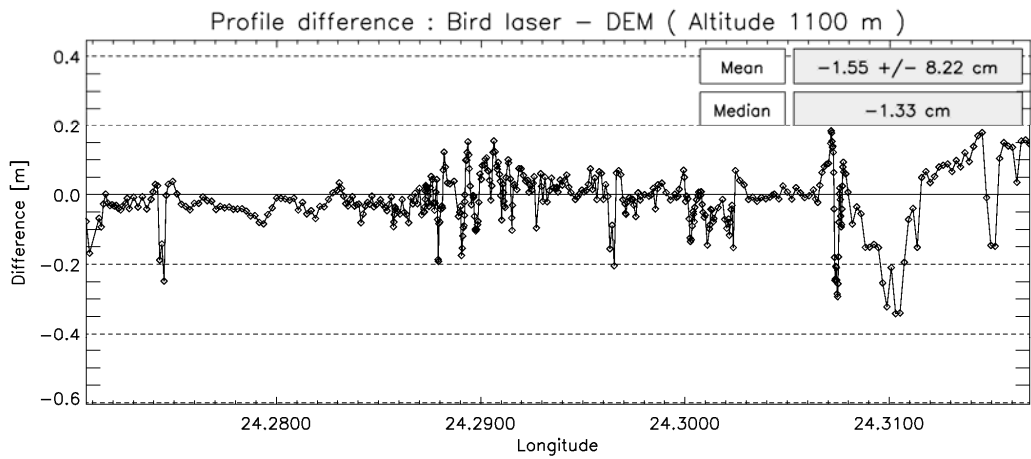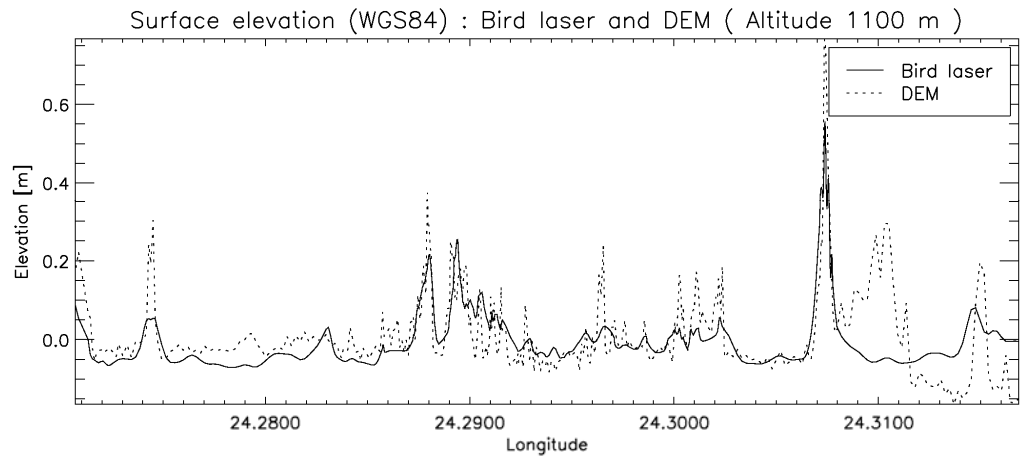
Figure 6.10-9 Comparison of ALS surface elevation profile and surface roughness profile obtained with EM Bird laser (1100 m)

6.10.3   Comparison ASIRAS – ALS
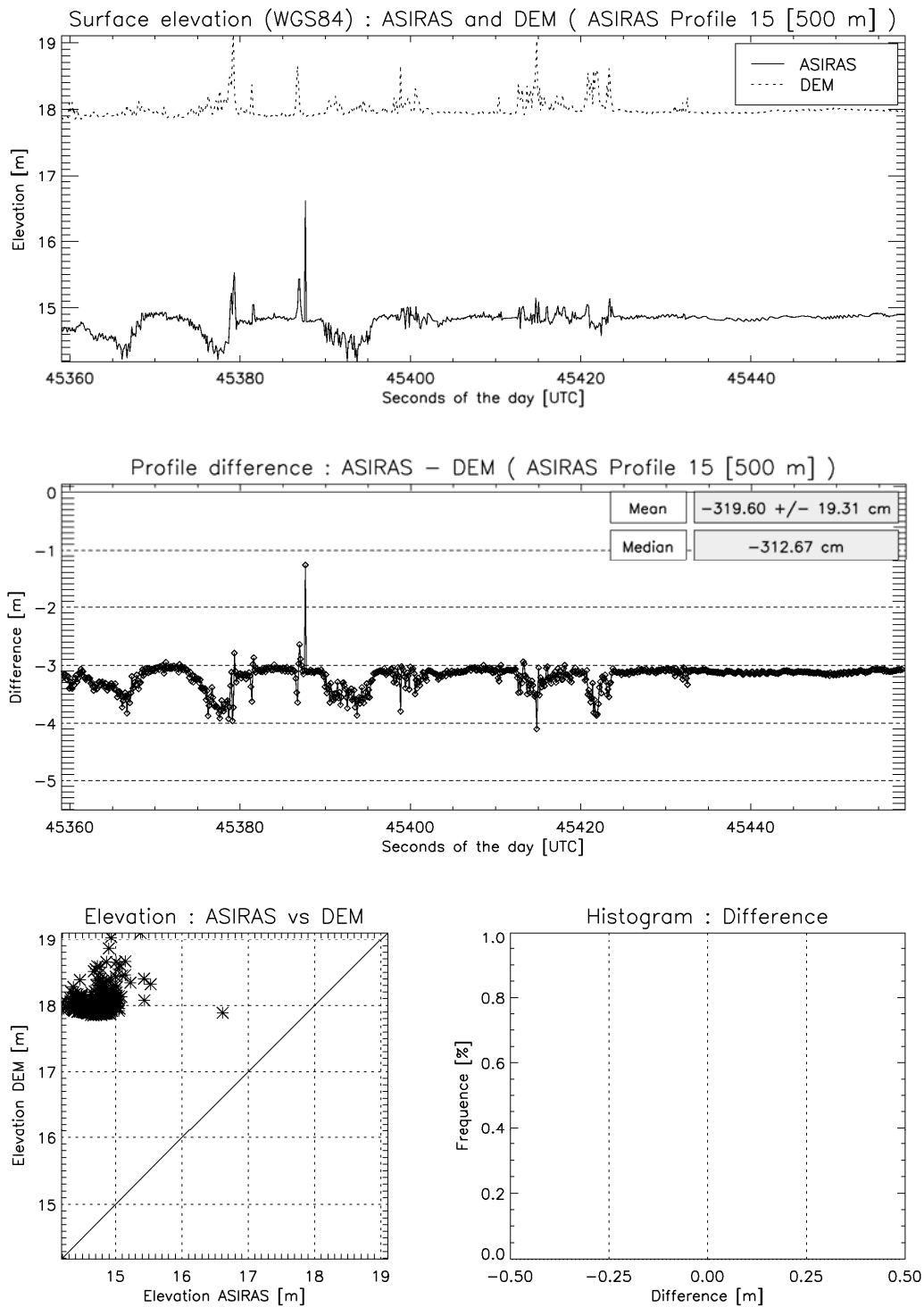
Figure 6.10-10 : Comparison of ASIRAS and ALS surface elevation, (Profile 15, 500m)

Surface elevation (WGS84) : ASIRAS and DEM (ASIRAS Profile 17 [500 m])

Profile difference : ASIRAS − DEM (ASIRAS Profile 17 [500 m])

Mean	−331.04 +/− 12.05 cm
Median	−326.84 cm

Elevation : ASIRAS vs DEM

Histogram : Difference
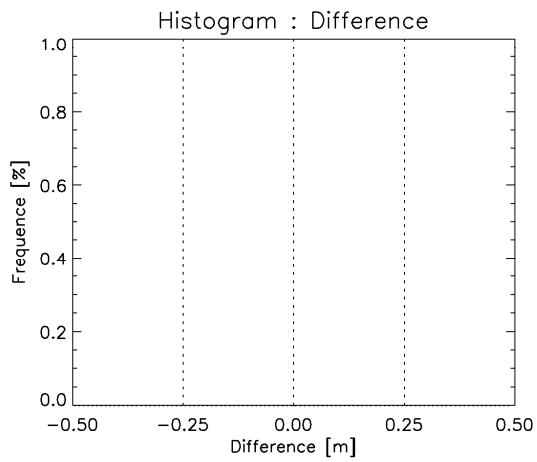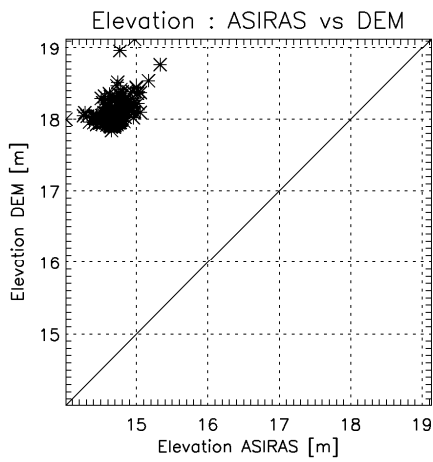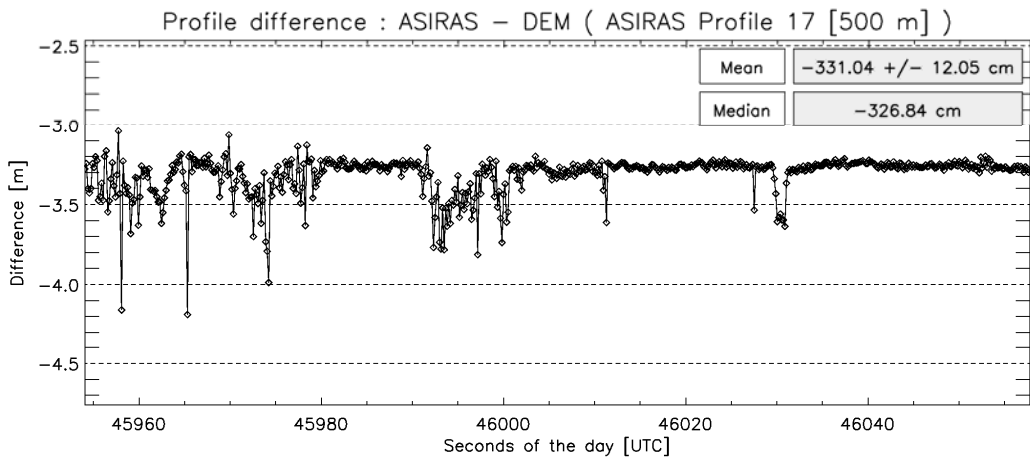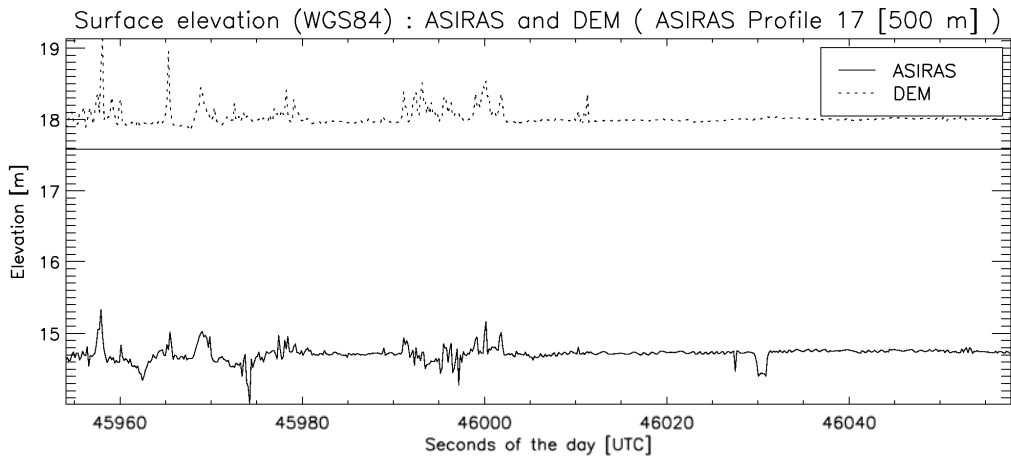
Figure 6.10-11 : Comparison of ASIRAS and ALS surface elevation, (Profile 17, 700m)

Surface elevation (WGS84) : ASIRAS and DEM (Oulu runway)

Profile difference : ASIRAS − DEM (Oulu runway)

| Mean | −401.57 +/− 294.00 cm |
| Median | −313.14 cm |

Elevation : ASIRAS vs DEM

Histogram : Difference
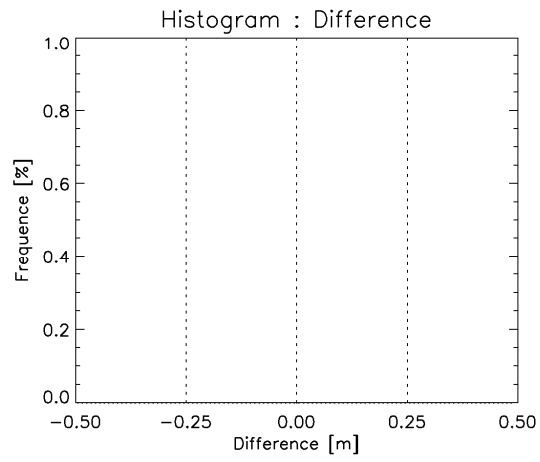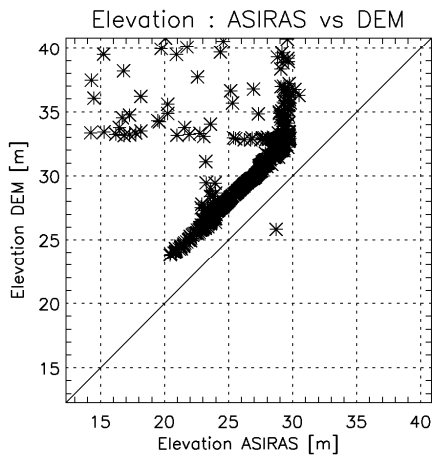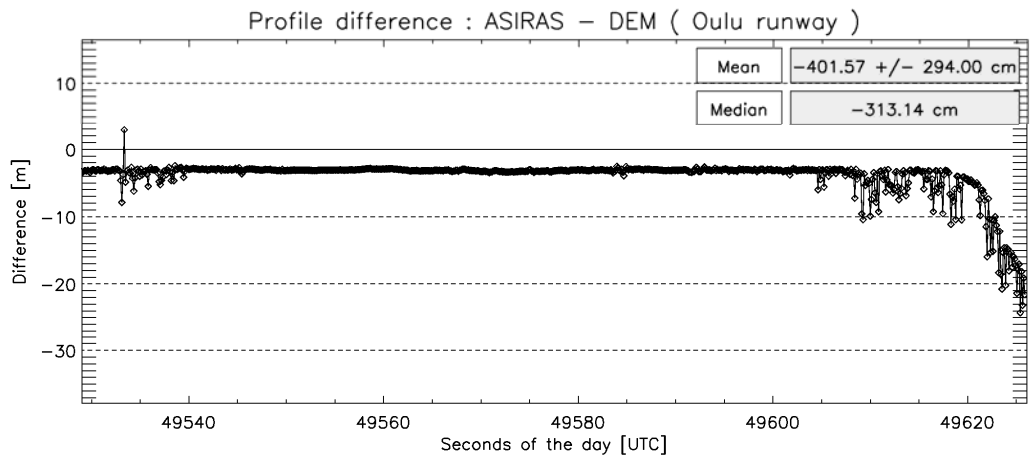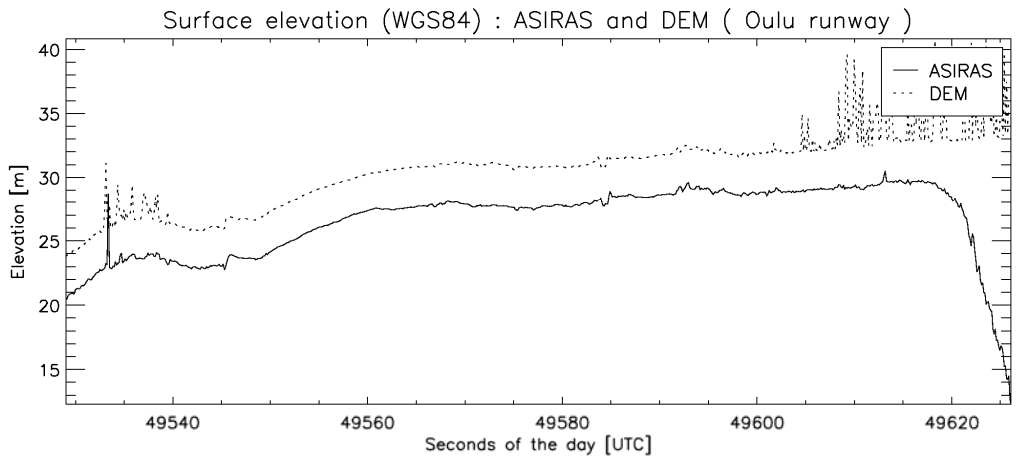
Figure 6.10-12 Comparison of ASIRAS and ALS surface elevation, (Oulu runway)

6.10.4 ASIRAS echoes

Displayed are the power echoes for the validation line passes at different altitudes. The black line in the plot shows the surface levelling data for comparison. Time shifts between power echoes and GPS have not been removed from these plots.
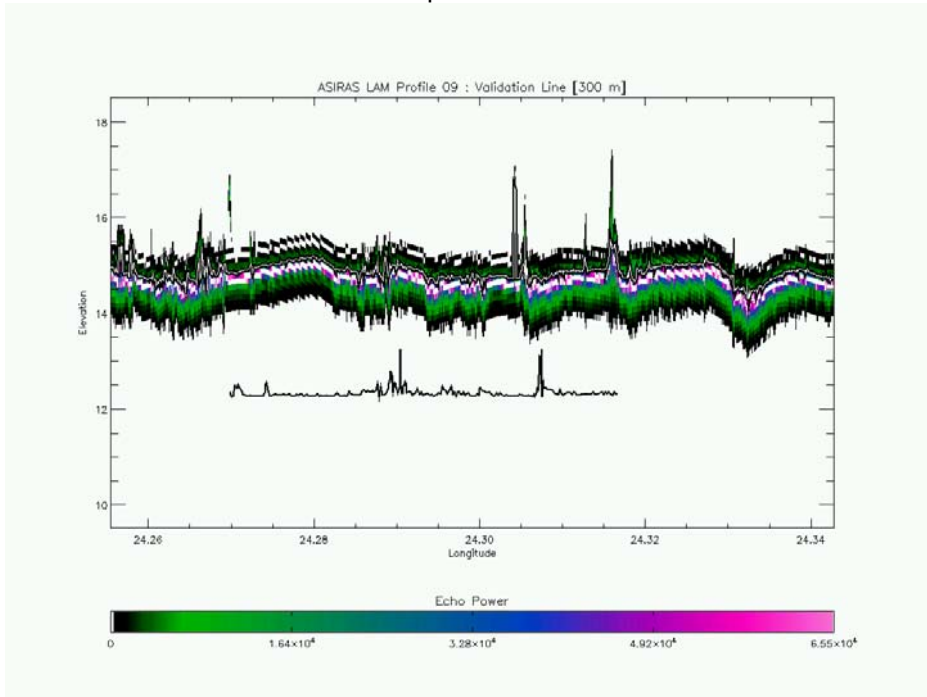
Figure 6.10-13 : ASIRAS LAM power echoes and retrieved surface elevation (Profile #9, 300 m)
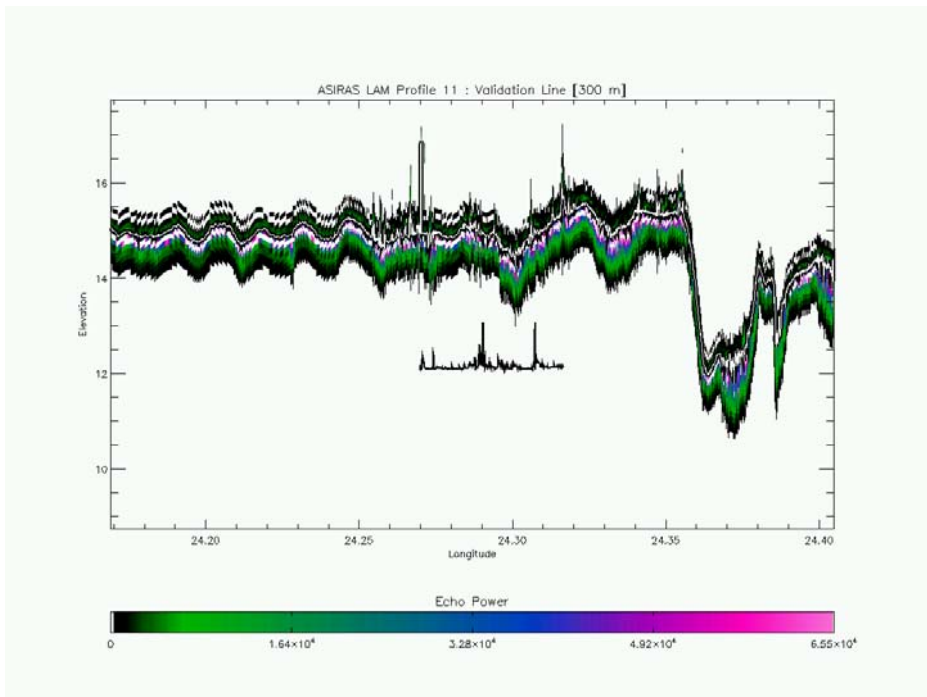
Figure 6.10-14 : ASIRAS LAM power echoes and retrieved surface elevation (Profile #11, 300 m)
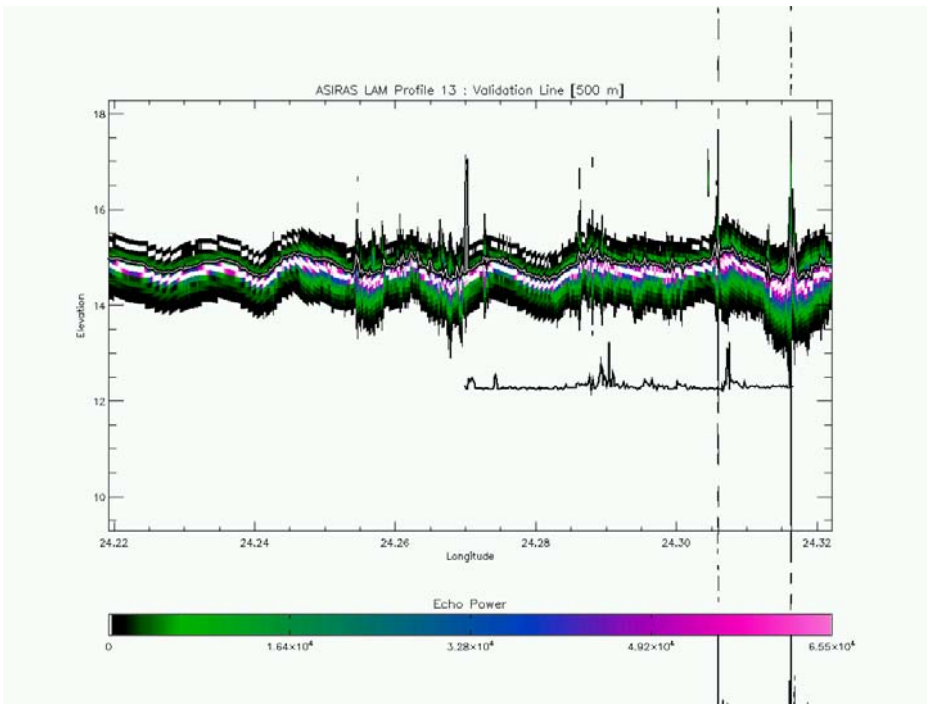
Figure 6.10-15 : ASIRAS LAM power echoes and retrieved surface elevation (Profile #13, 500 m)
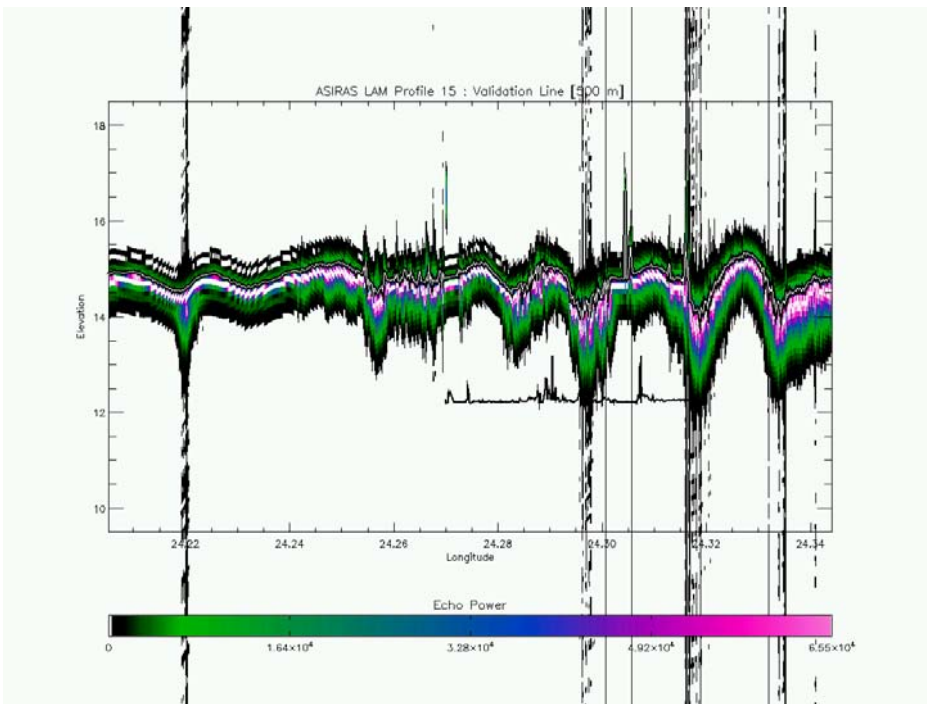
Figure 6.10-16 : ASIRAS LAM power echoes and retrieved surface elevation (Profile #15, 500 m)
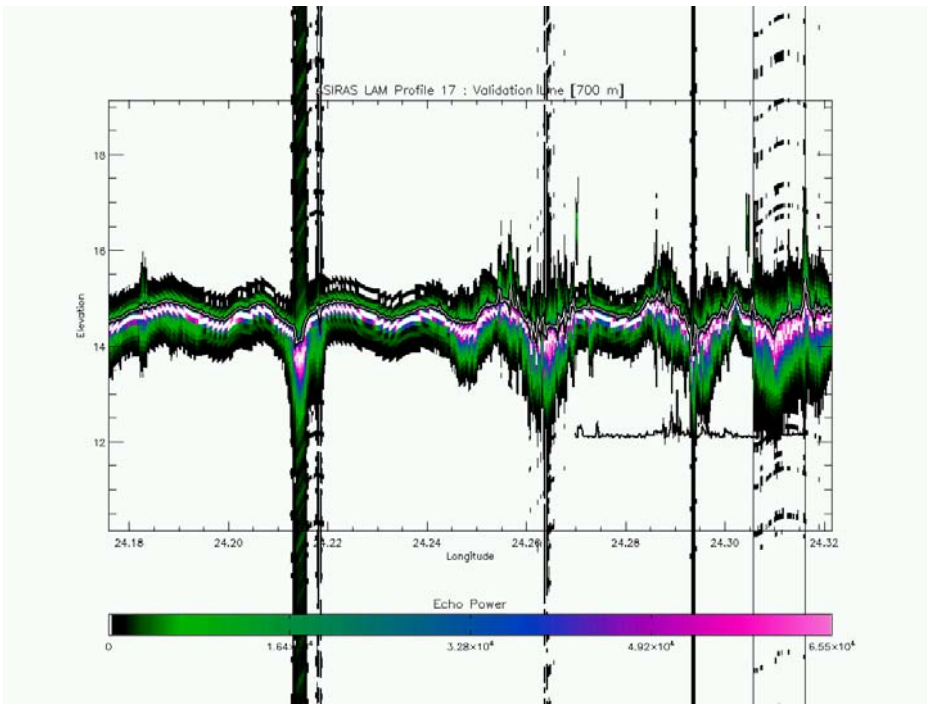
Figure 6.10-17 : ASIRAS LAM power echoes and retrieved surface elevation (Profile #17, 700 m)
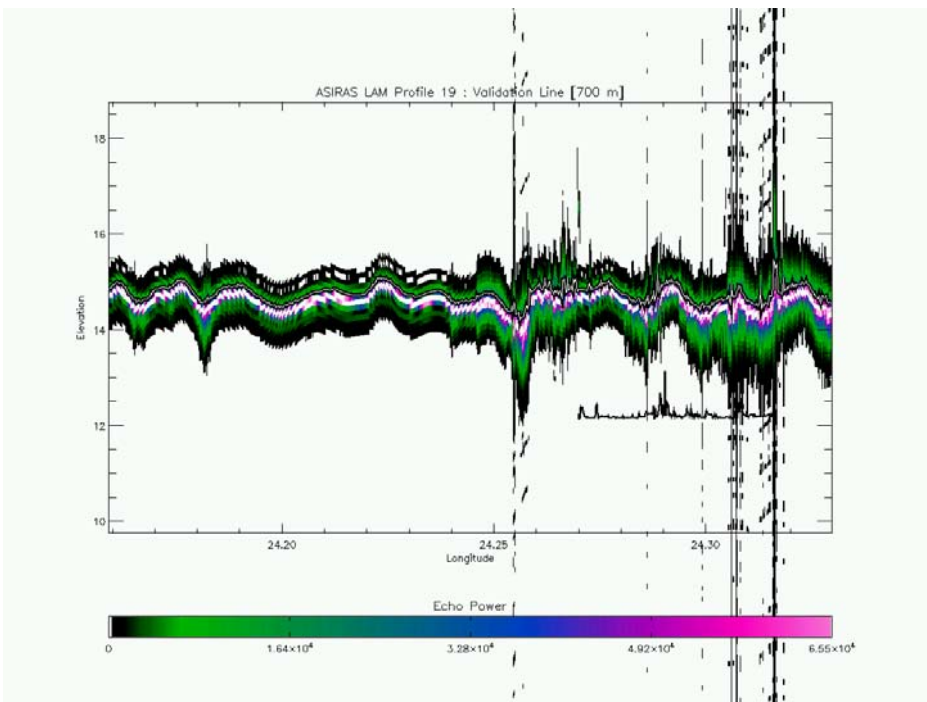
Figure 6.10-18 : ASIRAS LAM power echoes and retrieved surface elevation (Profile #19, 7300 m)
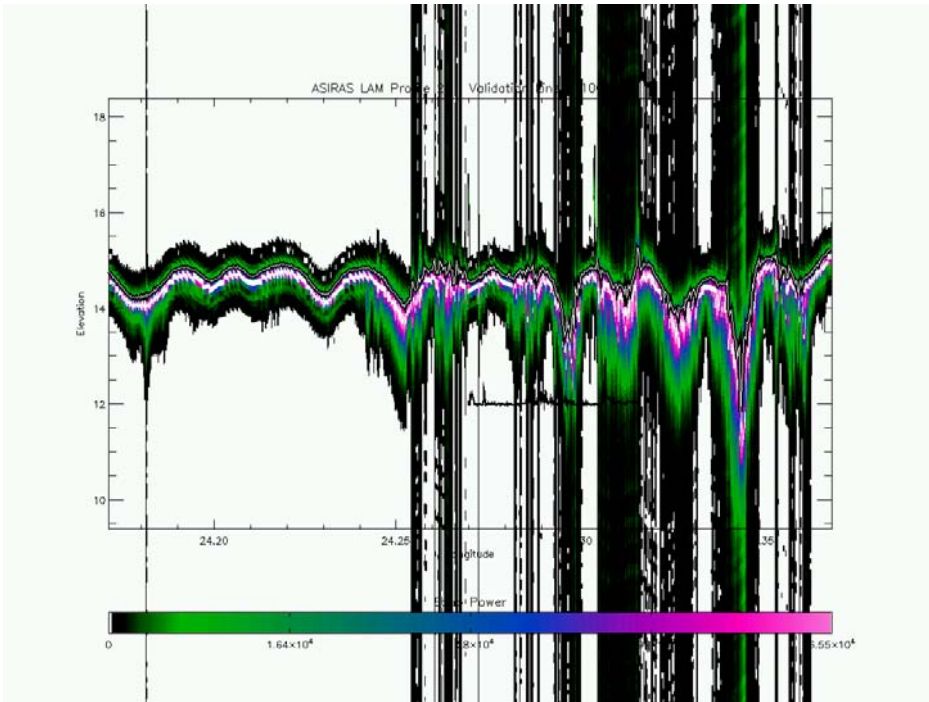
Figure 6.10-19 : ASIRAS LAM power echoes and retrieved surface elevation (Profile #23, 1100 m)

7 Data delivery

7.1 Directory structure and file naming convention

Delivered data will have the following structure. Filenaming convention is described in detail in ???.

7.1.1 Raw data structure

Campaign_name/FlightData/Measuring-day_name/RawData
(e.g. ASIRAS_04_03/FlighData/0409140501/RawData)

ASIRAS:
```
        /ASIRAS/Logs          ...log
        /ASIRAS/PC1                    ...dat
        /ASIRAS/PC2                    ...dat
```

GPS:
```
                /GPS/AirF              AIRF...dat, ...eph, ...mes, ...ion

                /GPS/AirR              AIRR...dat, ...eph, ...mes, ...ion
                /GPS/Ground            ...dat, ...eph, ...mes, ...ion
```

SCANNER (ALS):
```
                /MedusaP/als           rawdata..., trigdata...
```

LD90:
```
                /MedusaP/asciidata     NAVP_raw6_LD90.dat
```

INS:
```
                /MedusaP/asciidata     NAVP_raw0_INSGNS.dat
```

7.1.2 Processed data structure

Campaign_name/Measuring-day_name/ProcessedData
(e.g. ASIRAS_04_03/0409140501/ProcessedData)

ASIRAS:
```
                /ASIRAS/LEVEL_L1B   ...DBL
```
GPS:
```
                /GPS/GPS_F_01_name
                /GPS/GPS_R_01_name
```

ALS:
```
                /ALS/ALS_name
```

LD90:
```
                /LD90/LD90_name
```

INS:
```
                /INS/INS_name
```

7.2 Delivered files of CryoVex2004A

Table 7.2-1 Delivered files of 19th of April 2004, CryoVex2004A

Campaign	Day	Filetype	Filename
ASIRAS_04_02	0404190101	GPS	GPS_R_01_20040419T143812_174231
			GPS_F_01_20040419T143805_174232
		INS	INS_20040419T151008_174017
		LD90	LD90_L1B_20040419T152123_172932
		ALS	ALS_L1B_00_20040419T152540_152833
			ALS_L1B_01_20040419T152834_153302
			ALS_L1B_02_20040419T153856_154126
			ALS_L1B_03_20040419T154816_155700
			ALS_L1B_04_20040419T160217_160915
			ALS_L1B_05_20040419T161541_162319
			ALS_L1B_06_20040419T162631_162953
			ALS_L1B_07_20040419T163455_163939
			ALS_L1B_08_20040419T164250_164702
		ASIRAS	AS2TA00_ASIHL1B030320040419T152542_20040419T152832_0001.DBL
			AS2TA01_ASIHL1B030320040419T152836_20040419T153301_0001.DBL
			AS2TA02_ASIHL1B030320040419T153858_20040419T154125_0001.DBL
			AS2TA03_ASIHL1B030320040419T154818_20040419T155659_0001.DBL
			AS2TA04_ASIHL1B030320040419T160219_20040419T160914_0001.DBL
			AS2TA05_ASIHL1B030320040419T161543_20040419T162318_0001.DBL
			AS2TA06_ASIHL1B030320040419T162633_20040419T162952_0001.DBL
			AS2TA07_ASIHL1B030320040419T163457_20040419T163938_0001.DBL
			AS2TA08_ASIHL1B030320040419T164252_20040419T164701_0001.DBL

Table 7.2-2 Delivered files of 20th of April 2004, CryoVex2004A

Campaign	Day	Filetype	Filename
ASIRAS_04_02	0404200201	GPS	GPS_R_01_20040420T152348_202200
			GPS_F_01_20040420T152248_202204
		INS	INS_20040420T154049_202014
		LD90	LD90_L1B_20040420T155425_201705
		ALS	ALS_L1B_00_20040420T160235_160422
			ALS_L1B_01_20040420T170548_172514
			ALS_L1B_02_20040420T173331_174858
			ALS_L1B_03_20040420T180217_181114
			ALS_L1B_04_20040420T181226_183625
			ALS_L1B_05_20040420T185540_191515
		ASIRAS	AS2TA00_ASIHL1B030320040420T160237_20040420T160421_0001.DBL
			AS2TA01_ASIHL1B030320040420T170550_20040420T172513_0001.DBL
			AS2TA02_ASIHL1B030320040420T173333_20040420T174857_0001.DBL
			AS2TA03_ASIHL1B030320040420T180219_20040420T181113_0001.DBL
			AS2TA04_ASIHL1B030320040420T181228_20040420T183624_0001.DBL
			AS2TA05_ASIHL1B030320040420T185542_20040420T191514_0001.DBL

Table 7.2-3 Delivered files of 25th of April 2004, CryoVex2004A

Campaign	Day	Filetype	Filename
ASIRAS_04_02	0404250301	GPS	GPS_R_01_20040425T063022_092136
			GPS_F_01_20040425T063048_092120
		INS	INS_20040425T082020_085017
		LD90	LD90_L1B_20040425T083024_084340
		ALS	ALS_L1B_04_20040425T083907_084908
		ASIRAS	AS2TA00_ASIHL1B030320040425T073258_20040425T074312_0001.DBL
			AS2TA01_ASIHL1B030320040425T074535_20040425T075902_0001.DBL
			AS2TA02_ASIHL1B030320040425T080425_20040425T081056_0001.DBL
			AS2TA03_ASIHL1B030320040425T082049_20040425T082538_0001.DBL
			AS2TA04_ASIHL1B030320040425T083909_20040425T084907_0001.DBL

Table 7.2-4 Delivered files of 2nd of May 2004, CryoVex2004A

Campaign	Day	Filetype	Filename
ASIRAS_04_02	0405020401	GPS	GPS_R_01_20040502T172935_215833
			GPS_F_01_20040502T172934_215830
		INS	INS_20040502T174500_215702
		LD90	LD90_L1B_20040502T180552_215005
		ALS	ALS_L1B_01_20040502T190501_191528
			ALS_L1B_02_20040502T192202_193136
			ALS_L1B_03_20040502T193934_194321
			ALS_L1B_04_20040502T201949_203616
			ALS_L1B_05_20040502T213820_214246
		ASIRAS	AS2TA00_ASIHL1B030320040502T190156_20040502T190327_0001.DBL
			AS2TA01_ASIHL1B030320040502T190503_20040502T191527_0001.DBL
			AS2TA02_ASIHL1B030320040502T192204_20040502T193135_0001.DBL
			AS2TA03_ASIHL1B030320040502T193936_20040502T194320_0001.DBL
			AS2TA04_ASIHL1B030320040502T201951_20040502T203615_0001.DBL
			AS2TA05_ASIHL1B030320040502T213822_20040502T214245_0001.DBL

Table 7.2-5 Delivered files of 6th of May 2004, CryoVex2004A

Campaign	Day	Filetype	Filename
ASIRAS_04_02	0405060601	GPS	GPS_R_01_20040506T123221_171731
			GPS_F_01_20040506T123418_171733
		INS	INS_20040506T124241_171612
		LD90	LD90_L1B_20040506T125557_170601
		ALS	ALS_L1B_00_20040506T131850_132155
		ASIRAS	AS2TA00_ASIHL1B030320040506T131852_20040506T132154_0001.DBL

Table 7.2-6 Delivered files of 5th of May 2004, CryoVex2004A

Campaign	Day	Filetype	Filename
ASIRAS_04_02	0405050501	GPS	GPS_R_01_20040505T174421_202403
			GPS_F_01_20040505T174518_202406
		INS	INS_20040505T180708_202248
		LD90	LD90_L1B_20040505T181741_201526
		ALS	ALS_L1B_00_20040505T183945_185825
			ALS_L1B_01_20040505T193818_194543
			ALS_L1B_02_20040505T200147_200340
			ALS_L1B_03_20040505T200831_200956
		ASIRAS	AS2TA00_ASIHL1B030320040505T183947_20040505T185824_0001.DBL
			AS2TA01_ASIHL1B030320040505T193820_20040505T194542_0001.DBL
			AS2TA02_ASIHL1B030320040505T200149_20040505T200339_0001.DBL
			AS2TA03_ASIHL1B030320040505T200833_20040505T200955_0001.DBL

7.3 Delivered files of CryoVex2004B

Table 7.3-1 Delivered files of 4th of September 2004, CryoVex200B

Campaign	Day	Filetype	Filename
ASIRAS_04_03	0409040201	GPS	GPS_R_01_20040904T113835_134427
			GPS_F_01_20040904T113917_134423
		INS	INS_20040904T114320_134330
		LD90	LD90_L1B_20040904T121814_133147
		ALS	ALS_L1B_00_20040904T123115_123741
			ALS_L1B_01_20040904T123754_124131
			ALS_L1B_02_20040904T124258_124812
			ALS_L1B_03_20040904T125015_125350
			ALS_L1B_04_20040904T125719_125913
			ALS_L1B_06_20040904T130650_131053
			ALS_L1B_07_20040904T131139_131905
			ALS_L1B_08_20040904T132602_132934
		ASIRAS	AS2TA00_ASIHL1B030320040904T123117_20040904T123740_0001.DBL
			AS2TA01_ASIHL1B030320040904T123756_20040904T124130_0001.DBL
			AS2TA02_ASIHL1B030320040904T124300_20040904T124811_0001.DBL
			AS2TA03_ASIHL1B030320040904T125017_20040904T125349_0001.DBL
			AS2TA04_ASIHL1B030320040904T125721_20040904T125912_0001.DBL
			AS2TA06_ASIHL1B030320040904T130652_20040904T131052_0001.DBL
			AS2TA07_ASIHL1B030320040904T131141_20040904T131904_0001.DBL
			AS2TA08_ASIHL1B030320040904T132604_20040904T132933_0001.DBL

Table 7.3-2 Delivered files of 9th of September 2004, CryoVex200B

Campaign	Day	Filetype	Filename
ASIRAS_04_03	0409090301	GPS	GPS_R_01_20040909T144551_185314
			GPS_F_01_20040909T144522_185310
		INS	INS_20040909T144755_185114
		LD90	LD90_L1B_20040909T151610_184412
		ALS	ALS_L1B_00_20040909T160237_161213
			ALS_L1B_01_20040909T161229_161443
			ALS_L1B_02_20040909T161929_162108
			ALS_L1B_03_20040909T162758_164333
			ALS_L1B_04_20040909T182659_183126
			ALS_L1B_05_20040909T183510_183756
		ASIRAS	AS2TA00_ASIHL1B030320040909T160239_20040909T161212_0001.DBL
			AS2TA01_ASIHL1B030320040909T161231_20040909T161442_0001.DBL
			AS2TA02_ASIHL1B030320040909T161931_20040909T162107_0001.DBL
			AS2TA03_ASIHL1B030320040909T162800_20040909T164332_0001.DBL
			AS2TA04_ASIHL1B030320040909T182701_20040909T183125_0001.DBL
			AS2TA05_ASIHL1B030320040909T183512_20040909T183755_0001.DBL

Table 7.3-3 Delivered files of 11th of September 2004, CryoVex200B

Campaign	Day	Filetype	Filename
ASIRAS_04_03	0409110401	GPS	GPS_R_01_20040911T162722_181542
			GPS_F_01_20040911T164630_181536
		INS	INS_20040911T164143_181453
		LD90	LD90_L1B_20040911T174009_181139
		ALS	ALS_L1B_00_20040911T174234_174811
			ALS_L1B_01_20040911T175552_181059
		ASIRAS	AS2TA00_ASIHL1B030320040911T174236_20040911T174810_0001.DBL
			AS2TA01_ASIHL1B030320040911T175554_20040911T181058_0001.DBL

Table 7.3-4 Delivered files of 17th of September 2004, CryoVex200B

Campaign	Day	Filetype	Filename
ASIRAS_04_03	0409170701	GPS	GPS_R_01_20040917T130548_183113
			GPS_F_01_20040917T130451_183110
		INS	INS_20040917T133129_183048
		LD90	LD90_L1B_20040917T141207_182441
		ALS	ALS_L1B_00_20040917T141748_154034
		ASIRAS	AS2TA00_ASIHL1B030320040917T141750_20040917T154033_0001.DBL

Table 7.3-5 Delivered files of 14th of September 2004, CryoVex200B

Campaign	Day	Filetype	Filename
ASIRAS_04_03	0409140501	GPS	GPS_R_01_20040914T144157_183701
			GPS_F_01_20040914T144148_183657
		INS	INS_20040914T150439_183725
		LD90	LD90_L1B_20040914T150135_181740
		ALS	ALS_L1B_00_20040914T150628_150937
			ALS_L1B_01_20040914T151348_151531
			ALS_L1B_02_20040914T154822_162209
			ALS_L1B_03_20040914T163155_163804
			ALS_L1B_04_20040914T175938_180113
			ALS_L1B_05_20040914T180121_180127
			ALS_L1B_07_20040914T181331_181530
		ASIRAS	AS2TA00_ASIHL1B030320040914T150630_20040914T150936_0001.DBL
			AS2TA01_ASIHL1B030320040914T151350_20040914T151530_0001.DBL
			AS2TA02_ASIHL1B030320040914T154824_20040914T162208_0001.DBL
			AS2TA03_ASIHL1B030320040914T163157_20040914T163803_0001.DBL
			AS2TA04_ASIHL1B030320040914T175940_20040914T180112_0001.DBL
			AS2TA05_ASIHL1B030320040914T180123_20040914T180126_0001.DBL
			AS2TA06_ASIHL1B030320040914T180556_20040914T180828_0001.DBL
			AS2TA07_ASIHL1B030320040914T181333_20040914T181529_0001.DBL

7.4 Delivered files of BoB

Table 7.4-1: Delivered files of 13th of March 2004, CryoVex 2005 (BoB)

Campaign	Day	Filetype	Filename
ASIRAS_05_01	0503130301	GPS	GPS_F_01_20050313T143548_182804
			GPS_R_01_20050313T143536_182648
		INS	INS_20050313T143717_182527
		LD90	LD90_L1B_20050313T145302_180849
		ALS	ALS_L1B_20050313T170025_181138
		ASIRAS	AS1TA07_ASILL1B0303050313T162801_050313T164626_0001.DBL
			AS1TA08_ASILL1B0303050313T165531_050313T173042_0001.DBL
			AS1TA09_ASILL1B0303050313T174002_050313T175431_0001.DBL
			AS1TA10_ASILL1B0303050313T175916_050313T180757_0001.DBL

Table 7.4-2 : Delivered files of 14th of March 2005 (1. Flight), CryoVex 2005 (BoB)

Campaign	Day	Filetype	Filename
ASIRAS_05_01	0503140403	GPS	GPS_F_01_20050314T115946_135314
			GPS_R_01_20050314T115946_135313
		INS	INS_20050314T100249_135251
		LD90	LD90_L1B_20050314T120427_134918
		ALS	ALS_L1B_20050314T122925_135250
		ASIRAS	AS1TA06_ASILL1B0303050314T095137_050314T095214_0001.DBL
			AS1TA07_ASILL1B0303050314T113607_050314T113642_0001.DBL
			AS1TA08_ASILL1B0303050314T115907_050314T120203_0001.DBL
			AS1TA09_ASILL1B0303050314T120700_050314T120800_0001.DBL
			AS1TA09_ASILL1B0303050314T120700_050314T120800_0002.DBL
			AS1TA10_ASILL1B0303050314T121223_050314T121333_0001.DBL
			AS1TA11_ASILL1B0303050314T121607_050314T121853_0001.DBL
			AS1TA12_ASILL1B0303050314T122136_050314T122326_0001.DBL
			AS1TA13_ASILL1B0303050314T122721_050314T122833_0001.DBL
			AS1TA14_ASILL1B0303050314T123131_050314T123241_0001.DBL
			AS1TA15_ASILL1B0303050314T123601_050314T123742_0001.DBL
			AS1TA16_ASILL1B0303050314T124016_050314T124159_0001.DBL
			AS1TA17_ASILL1B0303050314T124556_050314T124742_0001.DBL
			AS1TA18_ASILL1B0303050314T125022_050314T125157_0001.DBL
			AS1TA19_ASILL1B0303050314T125511_050314T125712_0001.DBL
			AS1TA20_ASILL1B0303050314T125936_050314T130136_0001.DBL
			AS1TA21_ASILL1B0303050314T132005_050314T130715_0001.DBL
			AS1TA22_ASILL1B0303050314T131036_050314T131157_0001.DBL
			AS1TA23_ASILL1B0303050314T131508_050314T131721_0001.DBL
			AS1TA24_ASILL1B0303050314T131951_050314T132200_0001.DBL
			AS1TA25_ASILL1B0303050314T132442_050314T132711_0001.DBL
			AS1TA26_ASILL1B0303050314T132934_050314T133044_0001.DBL
			AS1TA27_ASILL1B0303050314T134531_050314T134713_0001.DBL

Table 7.4-3 : Delivered files of 14th of March 2005 (2. Flight), CryoVex 2005 (BoB)

Campaign	Day	Filetype	Filename
ASIRAS_05_01	0503140501	GPS	GPS_F_01_20050314T150050_174024
			GPS_R_01_20050314T150145_173955
		INS	INS_20050314T135251_173816
		LD90	LD90_L1B_20050314T152543_173756
		ALS	ALS_L1B_20050314T151011_173815
		ASIRAS	AS1TA30_ASILL1B0303050314T152857_050314T153047_0001.DBL
			AS1TA31_ASILL1B0303050314T153117_050314T153919_0001.DBL
			AS1TA32_ASILL1B0303050314T154131_050314T154300_0001.DBL
			AS1TA33_ASILL1B0303050314T154519_050314T155340_0001.DBL
			AS1TA34_ASILL1B0303050314T155638_050314T163833_0001.DBL

Table 7.4-4 : Delivered files of 15th of March 2005, CryoVex 2005 (BoB)

Campaign	Day	Filetype	Filename
ASIRAS_05_01	0503150601	GPS	GPS_F_01_20050315T110718_122038
			GPS_R_01_20050315T110723_122029
		INS	INS_20050315T110822_121953
		LD90	LD90_L1B_20050315T120540_121652
		ALS	ALS_L1B_20050315T112741_121952
		ASIRAS	-